GEOPHYSICAL LOGS FROM WELL KJ-17 IN THE KRAFLA GEOTHERMAL FIELD

Manuel C. Paete *
UNU Geothermal Training Programme
National Energy Authority
Grensasvegur 9, 108 Reykjavik
ICELAND

*Permanent address:
PNOC Energy Development Corporation
Geothermal Division
Merritt Road
Fort Bonifacio, Metro Manila
PHILIPPINES

ABSTRACT

Geophysical logs from well KJ-17 in the Krafla geothermal field were analysed in order to interpret the logs in terms of petrophysical parameters. The application of the acoustic cement bond log to the cementing operations in KJ-17 was also studied. Well KJ-17 penetrates 2190m of igneous rocks, extrusives and intrusives, of mainly basaltic and rhyolitic composition. The geophysical logs (caliper, 64" normal resistivity, neutron-neutron, and natural gamma ray logs) cover most of the productive section of the well. The acidic intrusions and a breccia layer from 920m to 1055m are associated with increased readings in the natural gamma ray log. In the 1191-1220m depth interval, the neutron-neutron and the resistivity log responses indicate the highest porosity for KJ-17, together with high resistivity. This inverse relation suggests that the total porosity in this interval is due to horizontal fractures. The minimum porosity for KJ-17 is in the 1225-1400m depth interval which is composed of dolerite intrusions. The cross plots and the large scale variations in this depth interval show that the resistivity increases with porosity. Unambigous explanation of this observation is not at hand. The possible pressure of metallic elements in the rock matrix causing it to have resistivities much lower than the resistivity of the formation fluid seems not to be in agreement with the geological data. The calculated silica content for each type of rocks in KJ-17 is comparable with the silica content of the same type of rocks in other areas in Iceland.

TABLE OF CONTENTS

LIST OF FIGURES

LIST OF TABLES

1 INTRODUCTION

1.1 Scope of work

This report is a part of the author's work during his training in borehole geophysics at the United Nations University and the National Energy Authority of Iceland in the period April - October 1983.

The 6 months training period commenced with 5 weeks of introductory lectures in borehole geophysics, geology, geohydrology, surface geophysical techniques, geochemistry, reservoir engineering, drilling, geothermal utilization, economics, etc. The next 5 weeks of the training period were devoted to the more specialized aspects of borehole geophysics and reservoir engineering with practical field exercises in between lectures. About 2 weeks were spent by the UNU Fellows in visiting the various geothermal fields, geothermal experimental stations and industrial establishments utilizing geothermal energy in Iceland.

The author also participated in running various geophysical logs during the completion tests of KJ-22 in the Krafla geothermal field such as temperature, pressure, neutron-neutron, natural gamma, resistivity and caliper logs. The rest of the training period was spent in preparing this report.

The aim of the training was for the author to gain experience in the interpretation of the various types of geophysical logs from drill holes. The authors's company, PNOC-EDC in the Philippines, has recently aquired logging equipment similar to that used in Iceland, but as yet there is limited experience at PNOC in the interpretation of the logging data.

1.2 Methods of interpretation

Well logging interpretation techniques for geothermal exploration is still in its infancy, especially for wells drilled in igneous and metamorphic formations.

The response of logging tools in fractured igneous rocks is not well known and the effect of thermal alteration has not been studied systematically so far.

Numerous interpretation methods are available from the petroleum industry, where well logging is a well defined discipline. However, many of these methods are not directly applicable to geothermal reservoirs, due to the difference in nature of these two kind of reservoirs.

Geophysical logs have been used systematically in geothermal investigations in Iceland during the last five years. There, it has been found that the geophysical logs are of great importance in mapping the lithological sections of geothermal reservoirs as well as in getting detailed information on temperature and pressure in the reservoirs (Stefansson and Steingrimsson, 1980). The work in Iceland has also included studies on the response of logging tools in igneous rocks (Czubek, 1981), intepretation methods of resistivity logs (Stefansson et al., 1982a) and gamma ray logs (Stefansson et al., 1982b). Applications of these interpretation methods are described by Jonsson and Stefansson (1982) and by Stefansson and Tulinius (1983). The interpretation methods used in this report relay on the works mentioned above.

2 GENERAL ASPECTS OF THE KRAFLA GEOTHERMAL SYSTEM

2.1 Geographical setting

The Krafla geothermal field is located within the northeast volcanic zone of Iceland and it is one of the high temperature fields in the neo-volcanic zones which traverse Iceland. The Krafla fissure swarm, which is presently active, extends from the Tjornes Fracture zone in the Axafjordur bay in the north and some 100 km to the south (Fig.2.1). It's width is approximately 5 km, but varies considerably along the swarm (Bjornsson et al., 1979). The swarm itself passes through the Krafla caldera, which was formed during the last interglacial period, but has since been filled to the rim with eruptive material. In post glacial time, it has been recorded that about 35 eruptions have taken place in this area or in Namafjall which is another high temperature area about 10 km south of Krafla.

The Krafla high-temperature geothermal field is situated within the Krafla caldera (10 x 8 km) which is elongated in the EW-NS direction. The geothermal field measures an area of about 7 km^2 according to the 10 ohm-m contour line defined by the resistivity measurements. However, the surface area covered by the thermal alteration and the geothermal activity is about 35 km^2 (Stefansson, 1981). The main surface activity is in the center of the caldera and in the southeastern part of the caldera where series of explosion craters have formed a gully called Hveragil (Fig.2.2). The drilling area in the Krafla geothermal field is situated east of the main fissure swarm intersecting the caldera.

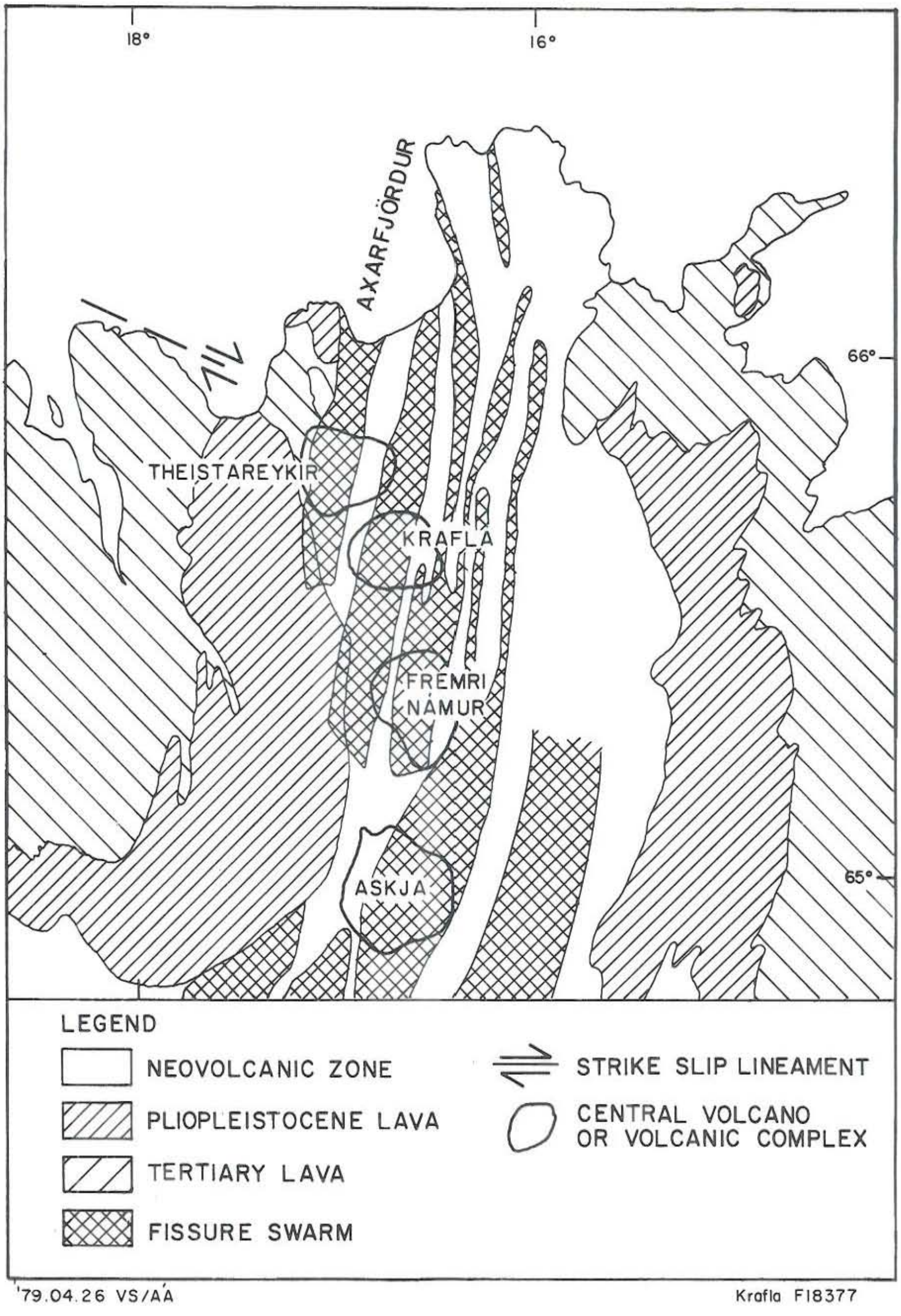

Fig. 2.1 The fissure swarms and central volcanoes within the northeast volcanic zone in Iceland. Mapped by K. Saemundsson.

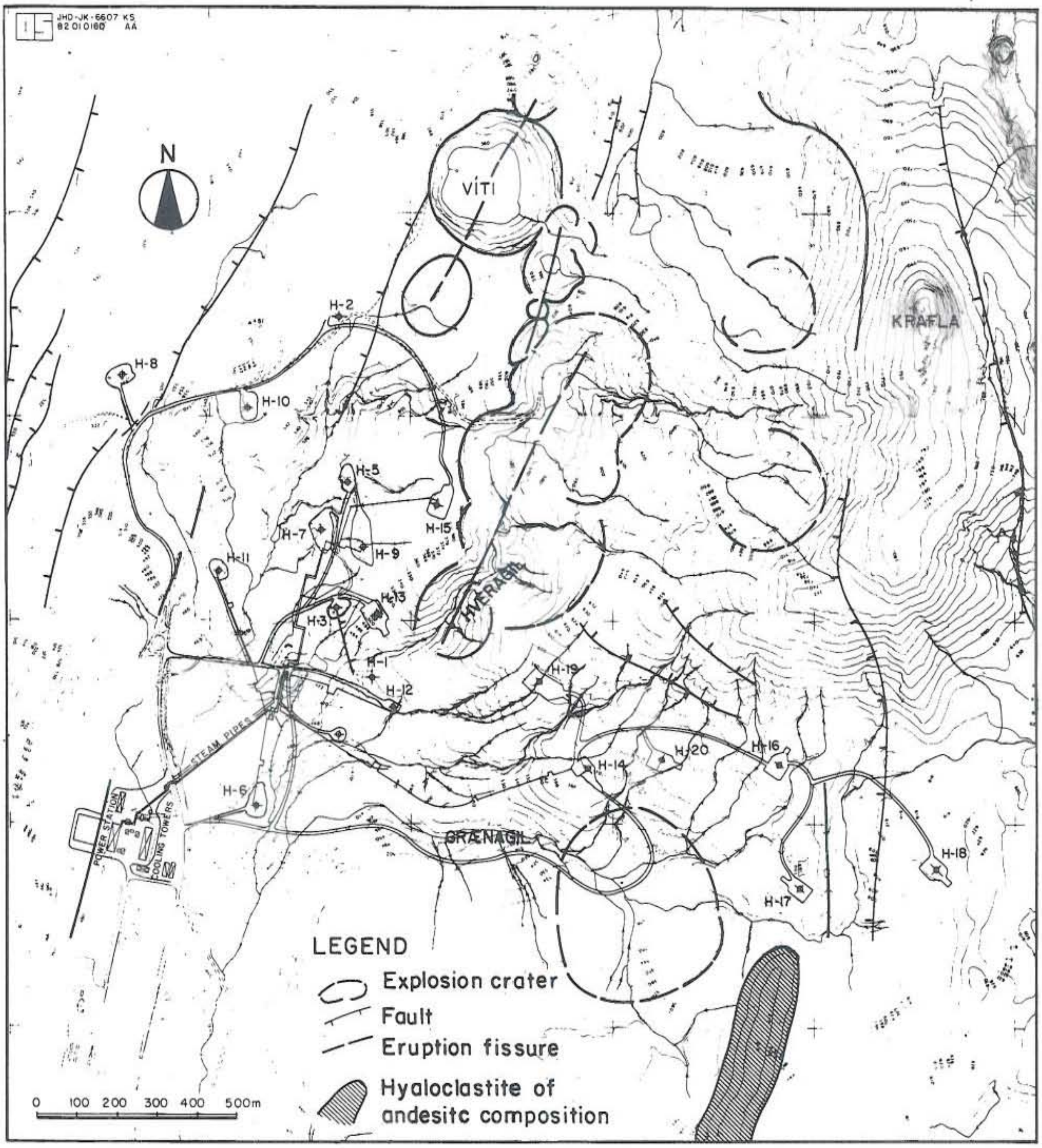

Fig. 2.2 Tectonic map of the Krafla area and the location of well sites and power plant. Mapped by K. Saemundsson.

2.2 Structure of the geothermal system

2.2.1 Geological structure

The rocks in the Krafla area have composition ranging from olivine tholeiite to rhyolite (Stefansson, 1981). Considerable basalt and granophyre intrusions have been encountered by drilling below the 1100m depth. As a result of the intensive study in Krafla, the rocks have been split into three main lithological units, the hyaloclastite, the lava, and the intrusive formations.

The hyaloclastite formation in the upper most 800-900m consists of primary and reworked products mainly from subglacial eruptions and is subdivided by a thick suite of subaerial lavas. Below this depth, alternating occurences of sub-aerial lava flows are dominant while hyaloclastites rarely exist. Sills are found to exist at about 1100-1300m while intrusive rocks have been found to be abundant below 1500-1600m.

The composition of the lavas and the hyaloclastites ranges from olivine tholeiite basalt to quartz normative tholeiite. The rocks in the hyaloclastite formation are recrystallized and the lavas are highly altered. Fig.2.3 shows a lithological cross section of the south eastern part of the Krafla geothermal field.

2.2.2 Geophysical structure

The surface investigations in the Krafla geothermal field were initiated in 1970. The investigations included geological mapping, geochemical analysis of natural springs and fumaroles, aeromagnetic survey, resistivity survey and seismic refraction measurements. The results of the resistivity survey at shallow depths (<800m) showed good correlation with the surface alterations. The aeromagnetic

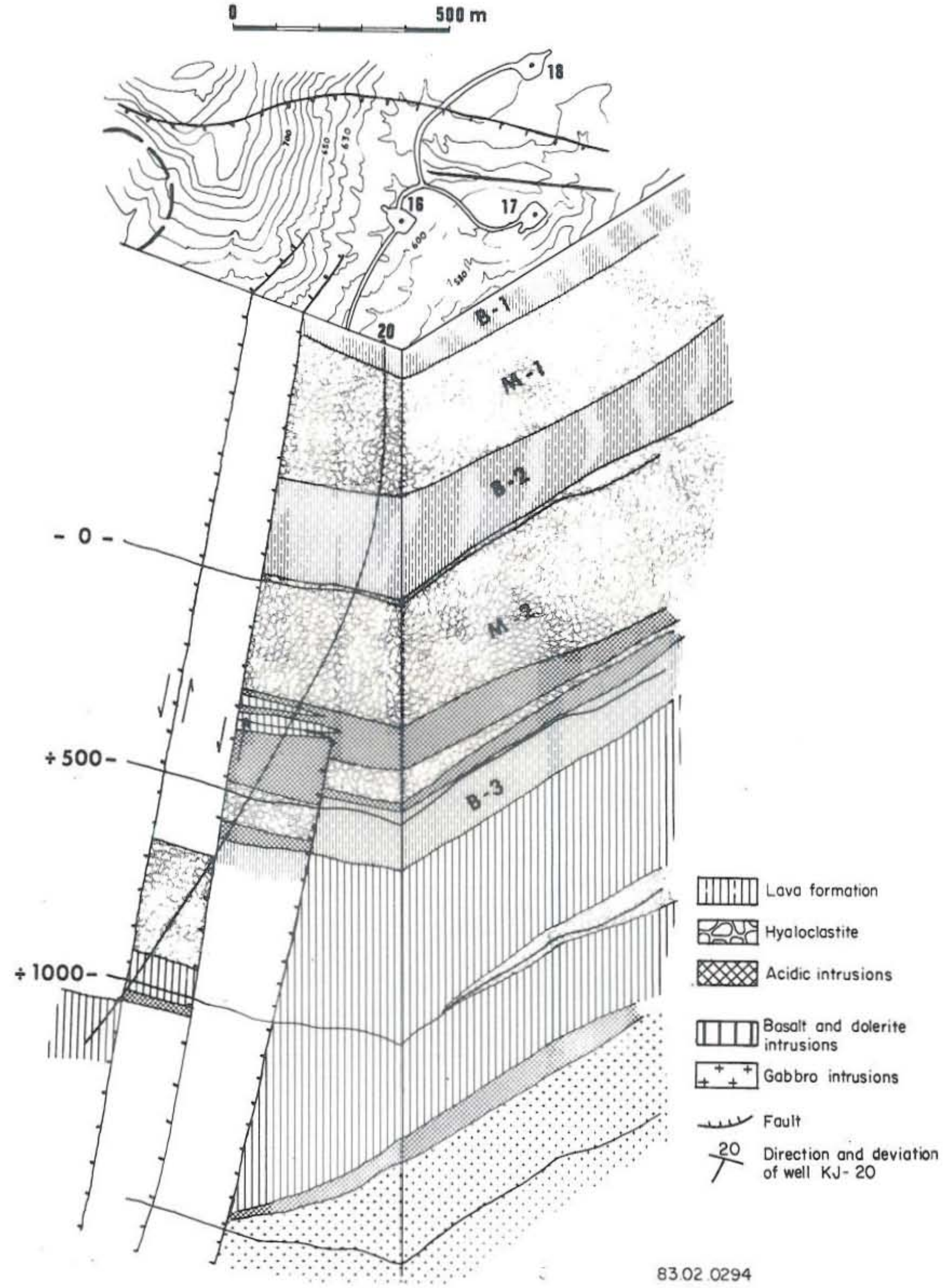

Fig. 2.3 Geological cross section northeast of the Krafla power plant. From Gudmundsson (1983).

survey showed a prominent magnetic low in the southern part of the caldera and the strongest magnetic anomally appears to be in the southern part of the geothermal field.

The drilling of exploratory wells in Krafla started in 1974. In one of these wells a temperature of 310°C was measured and it was assumed that the temperature in the system was close to the boiling point curve. However, it was not until 1977 that a model of the field was launched (Stefansson et al., 1977). It was proposed that two distinct zones exist in Krafla and that the lower zone (1100-1300m to at least 2200m) is the upflowing zone which feeds the upper zone (extending down to 1100m depth) near the Hveragil gully. The upper zone, which is water-dominated, has a mean temperature of 205°C, whereas the lower zone, which is a two-phase system, has temperatures ranging from 300°C to 350°C. Because of the relatively low temperature in the upper zone, production from this level was observed to cause precipitation of calcite in the wells. As a result of this, the production in Krafla has mostly been limited to the lower zone.

The rifting episode that started in the Krafla caldera in 1975 made some changes in the chemical characteristics of the fluid in the lower zone. In some areas of the field noticeable magmatic influence has been noted on the chemical composition of the fluid which caused serious deposition in some of the wells.

The mean permeability thickness of the upper zone has been calculated to be in the order of 10×10^{-12} m3 (Stefansson, 1981).

2.2.3 Geochemical features

The distribution of the H_2/H_2S ratio of gases in the discharges of the wells tapping the upper zone of the Krafla reservoir showed (Armannsson et al., 1978) that the fluid in the western part of the field is more degassed than the fluid in the area near Hveragil (Fig.2.2).

It has also been determined that calcite depositions are forming in some wells tapping the upper zone after considerable production time. This is mainly due to the low temperature in this zone.

For the lower zone of the Krafla geothermal reservoir, it has been determined that volcanic gasses (SO_2, H_2, CO_2) from the underlying magma body influence the geothermal fluid. The effect of SO_2 is such that it reduces to H_2S when the fluid flows through the formation and into the wells. Other gasses like CO_2, H_2, Hg,and Rn are observed also in some wells tapping the lower zone. In some cases, their concentrations influence the ph-value in the well (Armannsson et al., 1978).

2.3 Recent rifting episode

Prior to the present volcanic episode, there are historical records of one period of volcanic and tectonic activity within the Krafla fissure swarm, the Myvatn Fires of 1724 to 1729. A very small eruption in 1746 may be regarded as the last observed pulse in the Myvatn Fires episode (Bjornsson et al., 1979).

In early 1975 a rifting episode started to take place on the constructive plate boundary in northern Iceland after almost 100 years of tranquility. Some 3 meters of horizontal drift movement was observed in the Krafla caldera and the associated 80 km long fissure swarm. Since then the rifting occurs periodically in short active pulses at a few months intervals. These pulses have been found to be caused by the sudden east-west expansion of the fissure swarm and a contraction of zones outside the fissure swarm. Associated with these pulses are earthquake swarms and vertical ground movements of up to two meters and in some cases also volcanic eruptions and formation of new fumaroles. It has also been determined that after the initial subsidence in December 1975, periods of alternating subsidence and inflation followed and these have been observed to be taking place until the present time.

The inflation of the Krafla area between subsidence events is interpreted as being caused by inflow of magma from below into a magma chamber at shallow depth beneath the center of the caldera, and the subsidence is caused by the flow of magma out of the magma chamber (Bjornsson et al., 1979).

2.4 Previous Investigation

There have been numerous investigations conducted in the Krafla in the field of surface and sub surface geological, geochemical and geophysical investigations (Stefansson, 1981). A numerical simulation of the Krafla geothermal reservoir has also been carried out (Bodvarsson et al., 1983). The investigations have been the joint efforts of the National Energy Authority (NEA) and the State Electric Power Works of Iceland.

Among the geophysical investigations done in Krafla, geophysical well logging has made valuable contributions in understanding the characteristics of the field and in the drilling operations of the wells in Krafla since 1976 (Sarmiento, 1980; Stefansson et al ., 1982 a; Stefansson et al., 1982 b).

2.5 Facilities

To date, there have been drilled 23 wells in the Krafla geothermal field. Twelve of these wells (KJ 6,7,9, KJ 11-17, and KJ 19-20) are being connectedto the a 30 MW steam turbine. The location of the power plant and the wells is shown in Fig.2.2. As shown in Fig.2.2, well KJ-17 is about 620m southeast of KJ-14 and about 353m southwest of KJ-18.

Of the 23 wells, three are deviated or directional wells (KJ-13, 20 and 22). KJ-13 was deviated to the east of the field in an effort to intersect the Hveragil gully, and KJ-20 (situated between KJ-14 and KJ-16) was deviated towards the north. Of the three wells southwest of the power plant (KJ-21,22 and 23, not shown in the Fig.2.2), KJ-22 was deviated toward the west so as to intersect the north-south fissure swarm.

Most of these wells are drilled to about 2.0 km with the exception of KJ-1,2,5,8,9 and 21. The deviation of the wells has been proven to be successful in Krafla. In the case of KJ-13, its production was increased from about nil to about 6 MW, when the well was redrilled and deviated in the NE direction.

The decision to build a 2 x 30 MW power plant in Krafla was reached in 1975. By 1977, the power plant was already completed with one 30 MW turbine installed. And by Febuary 1978 it already started commercial operation. However, owing to some changes of the fluid characteristics in the lower zone, the power plant has been operational under partial load only. At the time of writing, the power plant is operating at 25 MW.

The future development strategy for Krafla geothermal field is to drill more holes in the southwestern part of the field where the fluid characteristics look favorable. When enough steam has been secured there, the second 30 MW turbine will be installed.

3 INSTRUMENTS AND DATA

The following discussion will deal with the two systems of data gathering and storing in logging presently employed by NEA. These were utilized in running the geophysical logs in KJ-17 in the Krafla geothermal field. Also included under this topic are the descriptions of the different tools used in logging KJ-17 as well as the presentation of the different data utilized in this report.

3.1 Data gathering and storing

Presently NEA is aquiring logging data by means of analog and digital recorders. The analog recorder is a built-in type of recorder attached to the panel box of the logging unit. The transmitted signal from the sonde is fed to this unit after it has gone through the necessary modules. The module itself is a processing unit where the processing of the signal is based on the calibration performed in the beginning of the logging operation. The analog recorder converts this signal on a paper strip which is driven synchronously by the logging cable. Figure 3.1. is a schematic diagram of a conventional analog logging system. In this system the line power module sends current to the probe. The signal from the sensor is converted to frequency and sent via the logging cable to the surface module which converts frequency to voltage. The converted signal is fed to the analog recorder. The final result of the log will be on the paper strip as measured values against depth. However, further processing of the data requires more time and effort. From the paper strip the data has to be digitized by using a digitizing equipment. Hence, there is the possibility that errors will be introduced. With the conventional rate meter used in the analog recording the record is continous, and the depth resolution depends on the scale used on the analog recorder.

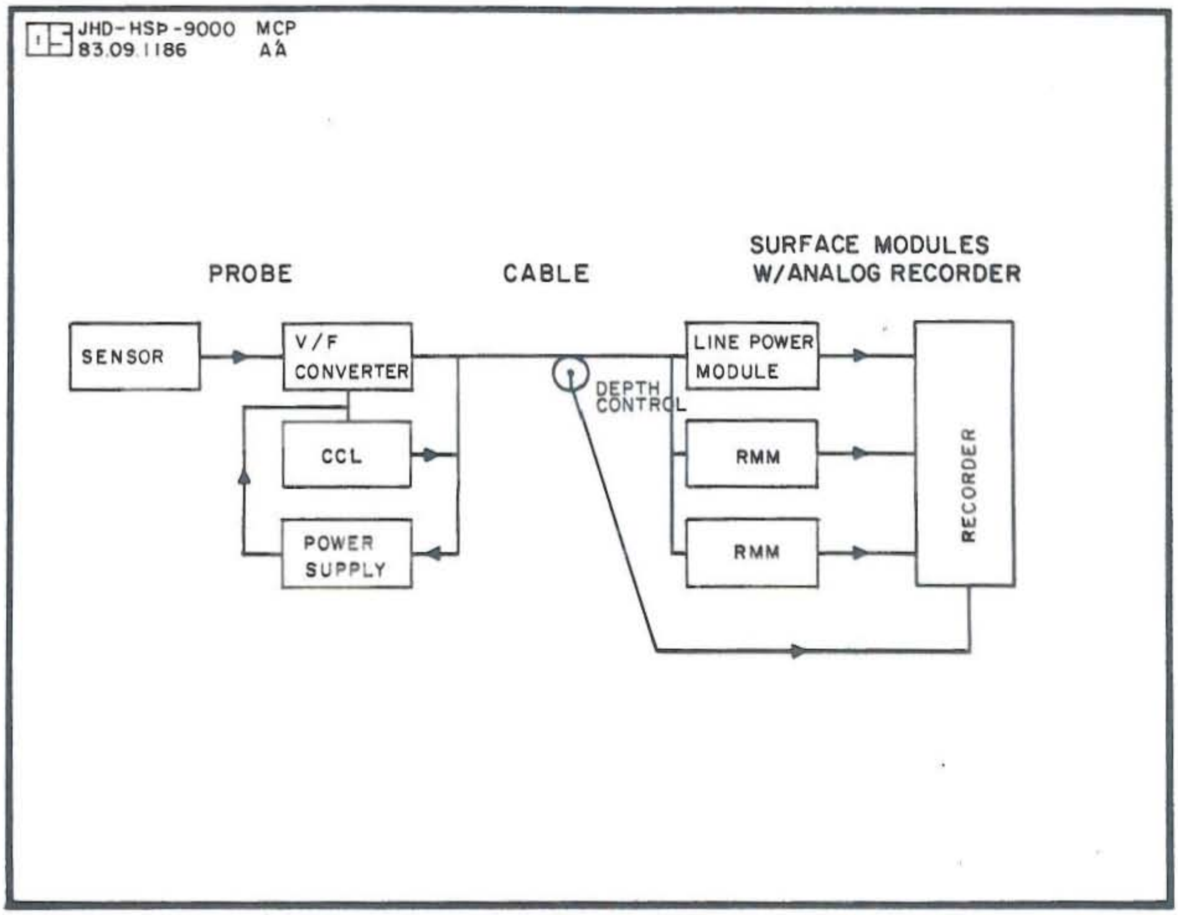

Fig. 3.1 Schematic diagram of a conventional analog logging system. From Halldorsson (1983).
RMM - rate meter module.
CCL - casing collar log.

To improve the situation, a digital recording system was introduced. A schematic diagram of the system is shown in Fig. 3.2. In this system various conditions are met such as:

a) Information concerning the log can be recorded on tape.

b) Calibrations can be received and recorded at any time during the log.

c) Flexibility on the selection of measurement intervals.

d) It can handle a maximum of four measured values from four different logs.

e) The resolution of the depth counter is 10 cm.

f) It has a sufficient recording rate for usual logging speed.

g) Both depth and data are visible on a display during the time of logging.

h) Final processing can be done on a computer (VAX/750 computer in the case of NEA).

Fig. 3.3 shows the flow diagram of how the raw data recorded on the tape is processed. From the tape (data is recorded in hexadecimal form), the data is read by a digital tape reader which is linked to a Cromenco computer. The computer transfers the data to a floppy disk. The reformatter programs are run in the same computer to convert the data to the floppy disk format suited for the VAX computer which has higher data storage capacity. The data now on the VAX floppy disk will be processed by the VAX computer and is calibrated with respect to the calibration coefficients recorded with the logs. The resulting

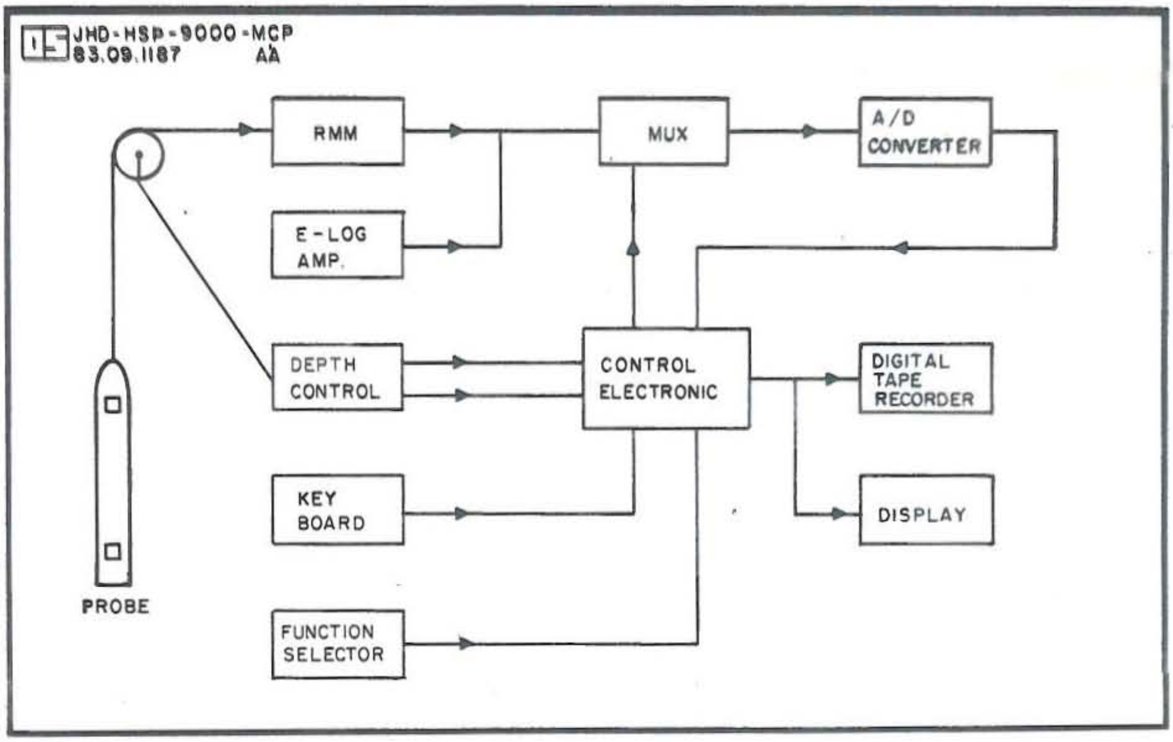

Fig. 3.2 Schematic diagram of the digital recording system of NEA using a digital tape recorder. From Halldorsson (1983). MUX - multiplexer; RMM - rate meter module; E-log = electrical log.

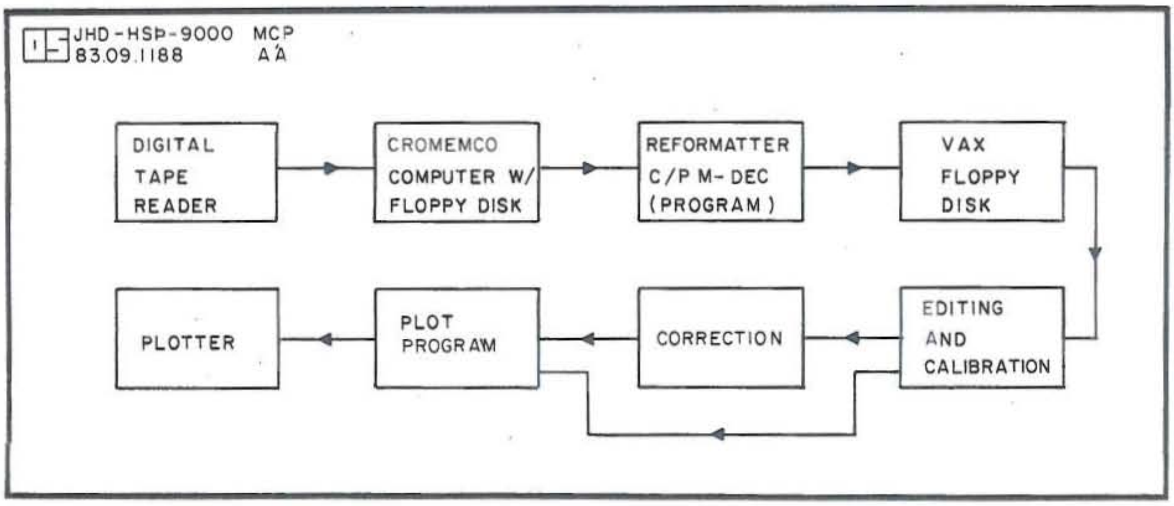

Fig. 3.3 Schematic diagram of the processing of data recorded on digital tape. From Halldorsson (1983).

data will then be in absolute values and is ready to be plotted. For more details on the logging data acquisition and storage systems one is referred to Maceda (1983).

3.2 Overview on tools and data

Pertinent information on the different tools used to gather the data in this report is presented in Table 3.1. Fig.3.4, 3.5 and 3.6 are illustrations of the different tools with the exception of 3.5 which is a newer version of the tool that was actually used. The sonic log tool will be presented separately in Chapter 6.

Table 3.2 summarizes the different types of data used in this report.

Table 3.1 Technical descriptions of the tools used in logging KJ-17

Type of tool	Outside Dia. (inch)	Length (inch)	Weight (lbs.)	Other descriptions
Caliper	1 1/4	75	18	3 Arm mechanical type (GOI)*
Gamma,CCL, Neutron	1 11/16	83 1/4	30	3 curie Am Be neutron source (GOI)*
Resistivity	2	79		64" normal and 16" normal (made by NEA)
Sonic	3 1/2	144	123	Single transmitter-single receiver with 3 ft. Transmitter-receiver spacing (GOI)*

* Gearhart Owen Industries, Inc.

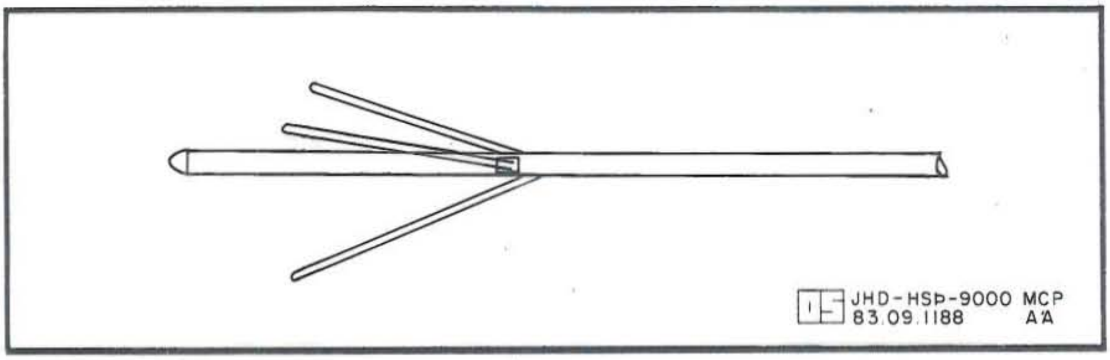

Fig. 3.4 Three-arm electro mechanical type caliper tool. From Gearhart Owen Industries, Inc. (1981).

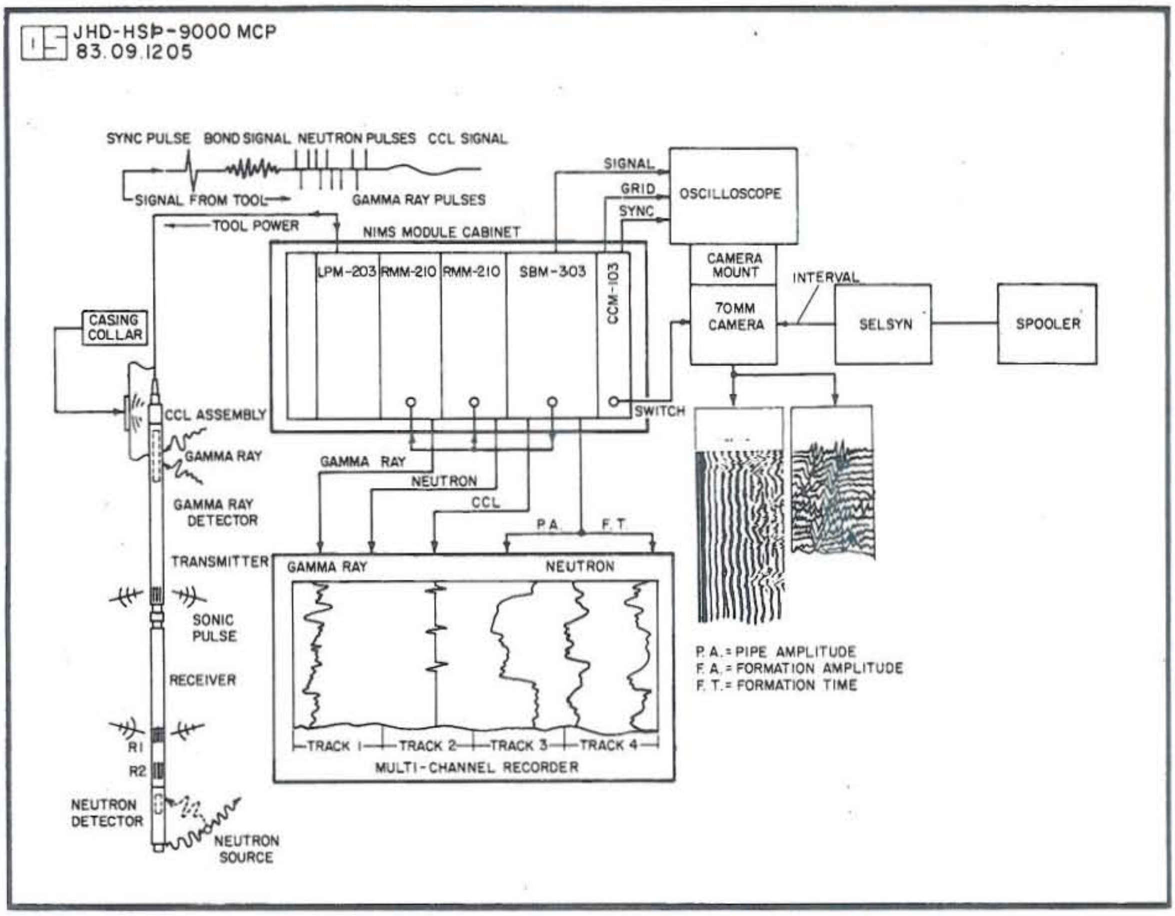

Fig. 3.5 CCL, Gamma ray, Sonic and Neutron combination tool. Also showing the analog and the VDL recording of the sonic log. From Gearhart Owen Industries, Inc. (1980).

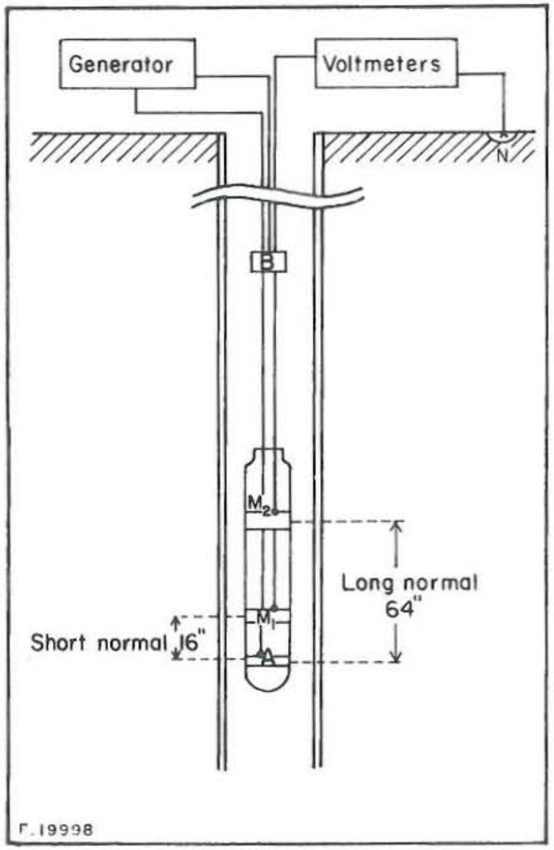

Fig. 3.6 Electrode arrangement of the 16" and 64" normal resistivity tool. (From Sarmiento, 1980).

Table 3.2 Summary of the different types of data used in this report with some pertinent information.

Type of log	Depth Interval (m)	Time constant (sec)	Logging speed (m/min)	Comments
Caliper	49.8-205.4	1	15	Analog
	200.4-688.4	1	15	Analog
	649.8-1726.8	1	15	Digital
Neutron-Neutron	17.9-206.5	5	9	Analog
	200.5-685.5	5	8	Analog
	680.7-1519.7	4	10	Digital
Natural gamma ray	678.8-1393.4	10	10	Analog
Resistivity 64" normal	695.5-1802.9	<1	35	Digital
Cement Bond (both pipe amplitude and VDL)	0-370	15		CBL after squeeze cementing at 453.1 - 454.2 m
	0-600	15		Calibration run
	0-640	15		CBL after initial cementing of 9 5/8" casing
	0-690	25		CBL after squeeze cementing at 453.1 - 454.2 and 207.9 - 209.0 m

4 CALIBRATION

4.1 Introduction

Geophysical well logs are generally continuous records of the various measurements plotted versus depth. For these measurements to have a meaning, they must be related to generally accepted standard units by a valid and specified system of comparison (Waller et al., 1975; Mills et al., 1977). Calibration data that is auxiliary to the log data will show the degree of log accuracy and indicate the reliability of the estimated subsurface geologic parameters, when the log data is reviewed with a knowledge of the calibration procedures (Schlumberger, 1974; Dresser Atlas, 1979; Welex, 1979; and Cochrane, 1966). The usual practice in geophysical logging is to calibrate tools before and after each run, because tool characteristics can drift with time.

Logging equipment can be calibrated by:

(a) Primary standards such as the API test pits situated at the University of Houston (Texas), the DOE Grand Junction Office test pits and the USGS Denver Federal Center test pits.

(b) Secondary standards. Those are private company owned test pits.

(c) Portable field calibration standards. These include devices that have been adapted or adjusted to primary or secondary standards and are carried in the logging truck.

(d) Laboratory analysis of core samples. These involve comparison of laboratory petrophysical measurements of core samples against log responses.

(e) Cross Plots. Involve log responses adjusted to local geological conditions encountered in a well.

4.2 The caliper log

The following discussion will deal with the calibration of a three-arm mechanical type caliper, similar to the tool used presently by National Energy Authority of Iceland. No effort will be made to discuss calibration of other mechanical type calipers and non-mechanical types such as the sonar calipers.

The caliper tool is sensitive to variations in hole size and is used to log wellbores. It is generally calibrated to read hole diameter in inches, millimeters or any appropriate units. For the case of NEA's three arm caliper, calibration is done using a calibrator supplied by the tool manufacturer. The calibrator is made from a rectangular aluminium plate with a hole on one edge (to allow the tool to be fitted to it) and from that hole succeeding smaller holes (to allow one arm to be inserted) are constructed every 2 inches on the 36 inches span (Fig. 4.1). Calibration is usually done in two ways, i.e (a) by flexing the arm through these different holes until the maximum of 36" span, and (b) the arm is made to collapse back to these holes. The recorded pen deflections (from the recorder unit in mm or cm) during the calibration is plotted against the different spans, in inches, that the tool was subjected to during the flexing and a relation is derived (usually the deflection versus arm span form a slope). The same thing is done to the deflections recorded when the arm was made to collapse. Usually, based on NEA's experience, these two calibrations give different readings. However, the difference between them is not large and a best representative slope can be drawn. This representative relation is used in determining hole size logs by the caliper.

4.3 The neutron-neutron log

This log is commonly referred to as a porosity log, as it is sensitive to the density of the hydrogen nucleus in the proximity of the tool. In all cases, neutron-neutron log readings are in counts per second (CPS). However, this unit of measurement is converted to API (American Petroleum Institute) neutron unit before it can be related to rock matrix porosity. 1000 API neutron units is defined as the response of the neutron tool in the 19% porosity Indiana limestone, which is inside the calibration pit situated at the University of Houston. Details of the calibrations pit is shown in Fig 4.2. However, it should be kept in mind that the above discussion on calibrating neutron-neutron logs involves the primary standards and is hard to accomplish, mainly because of the inconvenience in bringing the tool to and from the test pit every time a neutron-neutron log is done in a distant field. To remedy this situation, most logging trucks are equipped with portable field calibration standards. In the case of neutron-neutron log of NEA, a neutron calibrator supplied by the tool manufacturer is used for calibration (Fig. 4.3). When such a neutron calibration sleeve is positioned at given distance from the bottom end of the tool (distance A on the figure), the measured response in CPS is equivalent to 1000 API neutron units. Extra caution must be observed during calibration, namely, the tool should be at least four feet from the ground (in this way radiogenic elements present in the ground will not affect the reading) and people and objects must be at least ten feet from the tool.

4.4 The natural gamma ray log

The natural gamma ray log is used to measure the natural radioactivity of rocks, hence, in effect, it also determines the type of lithology, its position and thickness, along the borehole depth. This is possible as each rock type is characterized by its specific radioactivity. The widely used unit of measurement for the lithology gamma

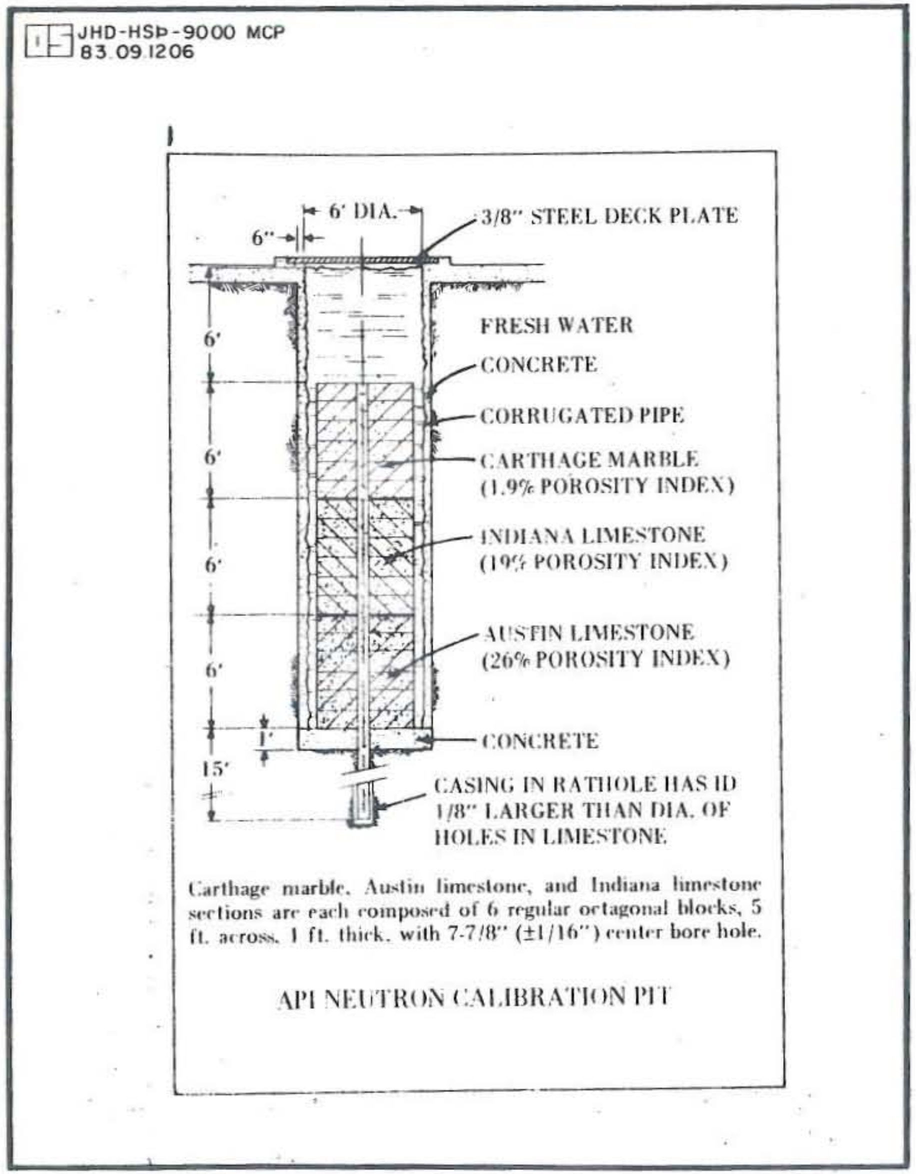

Fig. 4.2 API Neutron calibration pit.
From Dresser Atlas (1979).

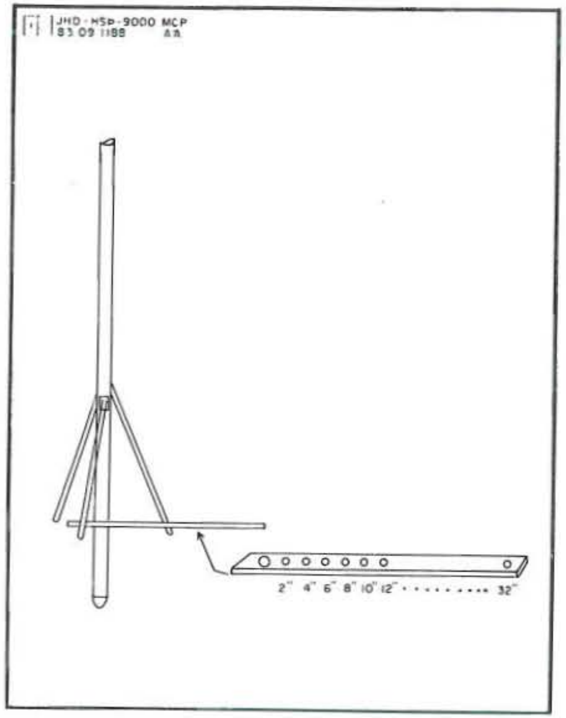

Fig. 4.1 Caliper tool calibrator.

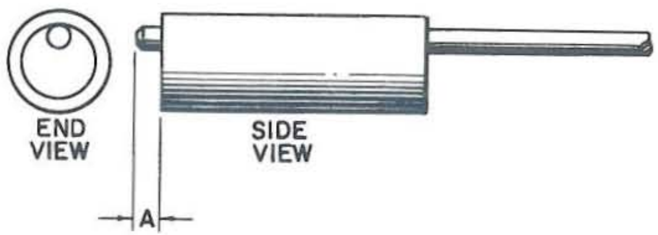

Fig. 4.3 Neutron log field calibrator. From
Gearhart Owen Industries, Inc. (1980).

ray log is the API gamma ray unit which is defined as the difference in the counting rate measured by a logging tool between the radioactive concrete and the low activity concrete in the test pit situated at the University of Houston. This difference is defined as 200 API gamma ray unit. The radioactive media in the calibration pit contains about 24 ppm Th, 12 ppm U and 4% K (U and Th being in radioactive equilibrium). The details of the test pit construction is shown in Fig.4.4. Like the neutron-neutron log, a calibrator is also being supplied by the tool manufacturer for gamma ray log calibrations (Fig. 4.5). The calibration procedure for this type of log involves background and calibrator in-place readings (Fig. 4.6). In proceeding the calibration, all radio-active sources must be in the shields and at least 50 ft away from the tool. The gamma calibrator must be at least 30 ft away when taking the background reading. The difference between the background and calibrator in-place readings is 120 API gamma ray units, for the calibrator used at NEA.

4.5 The resistivity log

Under this topic, the calibration of 16 inch short normal and 64 inch long normal resistivity device is discussed. As known in geophysical logging, the short normal and long normal involve the spacing of the two potential electrodes from the current electrode situated near the bottom end of the tool.

The resistivity log is performed to measure the electrical resistivity of a volume of earth by applying electrical current to this media. The calibration, therefore, can be done easily by subjecting the tool to a known current and resistors and measure the response of the two normal electrodes. In the case of NEA's resistivity tool, a calibration box is used to do this job. A schematic diagram of the resistors arrangement is shown in Fig. 4.7.

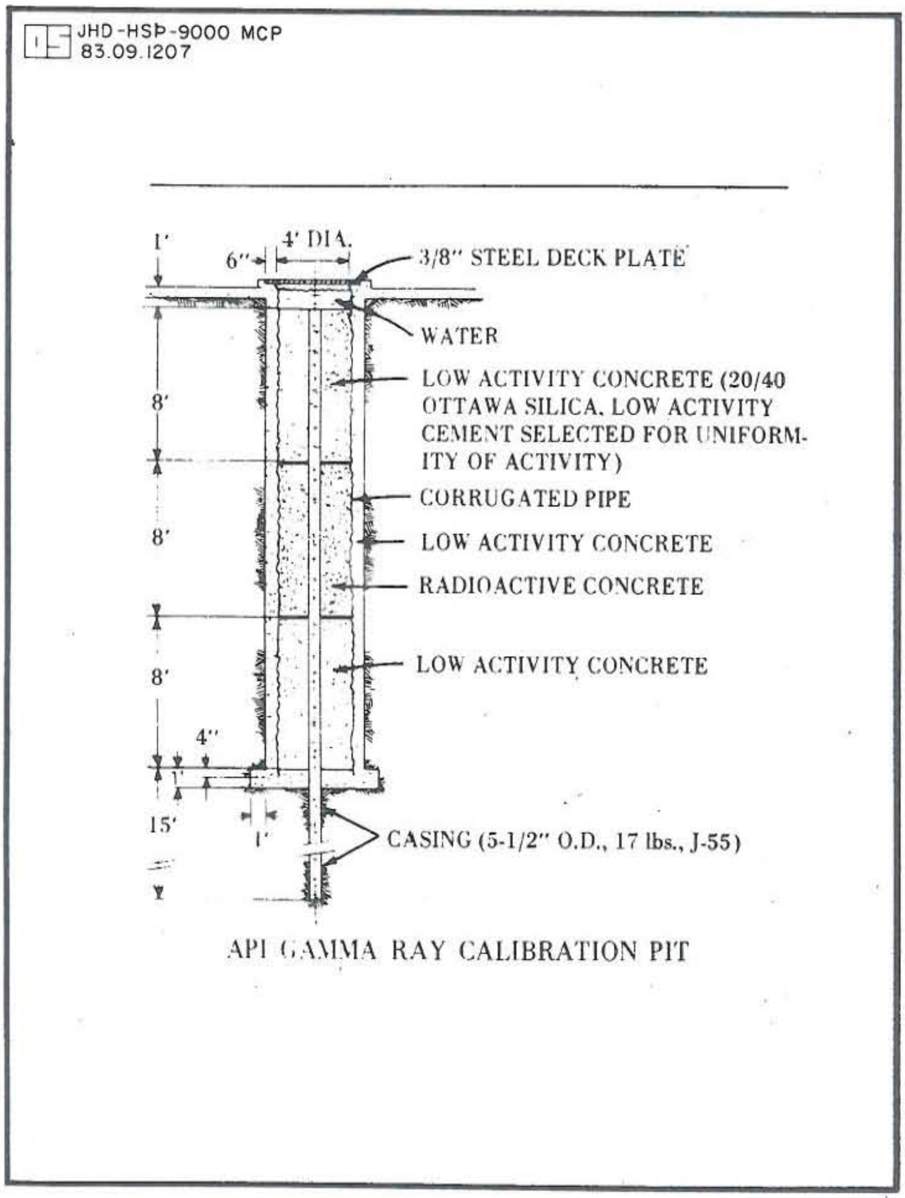

Fig. 4.4 API Natural gamma ray log calibration pit. From Dresser Atlas (1979).

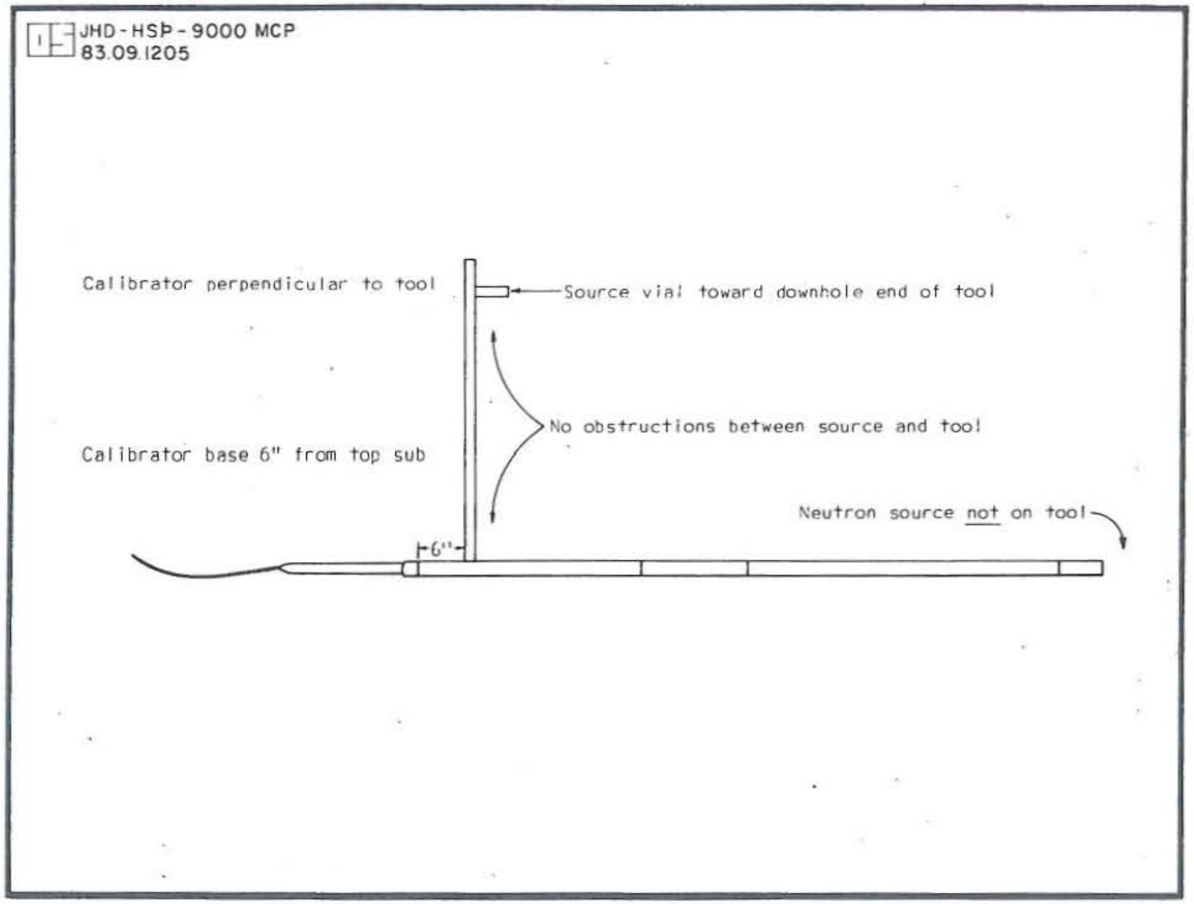

Fig. 4.5 Natural gamma ray log field calibrator.
From Gearhart Owen Industries, Inc. (1980).

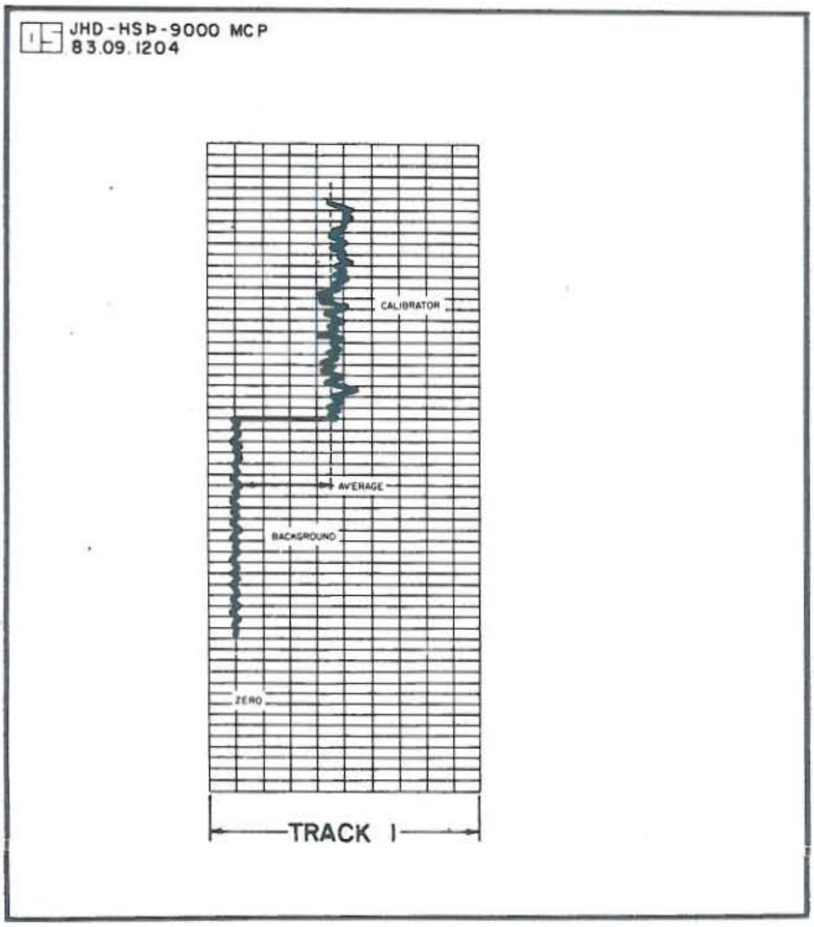

Fig. 4.6 Diagram of the background and calibrator in-place readings for the natural gamma ray log.

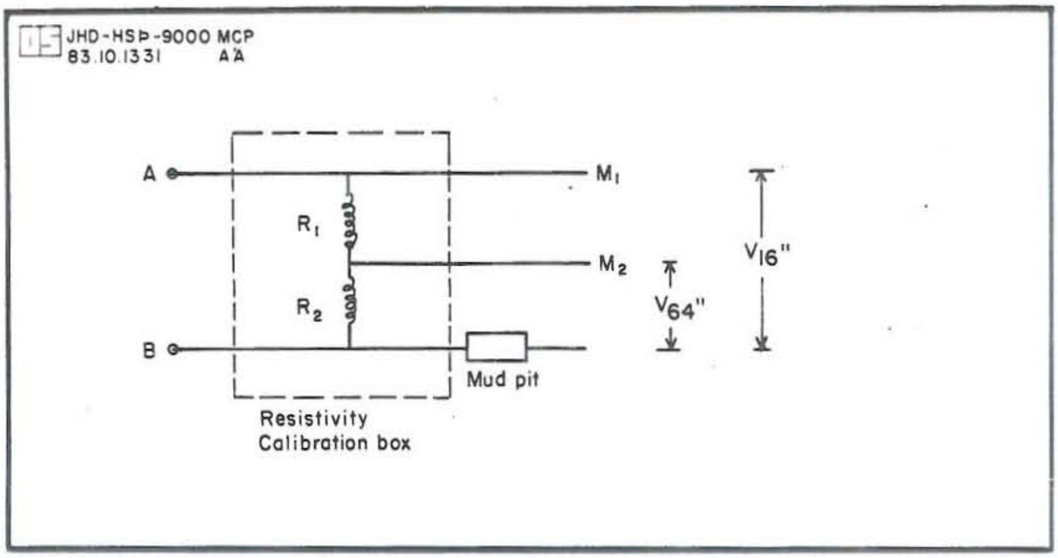

Fig. 4.7 Resistivity calibration box showing the resistors arrangement. Sketched by H. Halldorsson. M1 and M2 are the potential electrodes (16" and 64" normal). A and B are current electrodes.

5 WELL SIZE CORRECTIONS

5.1 Introduction

Most geophysical logs measured in wells are generally sensitive to well diameters to the extent that the realism of the interpreted log values depends much on how these values are being treated with respect to the different well bore diameters. Geophysical logs like the gamma-gamma and sonic logs (velocity logging) are heavily affected by well diameters. Other logs, like the neutron-neutron, resistivity 64" normal and the temperature logs are only moderately affected by the different well sizes. The purpose of this chapter is to discuss the corrections done to the various geophysical logs run in KJ-17 with respect to hole size variations. Also included in the dicussion is the correction done to the caliper log due to temperature effects.

5.2 The caliper log

In the case of the caliper log, a linear correction was applied to the recorded values. However, one should note that this correction was done not because of the well size variations, but because of temperature effects on the tool used.

5.3 The neutron-neutron log

The effect of the well size on the neutron-neutron log counting rate is such that the logarithm of the counting rate is a linear function of the well diameter. So that, if I_{nn} is the neutron intensity and D is the diameter of the well bore, I_{nn} is related to D by:

$$\log I_{nn} = a \times D + b$$

where:

a and b = particular constants for a given probe construction and are empirically determined.

Stefansson et al., (1982 b), from their numerous studies in the geophysical log responses to Icelandic basalts, determined the value of a (for the same tool used in KJ-17) to be:

$$a = -0.0015/mm$$

This value is also found to be in a good agreement with respect to the calibration curves published by Gearhart Owen Industries (GOI, 1976). For a particular well having a diameter Do, the neutron intensity is related by:

$$\log I_{nn} (Do) = a \times Do + b$$

Taking their ratio:

$$X = \frac{I_{nn} (Do)}{I_{nn}} = \frac{a \times Do + b}{a \times D + b}$$

$$X = 10^{a(Do-D)}$$

In this report, the neutron-neutron log response has been corrected to Do = 9" = 228.6mm. To demonstrate how corrected and uncorrected logs look the 1125-1225m portion of the neutron-neutron log run in KJ-17 was considered and is presented in Fig.5.1.

5.4 The natural gamma ray log

The recorded natural gamma ray intensity (I) is not equal to the true intensity (I_o) of the surrounding rocks due to the presence of drilling fluids (water or mud) which act as

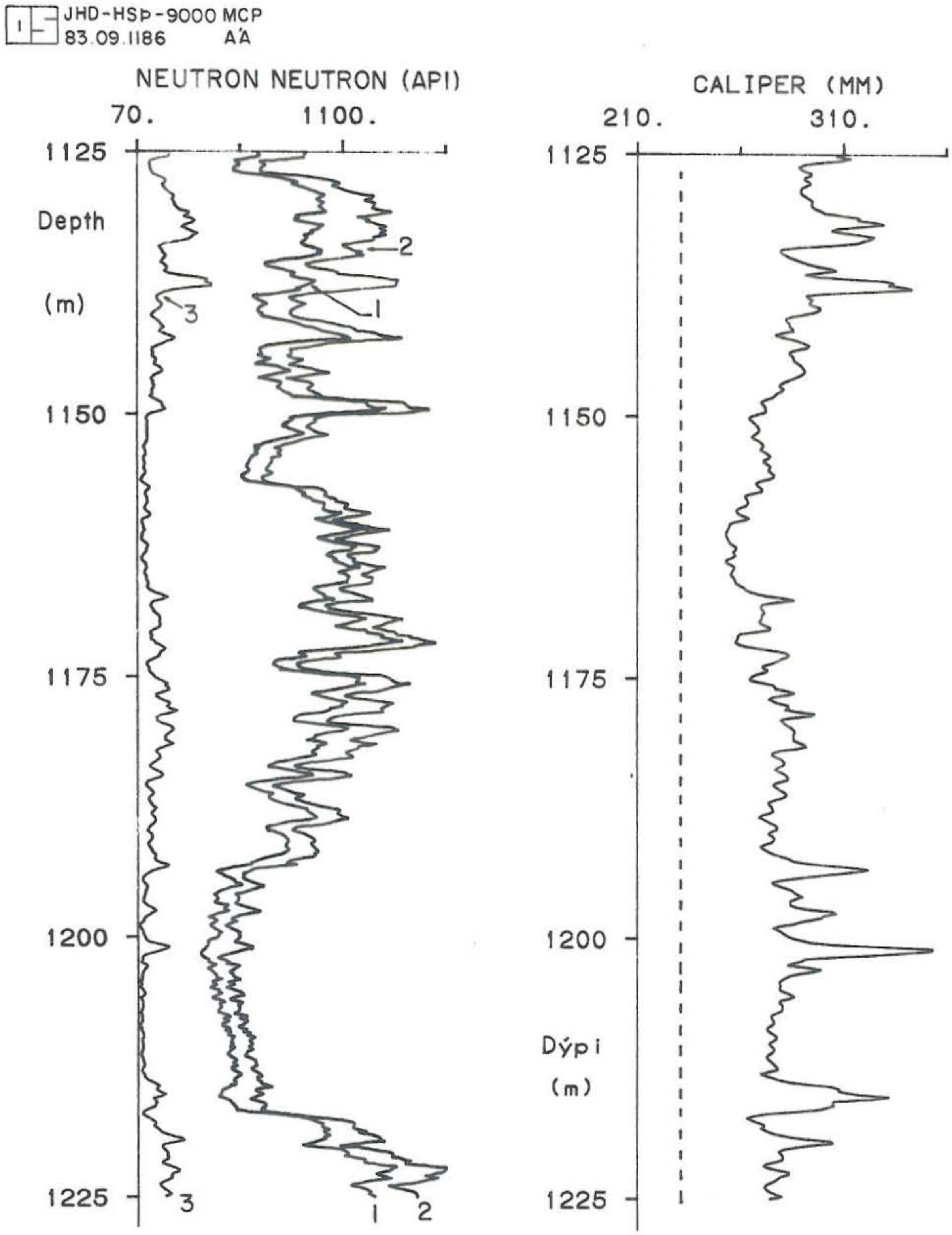

Fig. 5.1 Plotted uncorrected (1) and corrected (2) neutron log for the same depth interval. Magnitude of the correction calculated from the caliper log is also shown (3).

an extra absorbant to the surrounding natural radioactivity and also due to the wellbore and probe radii effects. Hence:

$$I_o = CF \times I$$

where: CF = correction factor

Czubek (1981) established the correction factor (CF) to be a function of the borehole radius (R), the radius of the probe (Rs), the density of the drilling fluid (ρ) and the effective mass absorption coefficient of the drilling fluid (μ_p). CF is calculated to be:

$$CF = \frac{1}{(1-Ap(\mu_p R))}$$

where $Ap(\mu_p R)$ = mass absorption function

Furthemore, Czubek (1981) established $Ap(\mu_p R)$ as a function of Rs/R. A curve for this relation is shown in Fig.5.2. In the case of KJ-17, Rs, μ_p and ρ are constants, and itwas assumed that $\mu_p = 0.03\rho$. Stefansson and Tulinius (1983) showed that with the above mentioned condition CF becomes a function of the well radius R alone. Hence:

$$CF = \frac{1}{1.192 - 0.3937\log R} + \frac{0.32}{R^2}$$

This relation was used in correcting the natural gamma ray log values of KJ-17. In this case the natural gamma ray log was corrected to 2R = 9" = 228.6 mm. To demonstrate this correction the 900-1000m portion of the natural gamma ray log of KJ-17 was considered and is presented in Fig.5.3.

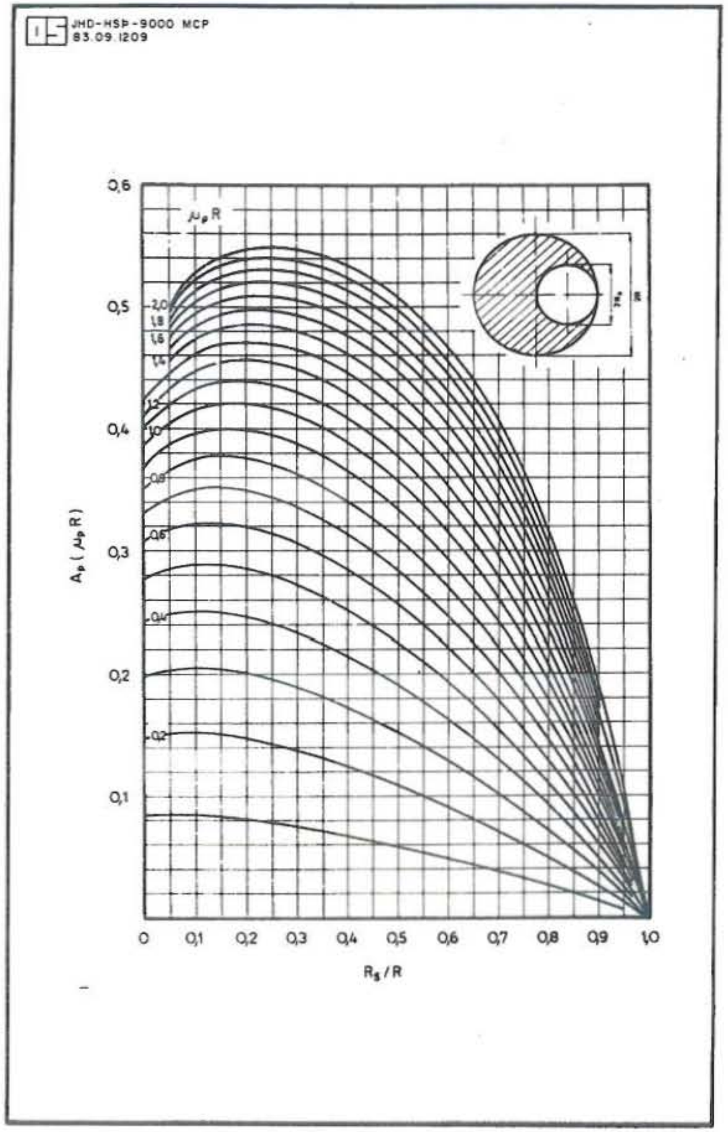

Fig. 5.2 Borehole absorption function used for well size correction of gamma ray log. From Czubek (1981). R = borehole radius; Rs = probe radius; $\mu_p = 0.3 \cdot \rho$; ρ = fluid density.

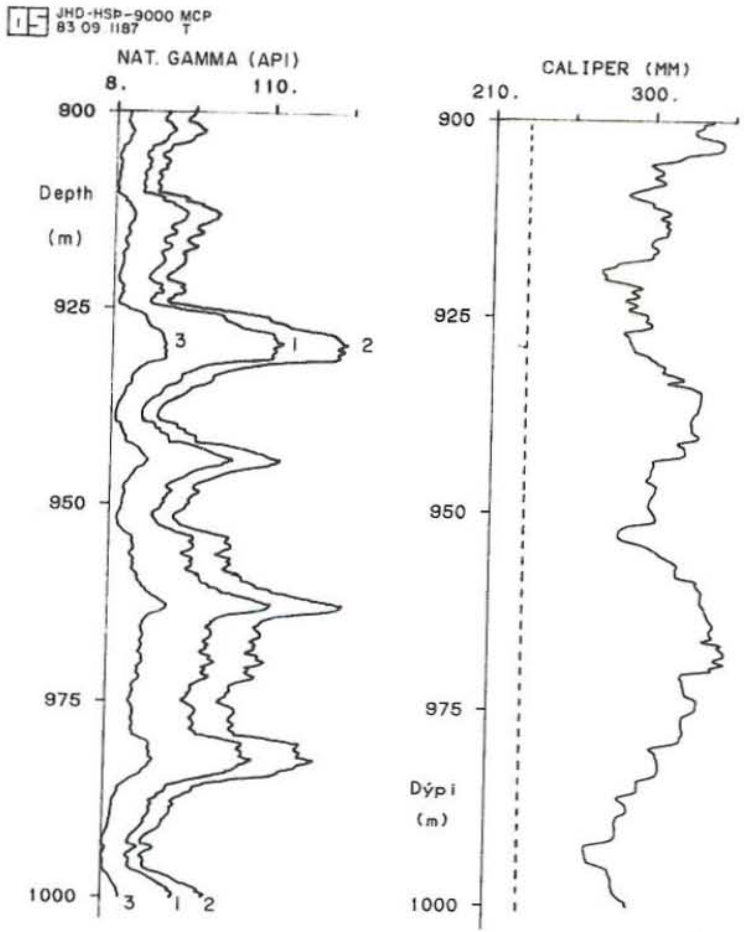

Fig. 5.3 Plotted uncorrected (1) and corrected (2) natural gamma log for the same interval. Magnitude of the correction calculated from the caliper log is also shown (3).

5.5 The resistivity 64" normal

The Gearhart Owen Industries, the manufacturer of the resistivity tool used in KJ-17, has published a correction curve for this type of tool against different borehole sizes (Fig.5.4). As can be seen in Fig.5.4, the effect of the KJ-17 well size on the resistivity response is very minimal considering that the observed Rf/Rw ratio was less than 500. No corrections were therefore made on the measured resistivity values of KJ-17.

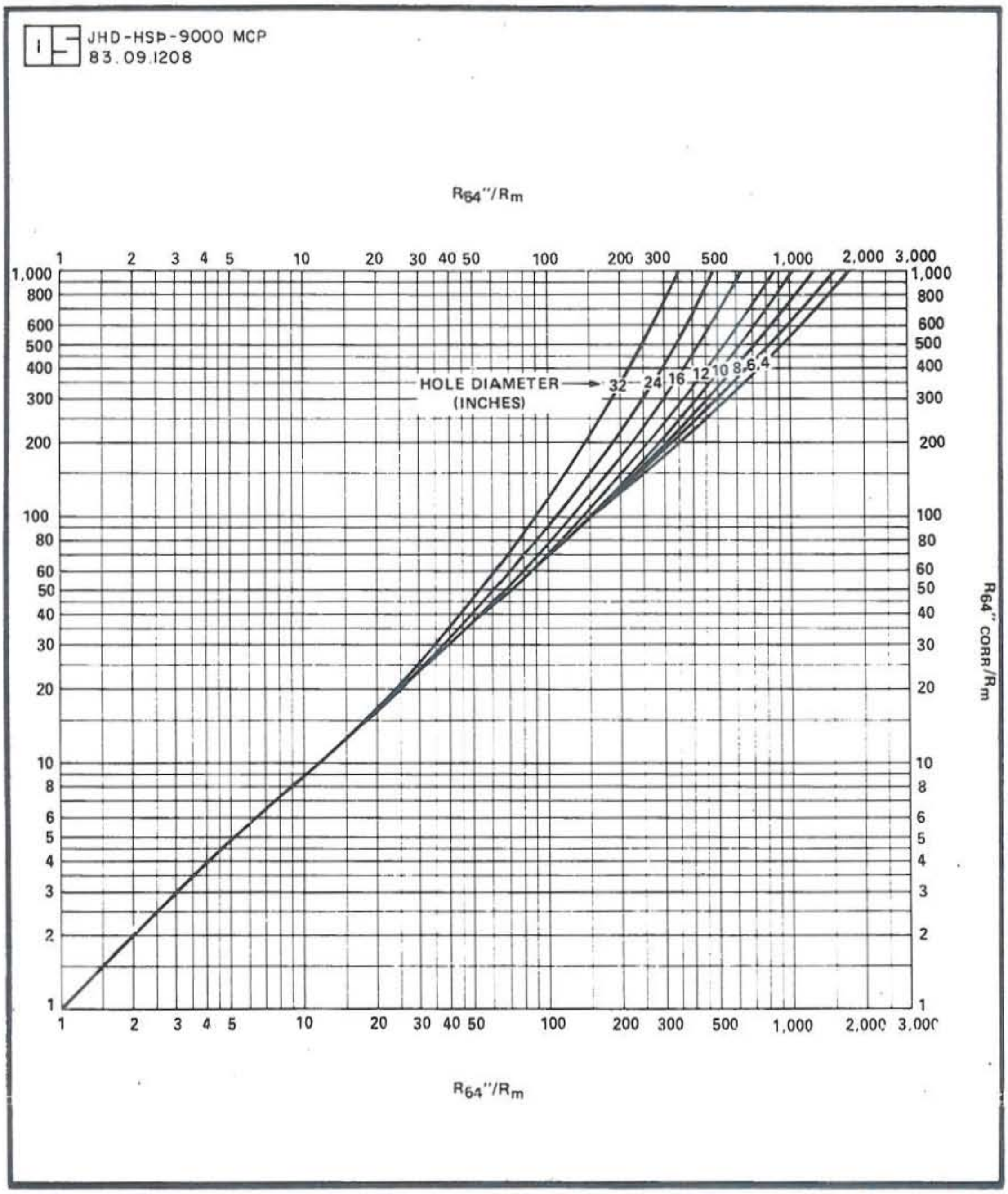

Fig. 5.4 Borehole correction for the 64" normal resistivity. From Gearhart Owen Industries, Inc. (1976).

6 ACOUSTIC CEMENT BOND LOG

6.1 Introduction

The success, safe operation and life span of a geothermal well depends on various important parameters. Two of these parameters are the casing and the cement conditions. Downhole conditions very often cause casing and cementing problems in geothermal wells. In some cases, the cement may be washed-out or dissolved by water in a crossflow or the cement may strike a permeable or lost circulation zone and may be displaced resulting in voids or water pockets in some sections of the casing. In the worst cases, the cement will not reach the surface. However, these conditions can be monitored and accurately determined during the cementing operations by means of an acoustic cement bond log (CBL) which is the most versatile and widely used tool in the field of cement inspection (Chang, 1981). When properly run and calibrated, an acoustic cement bond log can be used to determine the quality and extent of the physical bonding conditions between the casing and the surrounding cement sheath, and between the cement and the formation.

The acoustic CBL is an outgrowth of the acoustic velocity logging, and it has been used in field operations for more than twelve years (Chang, 1981). In acoustic velocity logging the time of arrival of an acoustic signal is measured. On the other hand, the acoustic CBL measures both the amplitude of acoustic signals propagated through the casing and the amplitude of later arrivals which are indicative of the bonding of the cement to the formation. This is possible as steel casing, cement, formation and water are media of different elastic properties. Hence they offer different pattern for the triggered acoustic wavefront. The acoustic velocity in a steel pipe is 17,544 ft/sec (or interval transit time of 57 microsecond/ft) while the velocities in the cement and in the formation are lower (Chang, 1981). Table 6.1 shows typical acoustic velocities and transit times. Normally, the acoustic cement bond log records the transit time, dt, the time required

Table 6.1 Typical acoustic velocities and transit times

Material	Velocity (ft/sec)	Normalized transit time (microsec/ft)
water*, drilling mud*	5,000	200
air	1,200	833
steel	17,000	58
cement	12,500	80
shale* (according to age)	7,000 - 11,000	91 - 143
sand, sandstone*, very porous limestone* (according to porosity)	10,000 - 15,000	67 - 100
hard formations* (low porosity limestone and dolorite)	17,000 - 22,000	45 - 58
volcanic rock	9,840 - 16,400	61 - 102

* Pressure and temperature dependent.

for the sound wave to travel a distance of 1 ft through the casing, cement and the formation. Transit time in microseconds per foot is related to the velocity, V, in feet per second by:

$$dt = 106/V \text{ (microsecond/ft)}$$

The unit of measurement in microsecond per foot is chosen so as to avoid small decimal fractions (Schlumberger, 1972).

6.2 Acoustic CBL tool

There are several types of acoustic CBL tools available commercially ranging from one transmitter - one receiver to two transmitter - two receiver types. The one transmitter - one receiver type comes also in different versions. Notably, the 3 1/2" O.D. sonde with 3 ft or 5 ft transmitter - receiver spacing (Fig.6.1), the 3 ft transmitter - receiver spacing, with a separate variable density log (VDL) receiver located 2 ft below from the first receiver, and the 3 1/4"O.D.sonicbond, gamma ray, neutron, CCL combination tool (Fig.3.5). The two transmitter - two receiver (borehole compensated tool as it is commonly known) offers more versatility. In contrast to the conventional acoustic CBL tool which is based on the absolute measurement of a peak amplitude (depending on transmitter-receiver spacing), the compensated tool is based on the measurement of the attenuation rate. This eliminates the attenuation effect experienced by the signal when travelling through the fluid when performing the ratio of amplitudes of the two receivers (Fig.6.2). The calibration problem in the two transmitter - two receiver tool is also eliminated as the attenuation measurement is independent of the absolute value of the signal (Gollwitzer and Masson, 1982). In most cases the two transmitter - two receiver tool has transmitter-receiver separations of 2.4 and 3.4 ft.

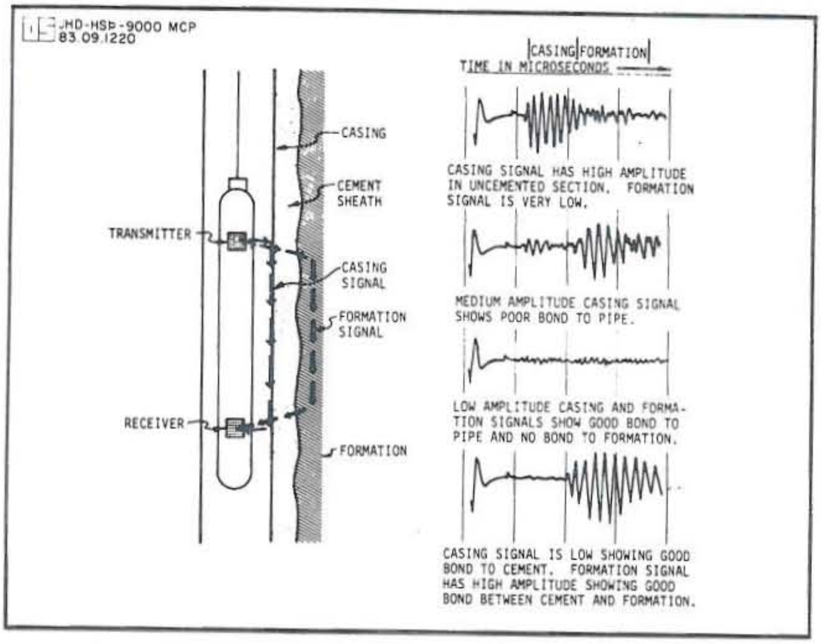

Fig. 6.1 Conventional single transmitter-single reciever CBL tool. From Chang (1981).

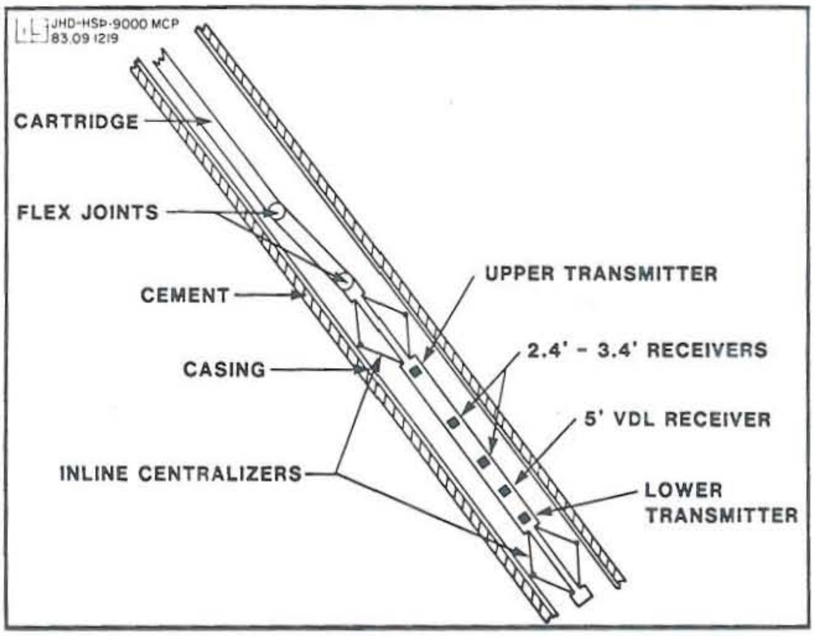

Fig. 6.2 Two transmitter-two reciever CBL tool with Separate VDL reciever. From Gollwitzer et al. (1982).

The NEA tool is of one transmitter - one receiver type obtained from Gerhart Owen Industries (3 1/2" O.D. 3 ft. transmitter - receiver spacing). It uses a single conductor cable, as most conventional tools do. The surface electronic panels include a variable intensity log.

6.3 Principles of operation

A fairly typical sonic receiver response to an acoustic wave transmitted through a compacted formation is illustratedin Fig. 6.3. The time at which the acoustic wave was initiated at the transmitter is also shown in the figure (To). The first arrival at the receiver is the compressional wave. This is followed by the Rayleigh wave (Rayleigh waves have essentially the same velocities as shear waves, but are usually dominant) wave which travels at slower rate. Arriving at much later time are the slower mud waves from the mud column and from the outside walls of the sonde itself.

The cement bond logging equipment measures the amplitude of pulsed sound energy after it has travelled through the casing between a transmitter - receiver system of the logging sonde. Fig.6.1 shows the cement bond sonde and the related signal paths. In a condition where there is no cement present between the casing and the formation, there is little acoustic energy transmitted beyond the casing wall,hence, the signal intensity seen by the receiver is high. When the casing is properly bonded with cement, the amplitude of the signal transmitted along the casing will be drastically reduced. If the cement bondings to both pipe and formation are good, the casing and its surrouding cement become relatively transparent to acoustic signals (Chang, 1981). On the other hand, if an annulus exists between the casing, the cement and the formation, little formation signal will be observed. The reason behind this (Chang, 1981) is that the low transmission coefficient across either of these boundaries will develop due to large acoustic impedance mismatch (e.g. air to steel and air to formation are examples of boudaries exhibiting large impedance mismatches). The amplitudes and arrival times of the pulsed sound energy can therefore be used to diagnose the degree of cement bonding. Laboratory results have supported the relationship between the strength of the pulsed sound energy signal and the degree of cement bonding (Grosmangin et al., 1961). Aside from the amplitude and arrival times (measured eletronically), the variable intensity log measurements or the variable density log (VDL) are also in most cases used during the acoustic CBL log. The VIL or VDL is a continous display of the acoustic signal in the form of a variation of light intensity on an oscilloscope. The simultaneous recording of the VDL (in the form of a film strip) and the first arrival amplitude (in the usefulness of acoustic information for the analysis of cement bonding. Fig. 6.4, shows the displays of the amplitude and the variable density log.

The fundamental scheme of a transmitter in a commercial acoustic CBL tool is shown schematically in Fig. 6.5. Capacitor, C1, in the circuit supplies energy through the SCR (semi conductor controlled rectifier) to the acoustic transmitter. After the SCR is fired, L1 boots the input voltage to a much higher value across C1, thus recharging it. On the other hand, L2 and C2 prevent the ripples from feeding back to the input. To provide a reference to the received signal, the capacitor C4 provides a high frequency path back to the input line for the detection of the pulse produced when the SCR conducts. R1, R2 and C5 limit the imposed voltage on the uninjunction transistor which will not be triggered until such a time that the capacitor C3 is sufficiently charged. Thus, the R3 and C3 time constants will determine the firing frequency of the SCR. The boosting of the amplitude of the trigger pulse to the SCR is done by a transformer T. In some tools, bipolar transistors are being used to generate the trigger signal. The received signal from the casing, cement and formation are sent to the surface through the receiver. The signals are processed in the surface modules which contain timing control and computation circuits. The signal is fead to the

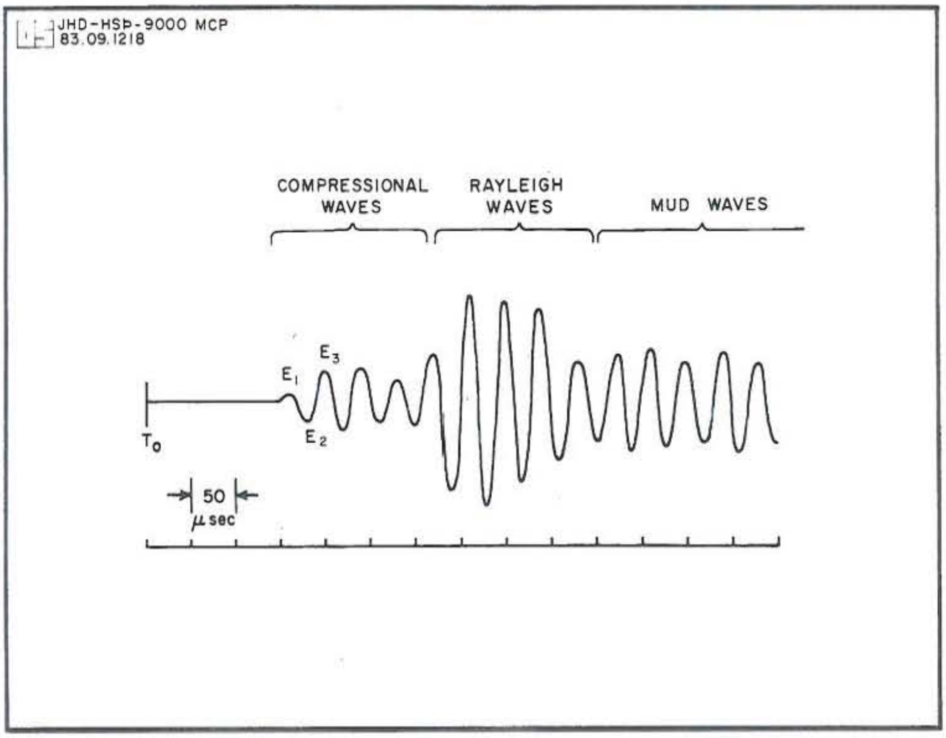

Fig. 6.3 Schematic figure of an acoustic wave in a compacted formation.

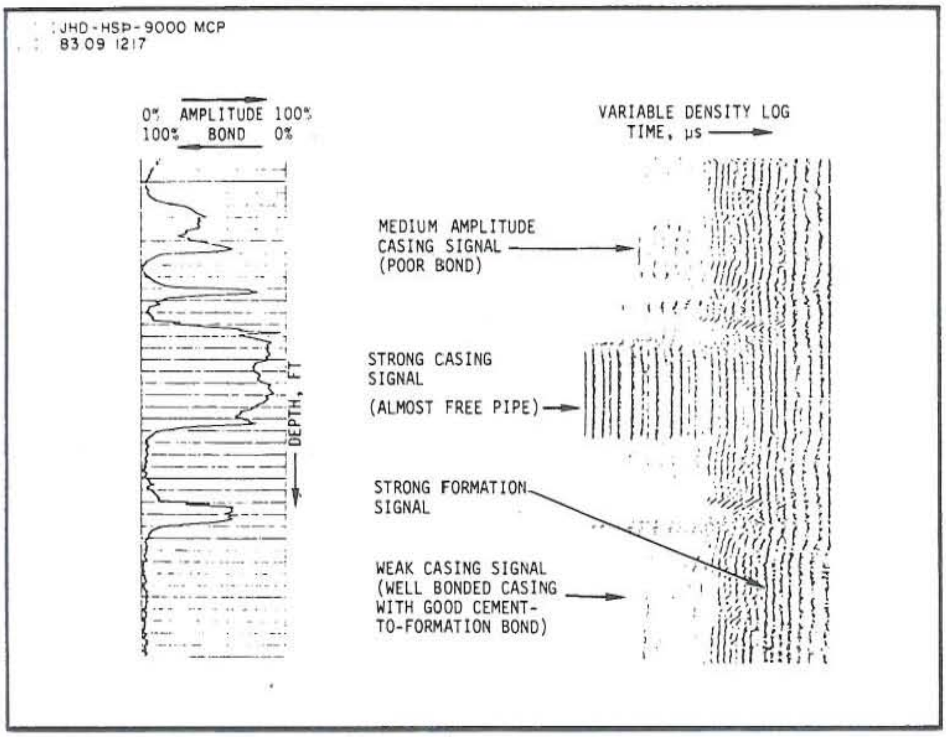

Fig. 6.4 Amplitude and variable density log displays for steel casing and surrounding formation. From Chang (1981).

amplitude measuring circuits which compute the CBL amplitude (Fig. 3.5). In a VDL incorporated acoustic CBL, part of the received signal goes to a cathode ray tube unit (commonly called oscilloscope), which is mounted on a optical recorder in the truck. In this unit, a reference pulse generated at the instant the transmitter is energized triggers the horizontal sweep which moves the electrone beam across the face of the cathode - ray display tube (Brown et al., 1970). In the same unit, the signal is fead to the light intensity circuit resulting in variations in brightness of the sweeping beam as a function of the signal amplitude (Z-modulation). Hence, generally speaking, what is appearing on the face of the tube is an intensity -modulated display, which in turn is used as the light source for the VDL optical record. The light source is then projected into the optical truck recorder through a system of mirrors and lenses (Fig. 6.6) and recorded on the logging film. One advantage of the VDL recording is that VDL scope face can be viewed during the logging operation without the film getting exposed. An acoustic CBL incorporated with VDL measurements, offers more information on the cement quality than instrument without VDL. Asidefrom measuring the first arrival both quantitatively (in analog strip) and qualitatively (from the film strip), it also records the relative amplitude of subsequent arrivals including formation compressional and Rayleigh wave arrivals, mud-wave arrivals, etc. (in the film strip) and the travel time of the first and subsequent arrivals (in the film strip). Typically the logging speed of the cement bond log is about 20 m/min.

6.4 Calibration

The amplitude of the acoustic signal in a free pipe casing is normally used as a reference for evaluating other signals in order to determine the percentage of bonding. Hence, it is necessary to run an acoustic CBL after setting the casing and before the actual cementing operation. The first step in calibrating the tool is to choose the right

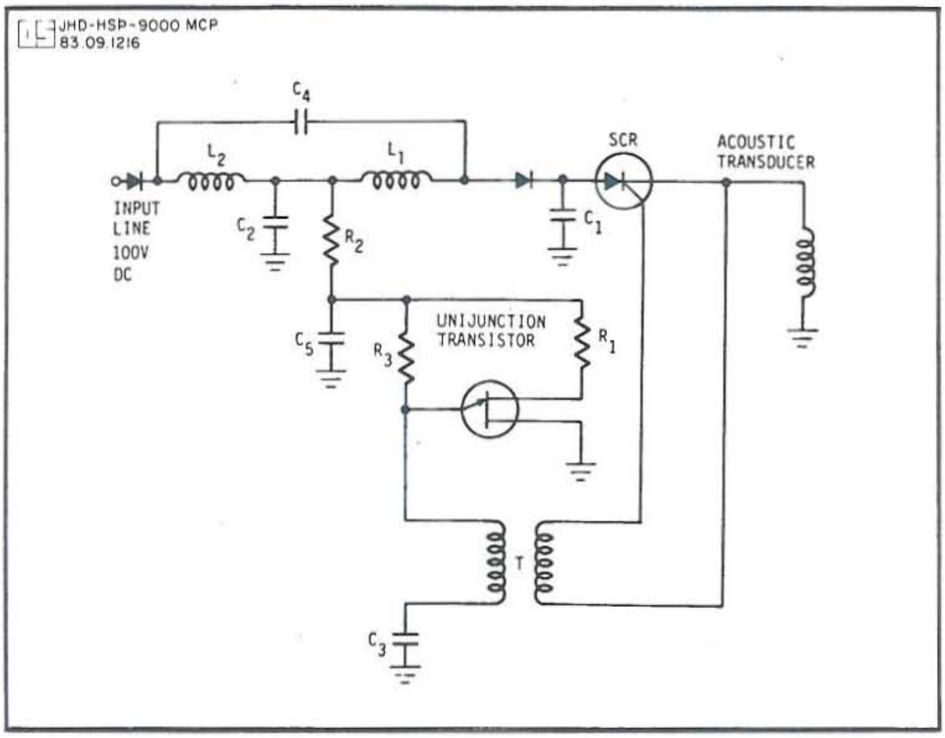

Fig. 6.5 Schematic figure of transmitter in a CBL tool.
From Chang (1981).

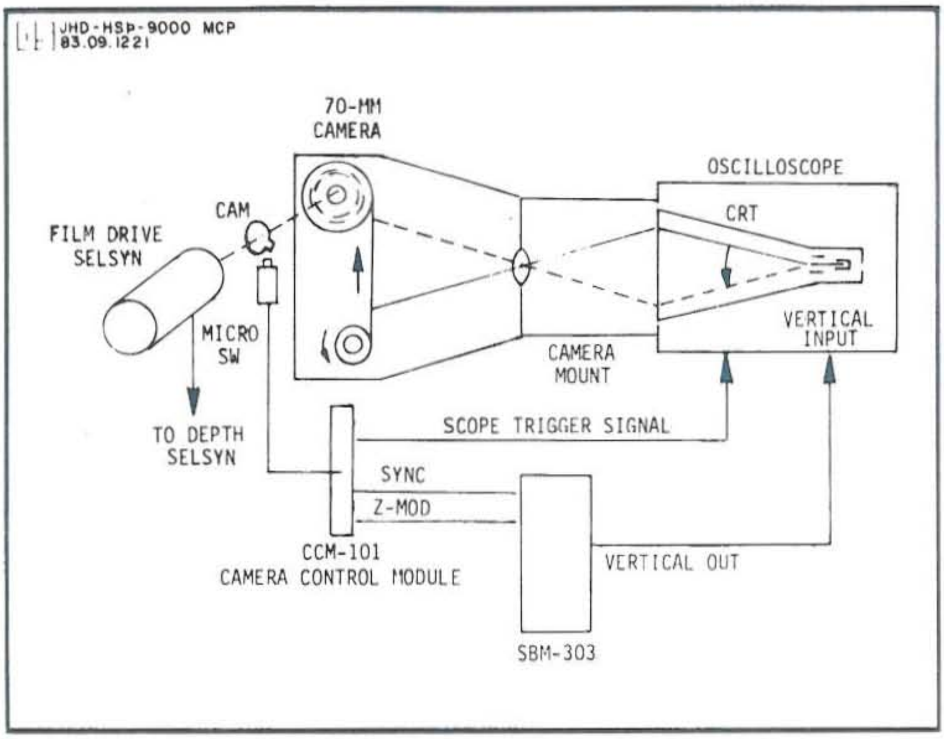

Fig. 6.6 Conventional CBL optical/photographic recording unit.
From Gearhart Owen Industries, Inc. (1980).

electronic gadgets or panel (e.g. sonic bond module, oscilloscope, recorder, line power module, line termination module, etc.) and connect the properly centralized tool to the line. The tool must be lowered to the casing and must be positioned below the water level and between the casing collars. To proceed in amplitude calibration, the vertical sensitivity of the oscilloscope should be adjusted to the desired voltage and set so that it shows only the gated interval. In contrast to the complete oscilloscope signal pattern, the gated interval will only show the first positive return (Fig.6.7) which represents the free pipe amplitude. Adjustment should be done next (probably the delay control) so that the gate will completely superimpose the entire length of the first positive return wave. In this way the area which corresponds to the amplitude of the return wave will be integrated and made as reference amplitude. The amplitude pen and the analog recorder will then measure the corresponding deflection which in this case is the 100% relative amplitude signal. Positioning the pen to the left side of the track will indicate the 0% relative amplitude signal (Fig.6.8). The oscilloscope settings for the intensity spectrum can be made possible by showing the complete wave train form and by controlling the time base panel.

6.5 Cementing and perforation operations in well KJ-17

TheKJ-17 drilling and casing program is shown in Fig. 6.9. From the beginning, it has been the practice in the Krafla geothermal field to run temperature surveys after completing the hole and right before setting the casing, and an acoustic CBL after setting the casing and right before cementing. The reason for running temperature surveys is to determine whether further cooling is still needed before setting the casings as abrupt recovery of temperatures may pose hazardous blow-out in the well. During the temperature run, the well is usually pumped with water at a minimum of 6 l/s. On the other hand, the acoustic CBL on the free casing serves as a calibration run

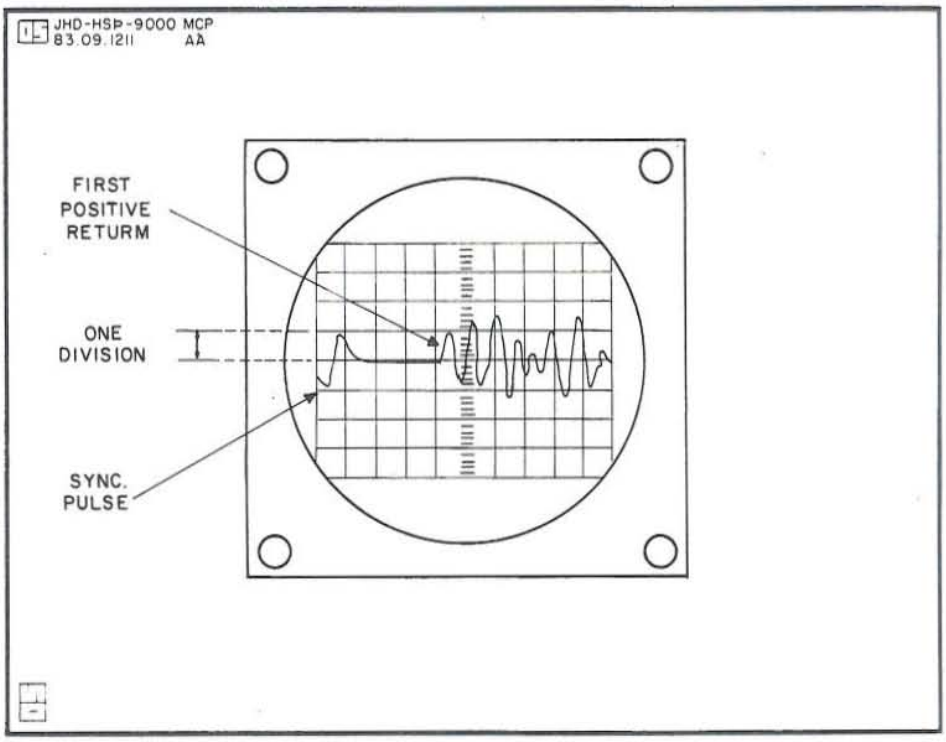

Fig. 6.7 Diagram of gated first positive return wave.

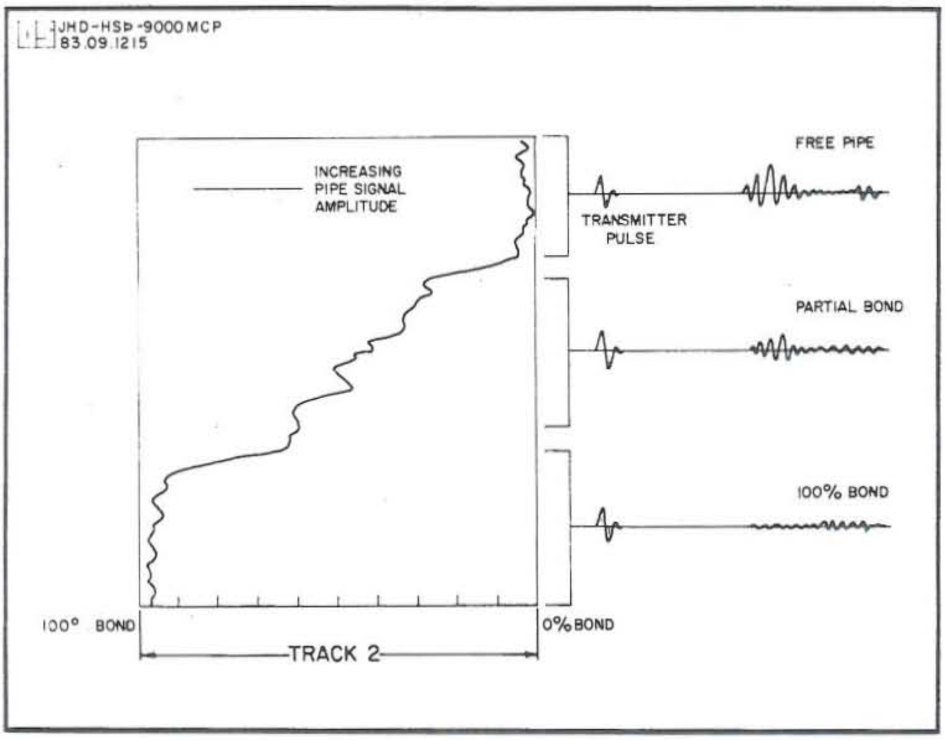

Fig. 6.8 Example of pipe amplitude and VDL signals recording.

to be used for comparison with further CBLs that may be made after the cementing of the casing in order to determine the top of cement level. The calibration run will also serve as a reference when the casing to cement and cement to formation bondings are evaluated.

On 11 July 1981, an acoustic CBL on the free 9 5/8" casing was run down to 600m (9 5/8" casing shoe is at 692m) in well KJ-17. This decision proved to be a vital one as during the cementing of the 9 5/8" casing the cement did not reach the surface (cementing was done by the inner string method). It is most likely that a considerable volume of cement was lost in the interval 600 - 692m where earlier a drilling circulation loss of about 4.5 l/s was recorded (this figure later increased to 8.5 l/s when this zone was cleaned). Temperature surveys conducted before setting the casing also indicated a likely loss zone at the bottom. At around 19:10h on the following day, an acoustic CBL (10m - 613m) was run to determine the top of the cement. As gathered from the amplitude curve and from the variable density log (Fig.6.10), the top of the cement was at about 442 - 451m. The casing perforation was then initiated in the interval 453.1 - 454.2m using a formed wire perforating gun. Cement was then subsequently squeezed through the perforated holes in the 9 5/8 inch casing. However, this operation proved to be unsuccessful as no return of cement was observed at the surface. A check acoustic CBL was run on the 13 July after considerable cement curing time. The CBL pointed out that the top of the cement was at about 209m (Fig.6.11). A second casing perforation was done in the interval 207.9 -209.0m. This time the cementing of the 9 5/8 inch casing proved to be successful as cement did reach the surface. A final CBL was run and the outcome confirmed that satisfactory level of cementing had already been attained (Fig.6.12).

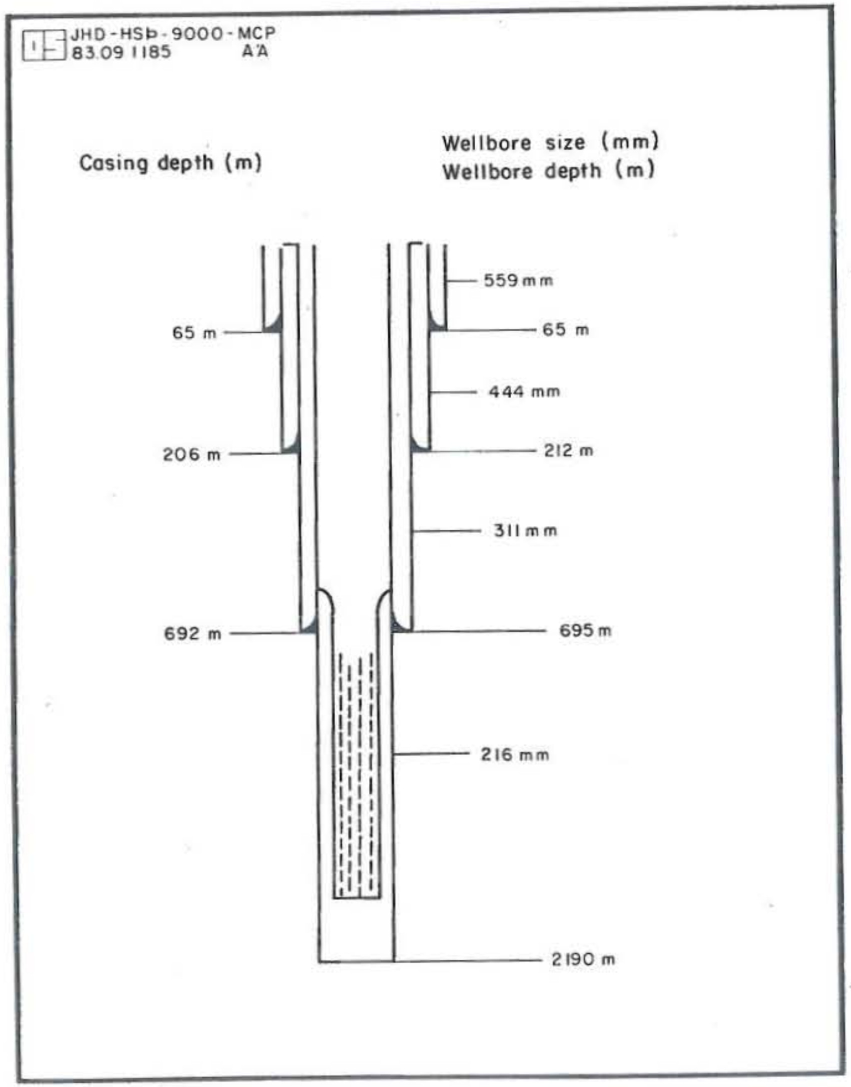

Fig. 6.9 KJ-17 drilling and casing program.

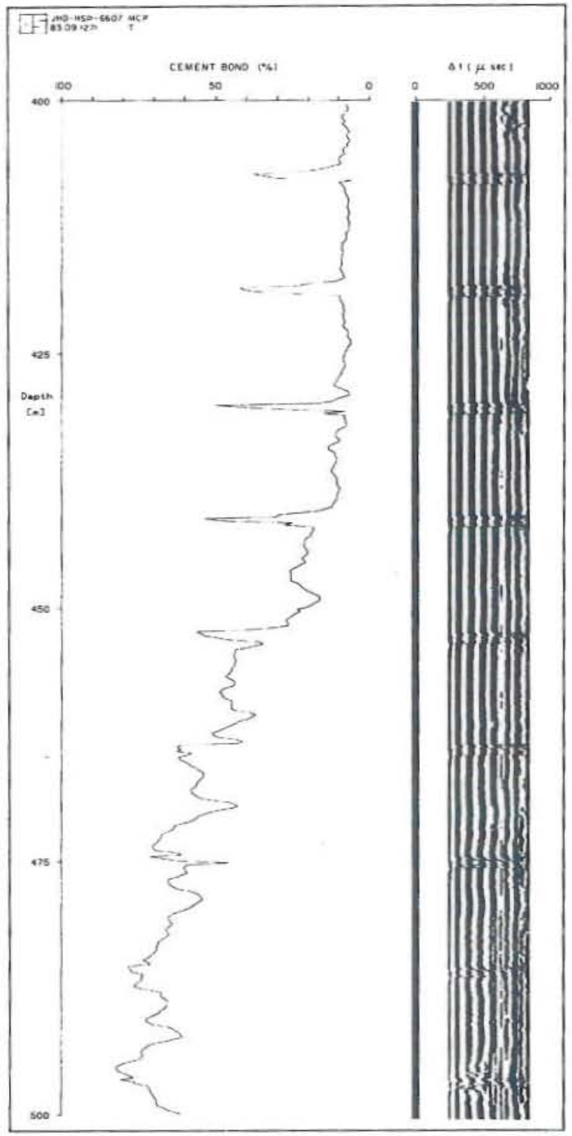

Fig 6.10 CBL run showing the top of the cement at 442-451 m.

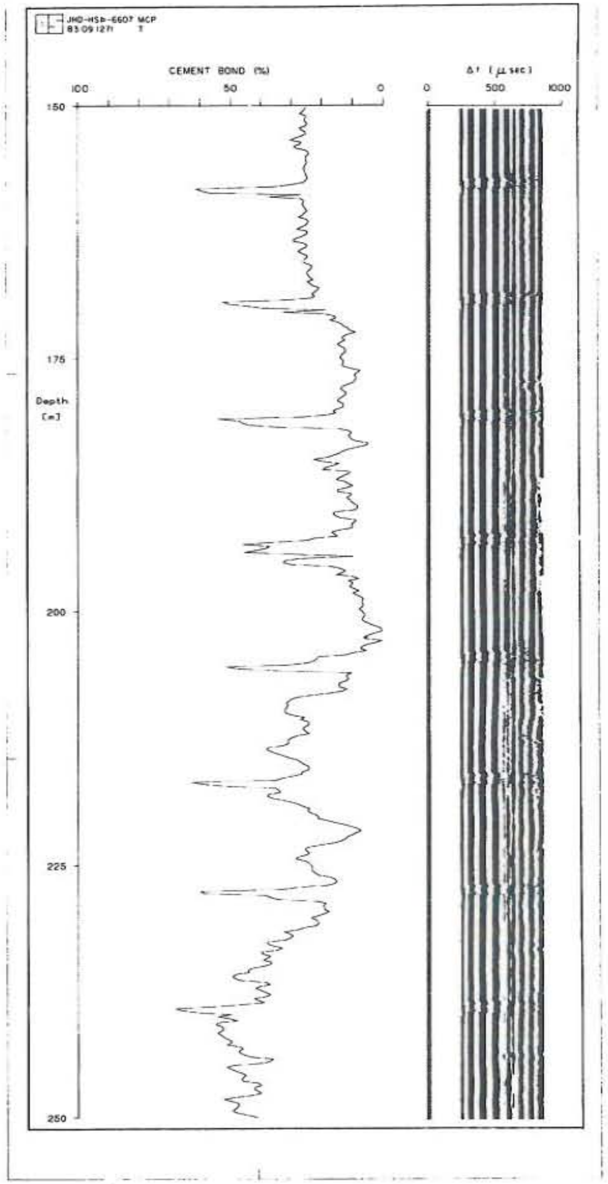

Fig. 6.11 CBL run showing the top of the cement at about 209 m.

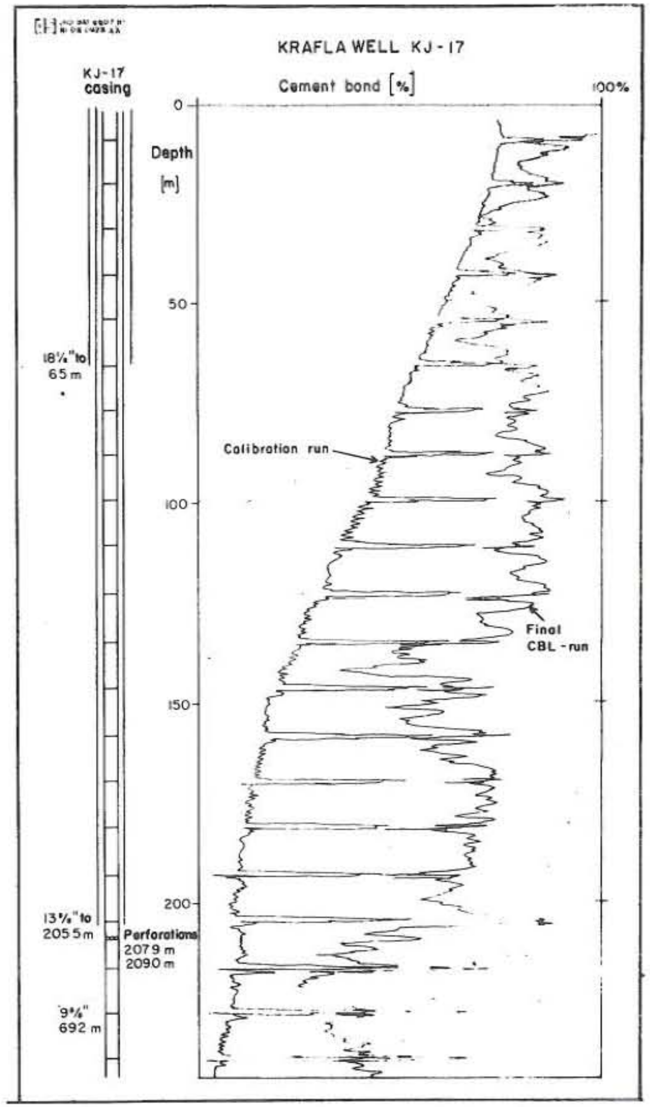

Fig. 6.12 Final CBL run after the two squeeze cementing operations together with a part of the calibration curve.

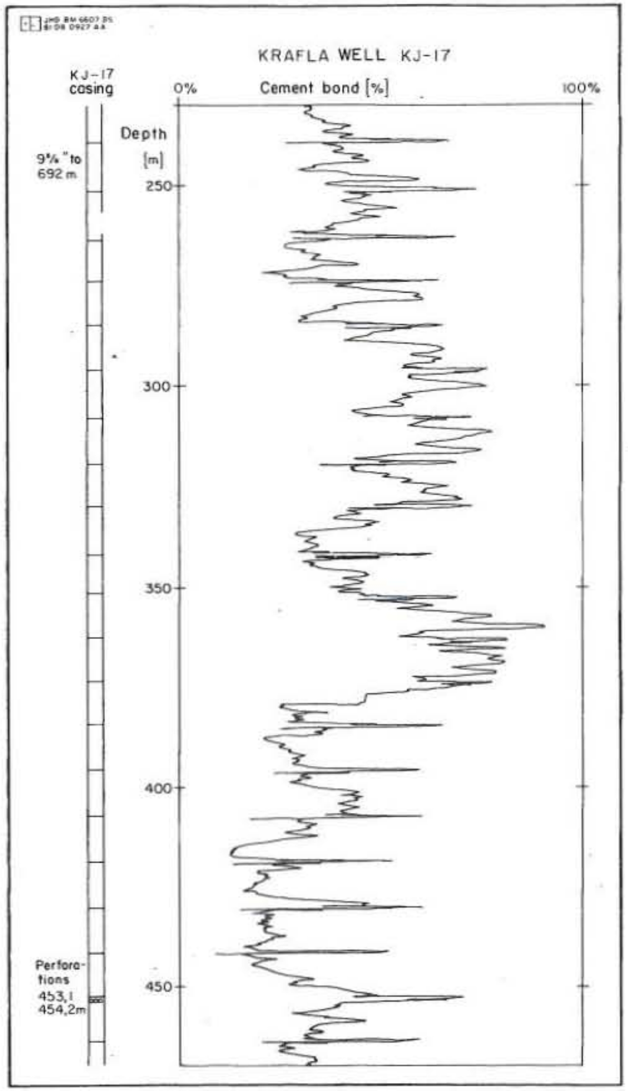

Fig. 6.12 Continued.

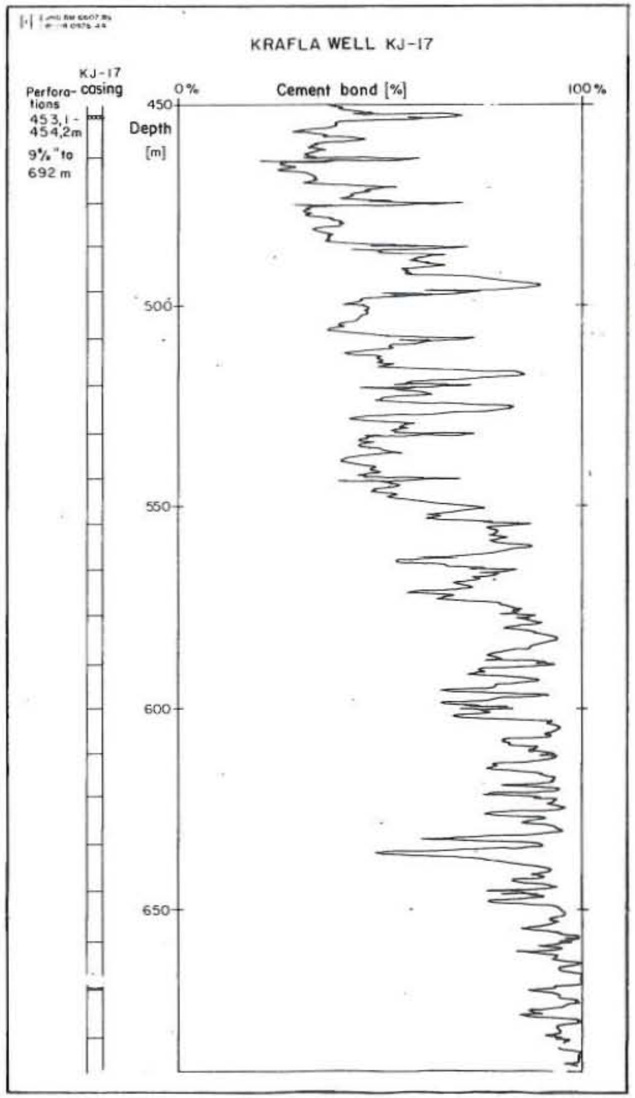

Fig. 6.12 Continued.

6.6 The KJ-17 CBL interpretation

The acoustic CBL logs run in KJ-17 have been interpreted by comparing them with the results obtained during the calibration run and also by applying the knowledge of transmitted acoustic sound wave behaviour in a steel casing, cement sheath and the surrounding formation. The calibration log in KJ-17 was done in such a manner that it recorded the amplitude of the first sound wave arrival (compressional wave) separately in the analog paper strip. The variable intensity of the complete sound wave train pattern, as it travelled from the three different media (e.g. the free casing, annulus and the formation) was recorded in the film strip. Figs.6.13, 6.10 and 6.14 show the 400 - 500m portions of the CBL run during the calibration, before the squeeze cementing and after the squeeze cementing at 453.1 - 454.2 m respectively. The amplitude calibration as seen in the figure is scaled 0% to 100% relative amplitude whereas the resulted VDL log is scaled in microseconds transit time (dt). The 100% relative amplitude represents the maximum recorded free casing amplitude, and 0% represents the absence of amplitude signals. The succeeding CBL run as seen in Figs. 6.10 and 6.14 are scaled 100% to 0% cement bonding. Since nothing had been changed in the equipment set up when these logs were conducted, the three measurements are related to each other. From this relation, it can be said that the 0% and 100% relative amplitude is equivalent to 100% and 0% cement bonding respectively. The explanation behind this inverse relationship is the fact that in the free casing most of the acoustic energy will travel through the casing to the receiver, with very little coupling to the formation. In this case the casing arrivals will be strong with weak formation arrivals (in some cases formation arrivals are not detected) and minimal or no change is observed in neither the arrival time (dt) nor the amplitude versus depth. In the case of Fig.6.13, the recorded amplitude is in the range of 90 - 100% relative amplitude and a fairly constant transit time of 223 microseconds. In contrast to an unbonded casing, well bonded casing (also with good

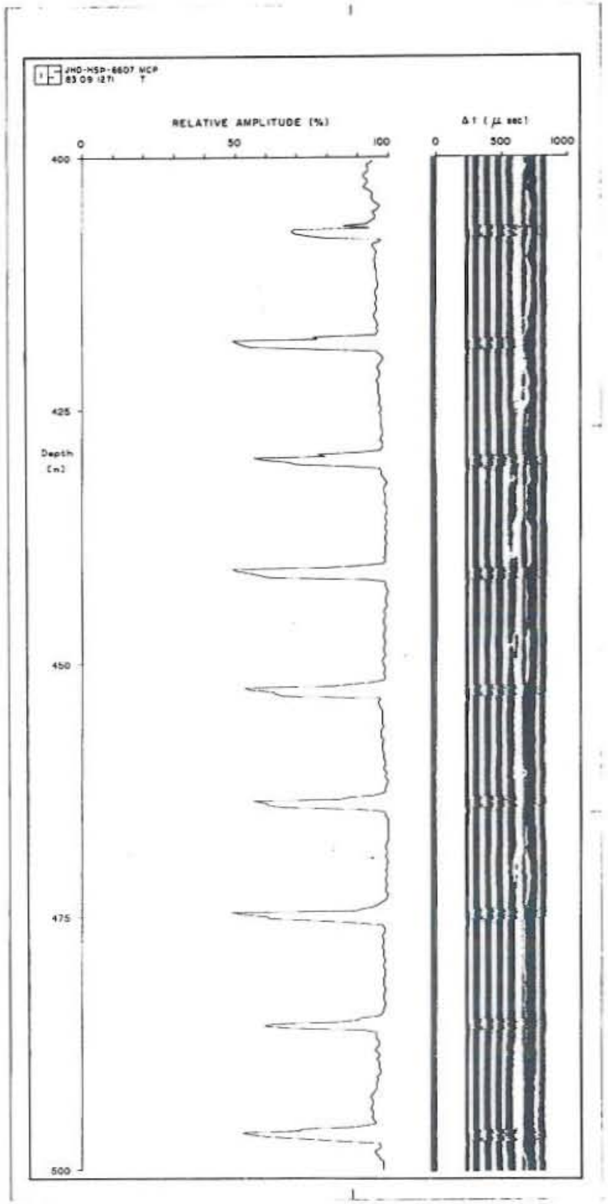

Fig. 6.13 The 400-500 m portion of the CBL calibration run showing both the analog and VDL signals.

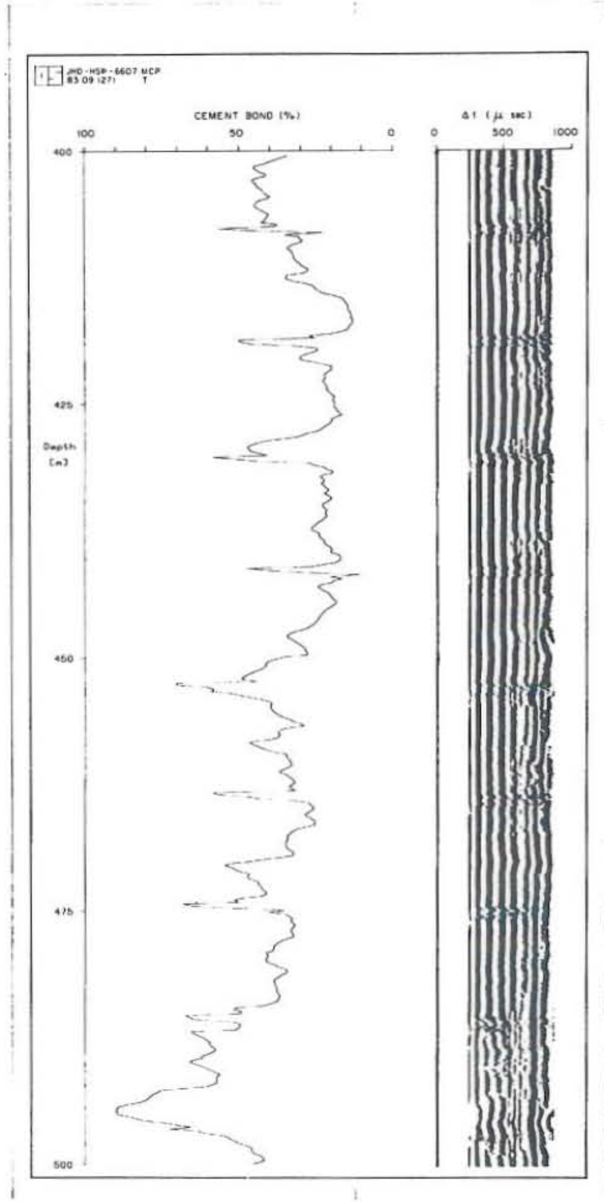

Fig. 6.14 The 400-500 m portion of the CBL run after squeeze cementing through the perforated holes in the 453.1 - 454.2 m interval.

cement to formation bonding) will result in weak casing arrivals coupled with strong formation signals (depending on the formation characteristics). This develops as the acoustic energy is transmitted very efficiently from the casing to the cement to the formation, thus leaving little acoustic energy in the casing. In Figure 6.10 (CBL to find the top of the cement) there is a fairly significant change in the recorded amplitude against depth hence suggesting two distinct sections in the 400 - 500m depth interval. From the knowledge of the calibration run, Fig. 6.11 suggests the top of the cement at about 442 - 451m where relative amplitude almost approaches that of the free casing. This is also being collaborated by the VDL results at this depth. In the VDL one can notice the compressional wave to be more intense above 450m. Furthermore, the latter signals appear to be less attenuated suggesting that these signals are purely from the casing. The check CBL, conducted after the squeeze cementing, proved the success of the cementing in the 400 - 500m depth interval as seen in Figure 6.14. However, during this operation the cement did not reach the surface and the check CBL run also pointed out another top of the cement.

Figures 6.15, 6.11 and 6.16 show the 150 - 250m portions of the calibration run, the CBL log before the squeeze cementing and after the squeeze cementing in the 207.9 -209.0m interval respectively. Figure 6.11 clearly indicates the top of the cement at about 209.0m. This is also closely supported by the VDL results at this depth where it shows that the received signals above 200m appear to be the strong casing signals only. Although there is only a very minimal difference in the transit time for the compressional wave above and below 200m, yet the signal attenuation below 200m is noticeable due to the good bonding. Figure 6.16 shows the squeeze cementing in the interval 150 - 250m to be satisfactory. The final CBL run from 0 - 692m, after the two successful squeeze cementing operations, is presented in Fig. 6.12. In the figure, the 0 - 244m depth interval of the calibration run is also included to demonstrate some characteristics inherent in

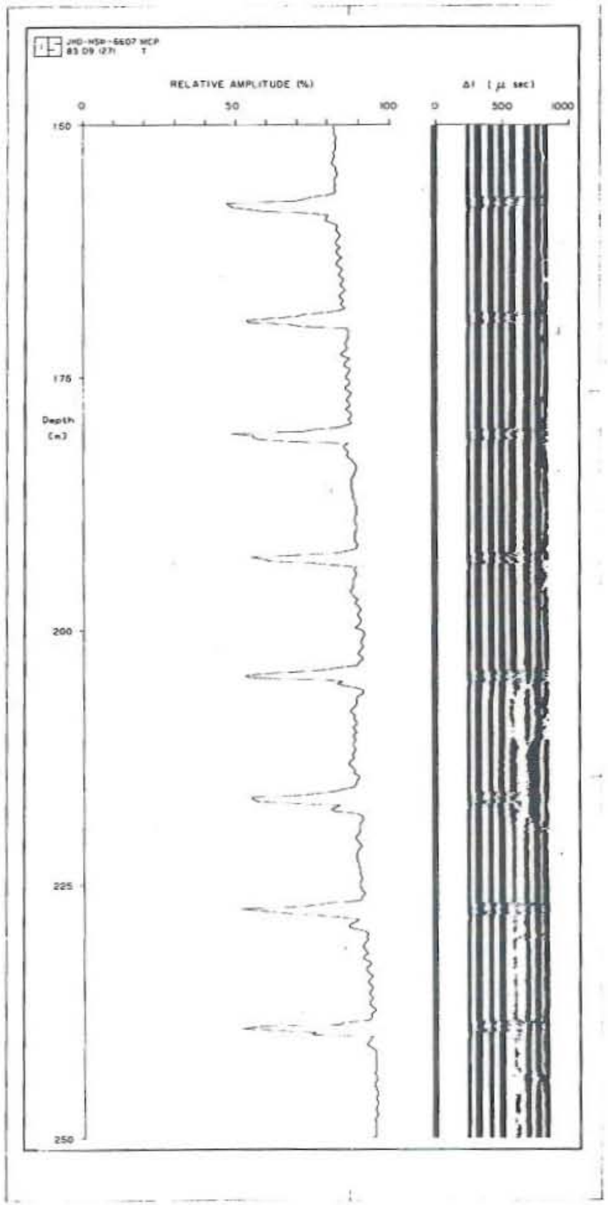

Fig. 6.15 The 150 - 250 m portion of the CBL calibration run showing both the analog and VDL signal.

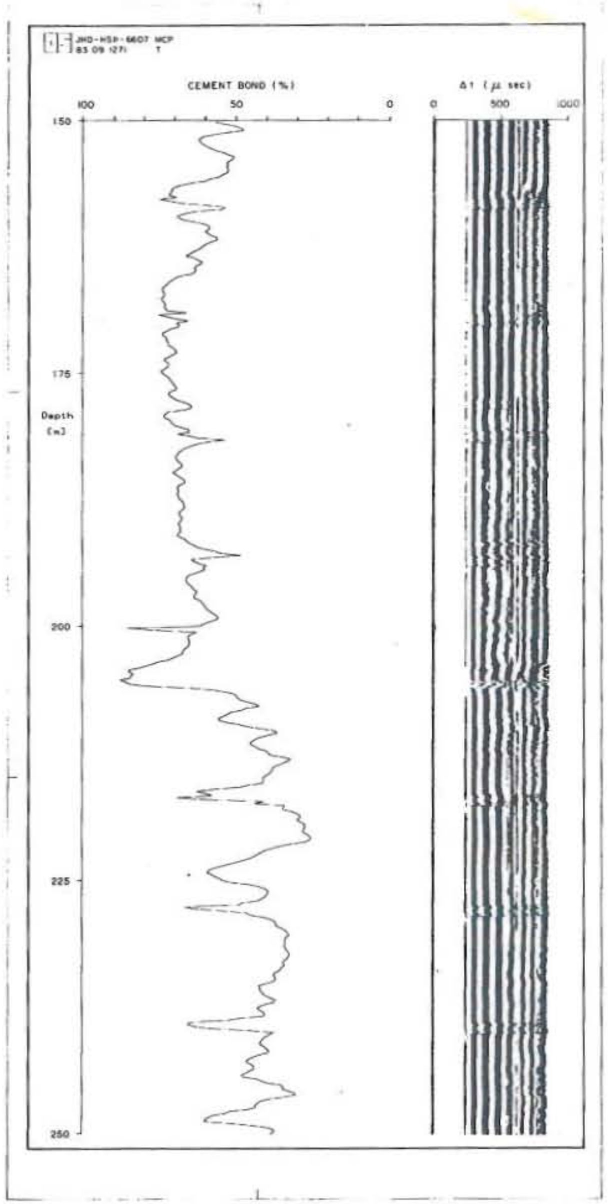

Fig. 6.16 The 150 - 250 m portion of the CBL run after squeeze cementing through the perforated holes in the 207.9 - 209.0 m interval.

other CBL tools as in the case of NEA's one transmitter - one receiver tool. In this case, the log appearance near surface showed the amplitude to de decreasing. One explanation for this effect could be the effect of gas expansion in the probe around the transducers. The coils of the transducers are likely to retain small bubbles of air which can severely affect the tool readings. The interpretation of the CBL for this part of the casing should therefore be made with reference to the calibration curve. In this case the calibration curve should be treated as the 100% relative amplitude or 0% cement bonding. In all logs, there are noticable intervals of chevron patterns. These are actually produced by reflected signals at each casing collar caused by the extra thickness in this part of the casing.

6.7 Perforating gun, its principle and operation in KJ-17

Little is available in the literature about the perforating gun and how this tool is used for making holes along the sides of the casing so as to make squeeze cementing possible. What will be described here is the experience gained by the well loggers of NEA as well as their methods in performing this delicate operation on well KJ-17. As discussed under 6.5, two separate perforating operations were done in the 9 5/8" casing of KJ-17. During these operations formed wire perforating guns (formed wire carrier is of 100ft dual coil - 0.135" O.D.) were used. These perforating guns were equipped with 2 1/8" O.D. - 22.7g tornado jet charges (aluminium case material), with a maximum operating temperature of 163°C, and a detoning fuse rated at 20,000 psi (220°C max. operating temperature). A primacord of 80g RDX (nylon - 163°C) was used in the two perforation operations. For details of the formed wire perforating gun and the tornado jet charge see Fig. 6.17.

The formed wire perforating gun operates on the following principle. A current from a special shooting module, is sent to the detornator (the upper most part of the gun)

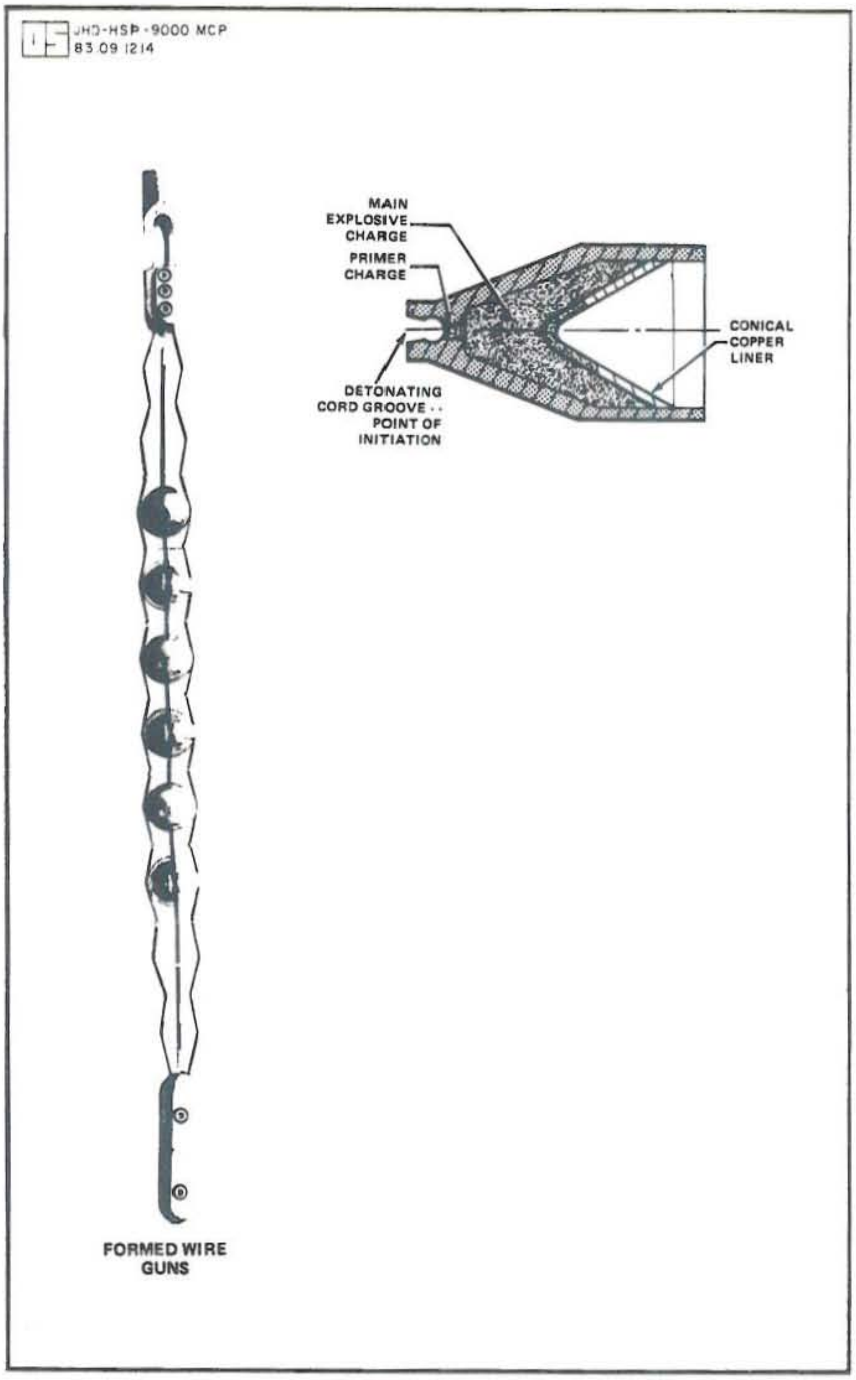

Fig. 6.17 Formed wire perforating gun and the Tornado jet charge. From Gearhart Owen Industries, Inc. (1981).

which has the resistivity of some 118 - 120 ohms and triggers the detonation. The energy released from this explosion is enough to detonate the connected primacord which in turn is connected to each of the charges. The detonation of the primacord will trigger the detonation of the charges. The detonation of two charges is expected to make two holes, one on each side of the casing. This develops as the charges are positioned such that they are facing opposite each other by 180 degrees.

There are two separate methods practiced by the well loggers of NEA to position and detonate the perforating gun in the bore hole. The first of this kind, which was applied in KJ-17, is done by first running a casing collar log (CCL) of the temperature sonde so as to locate the best depth for the perforation (the perforation depth should be in the part of the casing where there is no casing joint). The casing joint lowers the success ratio of making holes as the casing is extra thick along the joints. Once the best perforating depth has been established a reference mark is made on the cable (prefarably near the winch). The CCL is then retrieved and detached from the cable head. The formed wire perforating gun is attached to the cable head and lowered to the depth earlier established by the CCL (the mark on the cable). Detonation is accomplished by sending a current of about 50mA. In this method of operation only one conductor cable is used to detonate the gun.

The second method has only lately been practised by the well loggers of NEA. The running of a separate CCL is eliminated by using a shooting casing collar locator. The shooting casing collar is attached to the cable head and the perforating gun assembly to this tool. With this method, a two conductor cable is utilized. One is used for the CCL tool and the other for the perforating gun. To get the casing collar response, a positive current is sent through the conductor attached to the CCL tool. Once the perforation depth has been selected, the polarity in the line power module is reversed to negative and is sent through the other conductor linked to the perforating gun. A 500mA current is usually needed in this type of operation.

The success ratio of perforation jobs usually depends on many factors. One such factor is the unwanted perforation on the casing joint. This has already been explained. Other factors to consider is the proper selection of the number of charges to be used. This usually requires a good judgement and it is in this area of the operation where experience comes in. In the case of KJ-17, eight charges were used in each run (Fig. 6.18). Experience has shown the loggers that at least four charges out of eight will perforate the casing assuming all charges explode. It has been observed that four holes are enough to accomplish squeeze cementing with moderate pump pressure. The possibility of four out of eight charges making successful perforations could be expected when the perforating gun happens to lie on one side of the casing. As this develops there is the possibility that the four charges facing the opposite side of the casing by 180 degrees would only puncture the wall of the casing (Fig.6.19).

The other factors to consider is the clamping of formed wire to the firing head (detonator) and the slack in the primacord. If the former condition is not treated well there is a great risk that the formed wires will be detached from the detonator. The slack in the primacord is needed to allow shrinkage due to the high temperature in the well bore. This is to prevent the primacord from detaching from the detonator. Two more important factors are the proper selection of a sinker bar, and an awareness of the operating temperatures of the parts of the perforating gun. Too light weight sinker bars pose the possibility of the equipment becoming stuck. If this happens the weight will only get stuck and not the charges. With this condition, the perforation may end up in the wrong part of the casing.

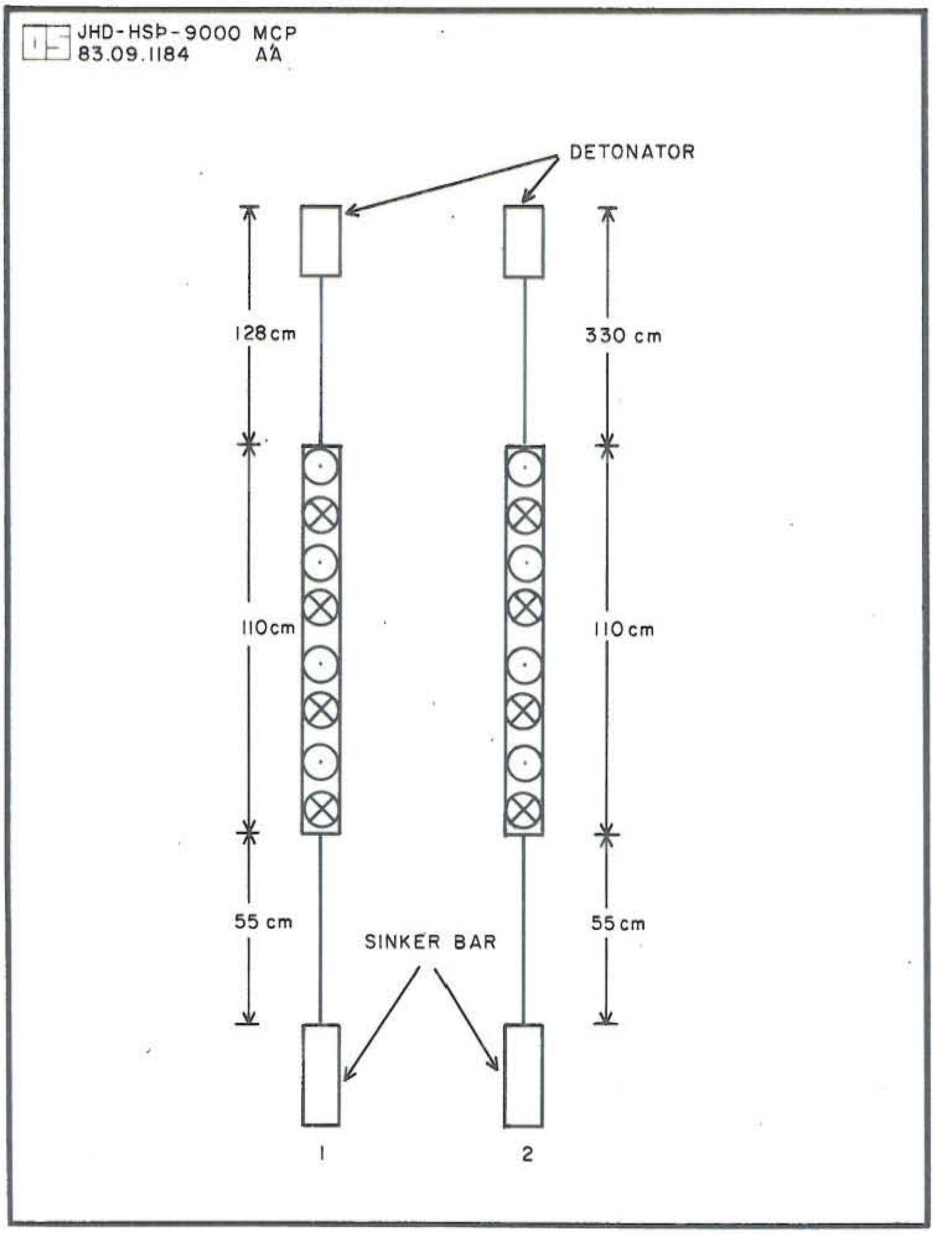

Fig. 6.18 Schematic diagrams of the formed wire gun and Tornado jet charges used in KJ-17. After Fridleifsson and Sigvaldason (1981).

1 - used in perforating the 453.1 - 454.2 m section of the 9 5/8" casing.

2 - used in perforating the 207.9 - 209.0 m section of the 9 5/8" casing.

6.8 Safety considerations

A perforating job is a delicate operation and involves the risk of accidents to human lives. Some safety precautions will therefore be discussed here and recommendations made for this kind of operation.

The safety precautions that must be observed in conducting perforation job can be listed as follows:

1. There must be a strong collaboration between the well loggers and the rig personnel as to what is going on.

2. All sources of electricity e.g. rig power plant, truck power, radio transmitters, welding machines etc. must be switched off when connecting the explosives. This is to avoid the presence of stray direct current potentials.

3. All effort must be made to check and eliminate other stray voltages in the vicinity.

4. Cable conductors must be grounded.

5. All personnel must keep out of line of the charges once the primacord has been connected to the charges.

6. The perforating gun must be lowered first to a safe depth (at least 50m down in the casing) before electrical power sources are switched on.

7. Extra precaution must be observed when pulling the expended gun from the well as there is possibility that some of the charges have not been detonated.

8. Safety/warning signs must be posted on strategic locations during the operation.

Since a perforating job is a delicate operation and involves the risks of accidents to human lives, it is recommended that the personnel who will be assigned to this operation must undergo training on the aspects of the handling of explosive, the operation and the safety precautions required before they are allowed to handle explosives for perforations.

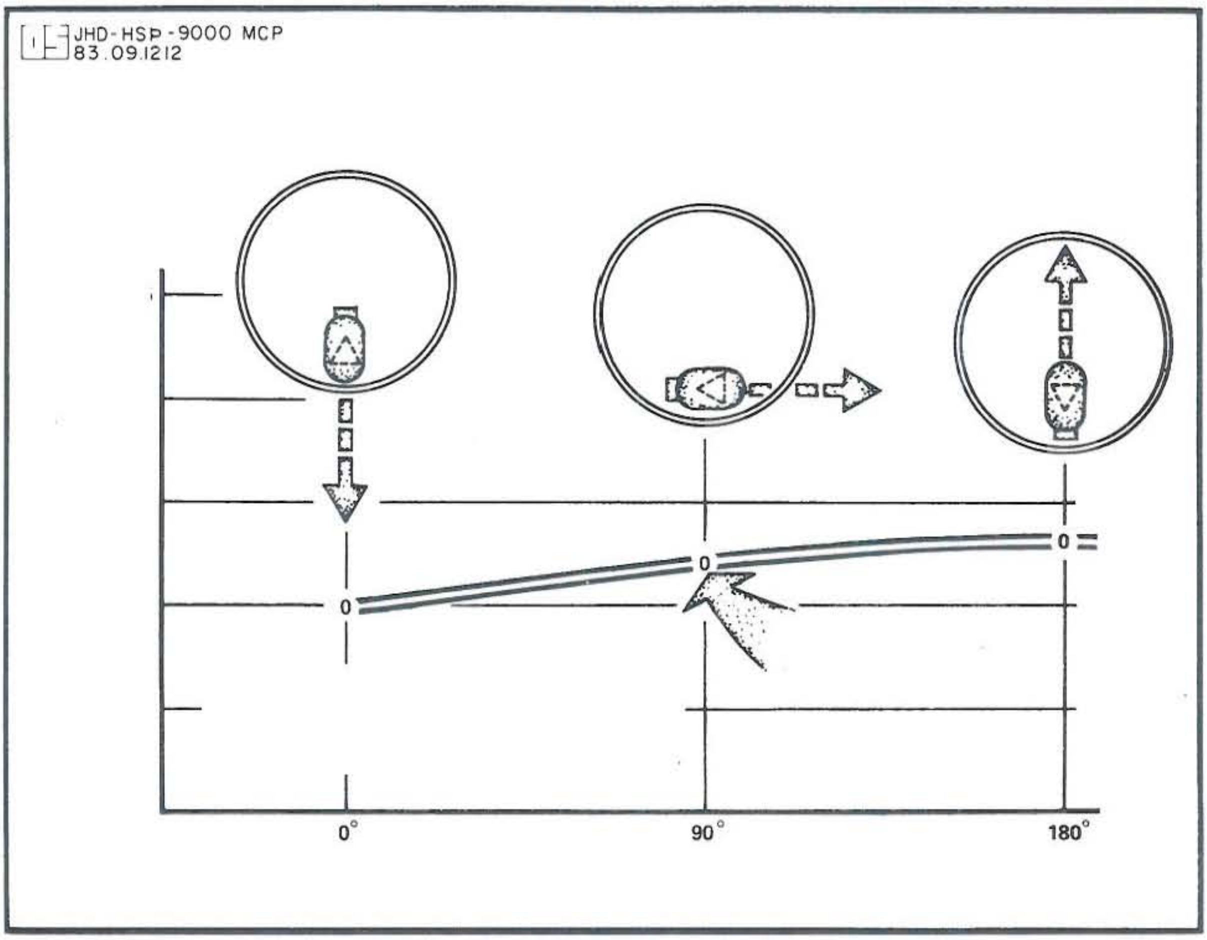

Fig. 6.19 Charge orientation against casing wall.

7 GEOPHYSICAL LOGS FROM KJ-17

In this chapter the various geophysical logs run in KJ-17 will be discussed, i.e., the caliper log (650-1726m), neutron-neutron log (680-1519m), natural gamma ray log (678-1390m) and the resistivity log (695-1802m). All these logs were limited to some specific depths due to the high temperature encountered in the well at the time of logging. Also included are the results of the calculated porosity from the neutron-neutron log as well as the calculated silica content of the rocks from the natural gamma ray log. The details of the drilling and casing program in KJ-17 are shown in Fig.6.9.

7.1 Interpretation of the geophysical logs from KJ-17

Well log interpretation techniques for geothermal exploration are still in infancy, especially for wells drilled in igneous and metamorphic formations. Although work in this direction has been reported in recent years, there remains a notable gap between petroleum and geothermal applications of log interpretation methods (Benoit et al., 1982). In petroleum logging the methods of interpretation are based on numerous case studies. In geothermal log interpretation problems associated with unknown matrix response, volcanic lithology, effects of hydrothermal alteration, and fracture systems cannot be solved directly with the methods used in the petroleum logging.

In the case of KJ-17, lithology logs derived from the drill cuttings have been drawn for the well. To fully understand both the lithology logs and the geophysical logs efforts were made to correlate them and techniques like cross plottting, use of histograms, large scale variations, porosity and silica calculations were applied to determine the lithological characteristics.

7.2 Correlation between the lithology and the geophysical logs

In general, there appears to be a good correlation between the lithology and the geophysical logs in KJ-17 (Fig.7.1). In most cases, boundaries and thin interbedded layers are resolved by the geophysical logs. One such example is in the 747-769m interval where the resistivity reading is observed to increase from what appears to be a baseline of 33 ohm-m to 219 ohm-m. The appearance of the resistivity and neutron-neutron logs indicate the presence of inter-bedded layers. This observation is closely supported by the lithology logs. From the study of the drill cuttings, alternating thin basalt and tuff layers are observed in this depth interval. However, the resolution of the resistivity log in the 753-769m depth interval is not very pronounced and this is mainly due to the effects of the thin layers. It is worth noting the apparent baselines in the three logs i.e., neutron-neutron, natural gamma and the resistivity logs in the 700-900m depth interval. They are expected in this interval since the formations are only of two types, i.e. tuffs and altered basalts.

From 900m to 1390m, the natural gamma ray log records higher intensities in the fine and coarsed grained intrusive acidic rocks. This type of rock is likely to have secondary minerals enriched in potassium feldspar. Stuckless et al. (1977) noted that in an oxidizing environment uranium is quite mobile. The log responses of the natural gamma and resistivity in the acidic units in the 1380-1390m interval are quite unusual. While the natural gamma records higher intensity, the resistivity log also shows higher resistivity values. However, this could be explained by considering the recorded neutron-neutron log. The neutron-neutron log shows some minima and maxima values in this interval. Keys (1979) has noted that very high resistivities are usually measured in low porosity formations (i.e. formations with higher neutron-neutronlog values).

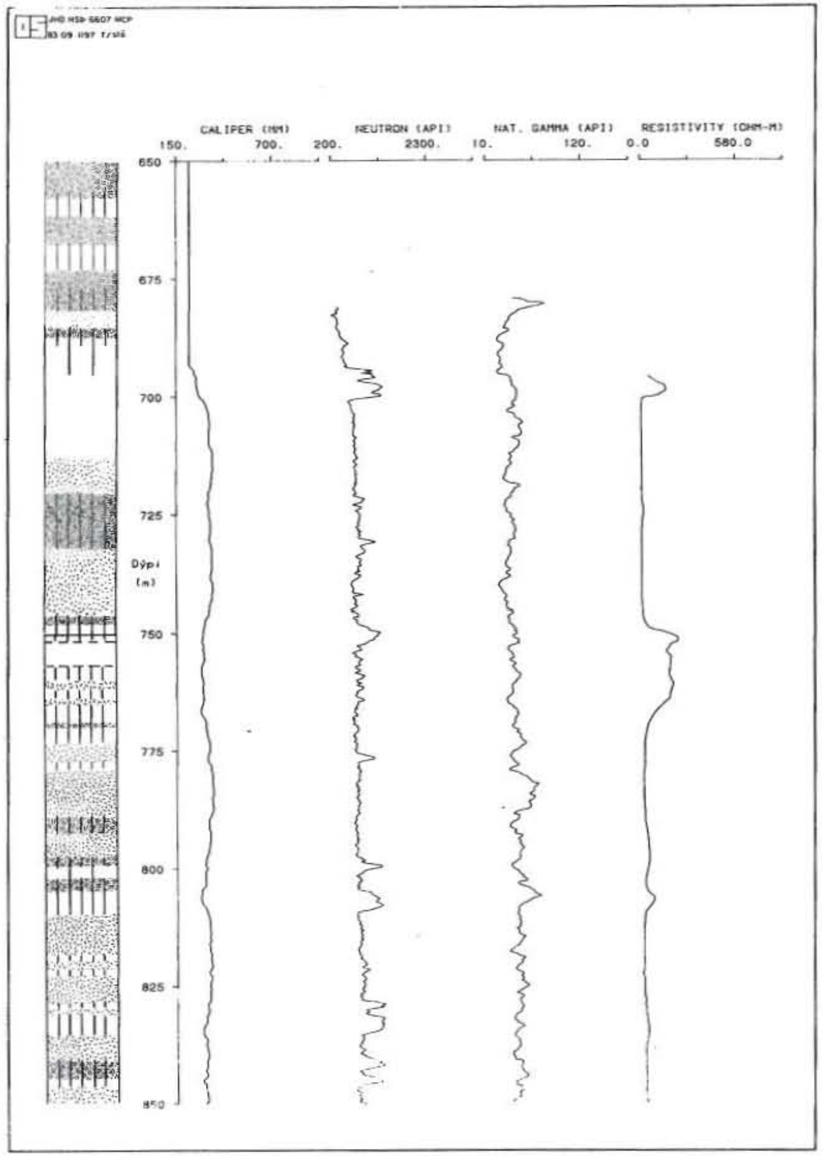

Fig. 7.1 Corrected caliper, neturon-neutron, natural gamma and 64" normal resistivity logs from 692 m to the maximum depth logged. Lithology log is also included.

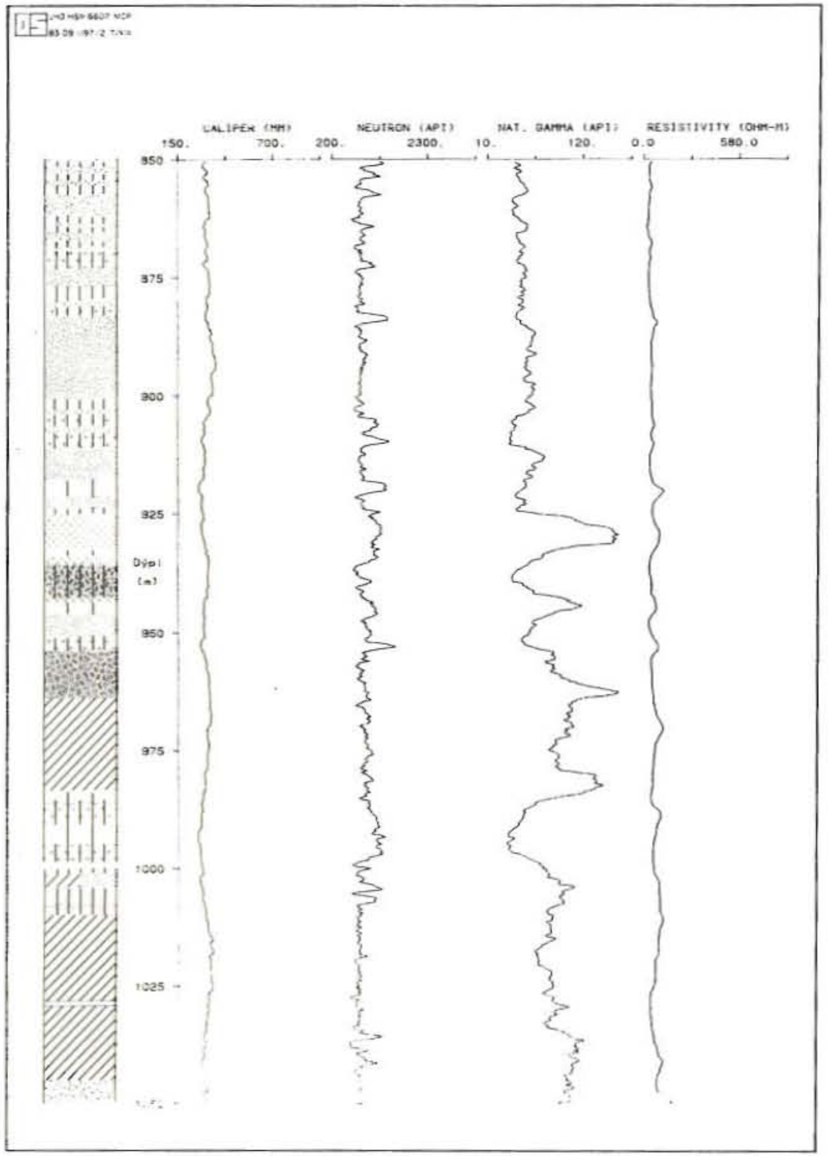

Fig. 7.1 Continued.

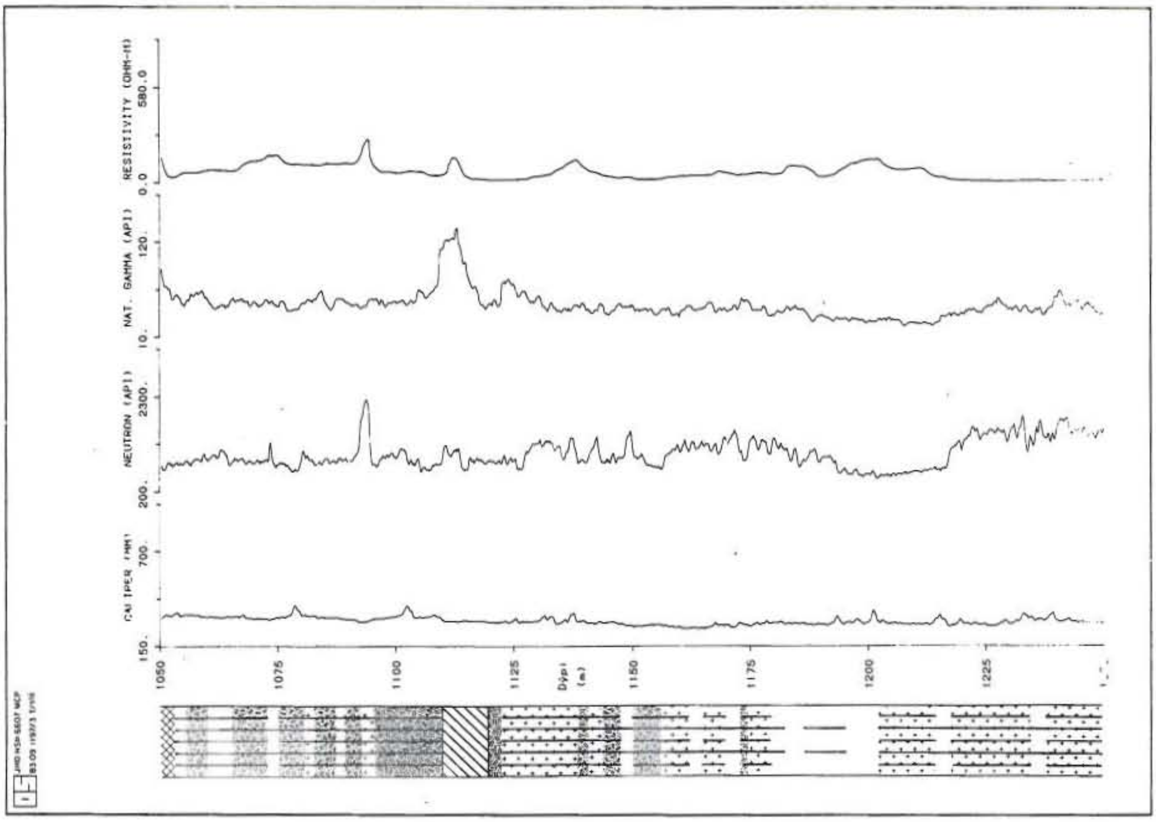

Fig. 7.1 Continued.

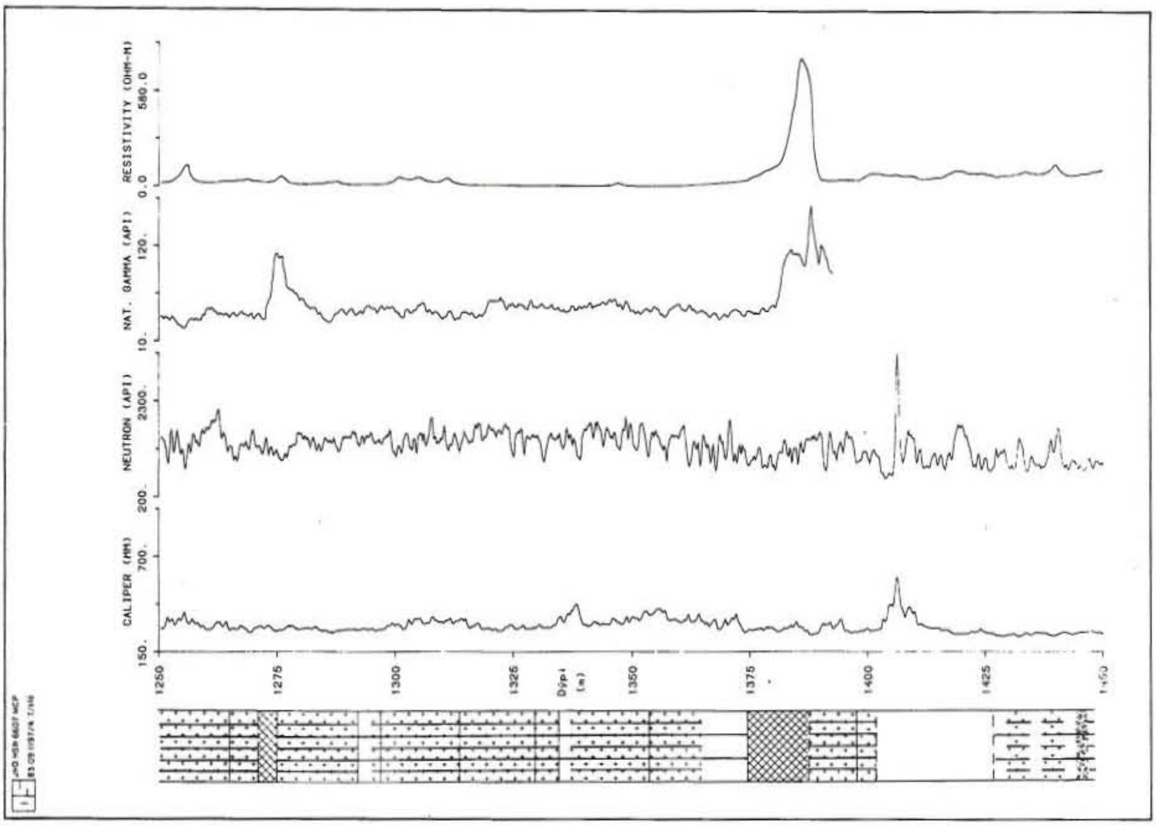

Fig. 7.1 Continued.

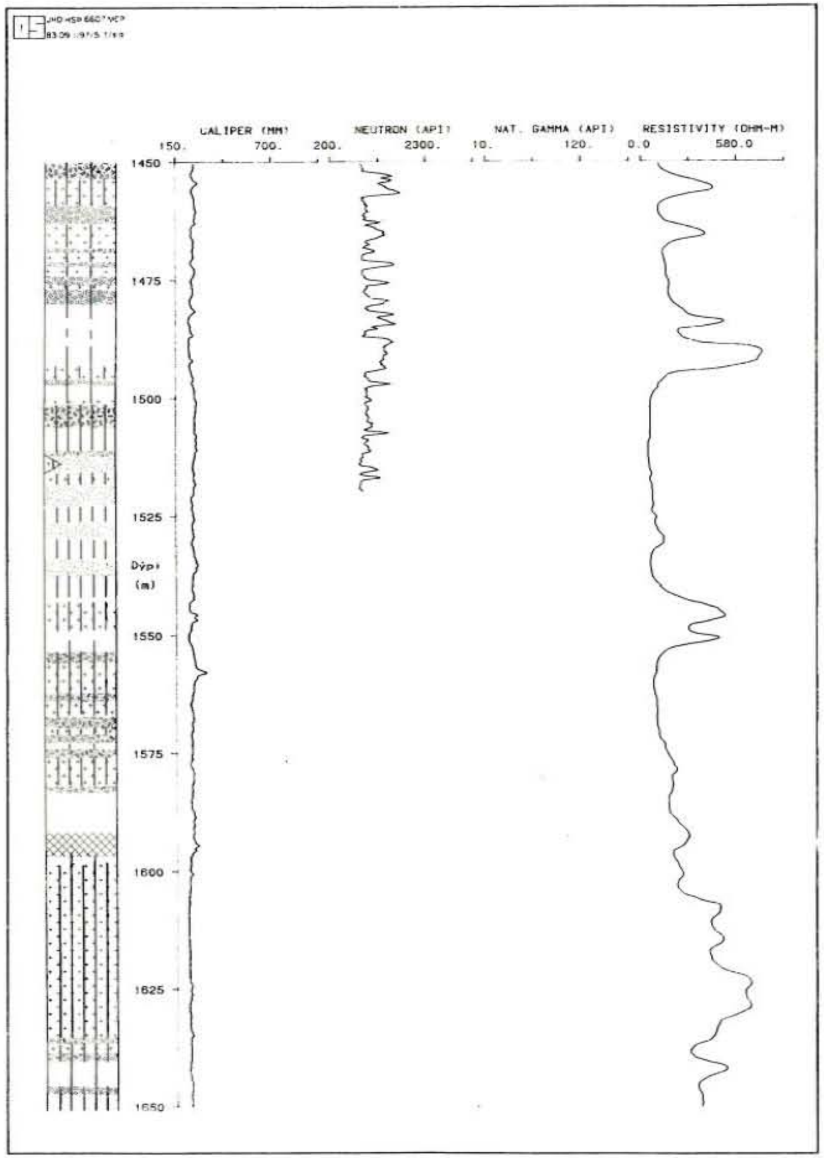

Fig. 7.1 Continued.

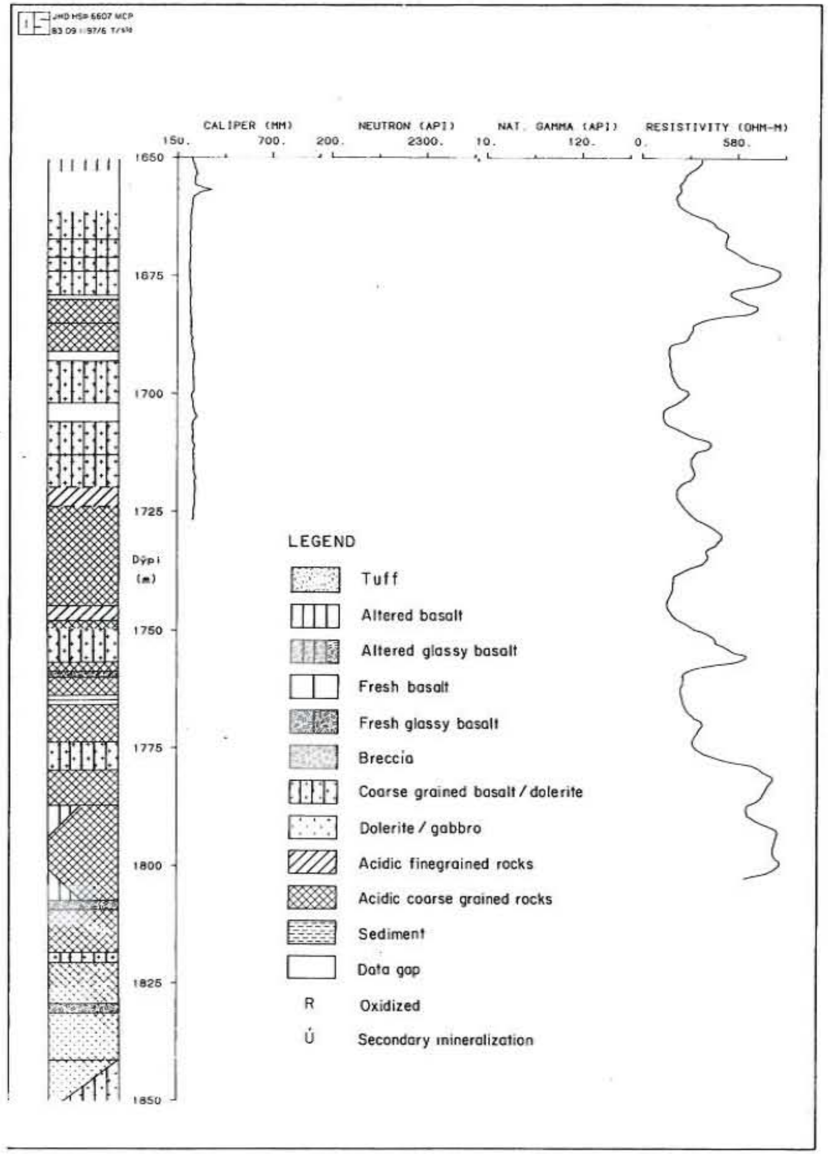

Fig. 7.1 Continued.

Attention is drawn to the log responses in the 1191-1220m depth interval. Here both the neutron-neutron and the natural gamma logs show low values, but the recorded resistivity log records high values. This behaviour is not easy to explain and may require further study. There is, however, one possible explanation based on a consideration of horizontal fractures only. Stefansson et al.(1982 b) noted that in a formation where the total porosity is dependent only on horizontal fractures the resistivity should be high. It is interesting to note that in this depth interval the caliper log shows some cavities.

7.3 Porosity versus depth

The porosity against depth for the KJ-17 is calculated by correcting the neutron-neutron log values to 9" well diameter and by using the calibration curve supplied by the tool manufacturer (Fig.7.2). Although this curve applies only for limestone formation, Czubek (1981) showed that the difference between igneous and limestone porosities does not exceed 3 %. Fig. 7.3 shows the resulting porosity plotted against depth. As expected the maximum porosity is in the interval 1191-1220m. The minimum calculated porosity for KJ-17 is in the 1225-1375m depth interval. From 1375-1519m, low porosity layers of basalt/dolerite units are also recorded.

7.4 Silica content of the rocks

It has been noted in the continuously cored IRDP (Iceland Research Drilling Project) hole in E-Iceland that there is a strong correlation between the concentration of U, Th, K and SiO_2 in the basaltic pile (Stefansson et al., 1982 a). The correlation constants for these relations are: R(K,Si) = 0.78, R(Th,Si) = 0.93, and R(U,Si) = 0.91. Heier et al.(1966) also noted that the thorium/potassium ratio in Icelandic basalts is similar to comparable basalts from many different environments, but that uranium is relatively

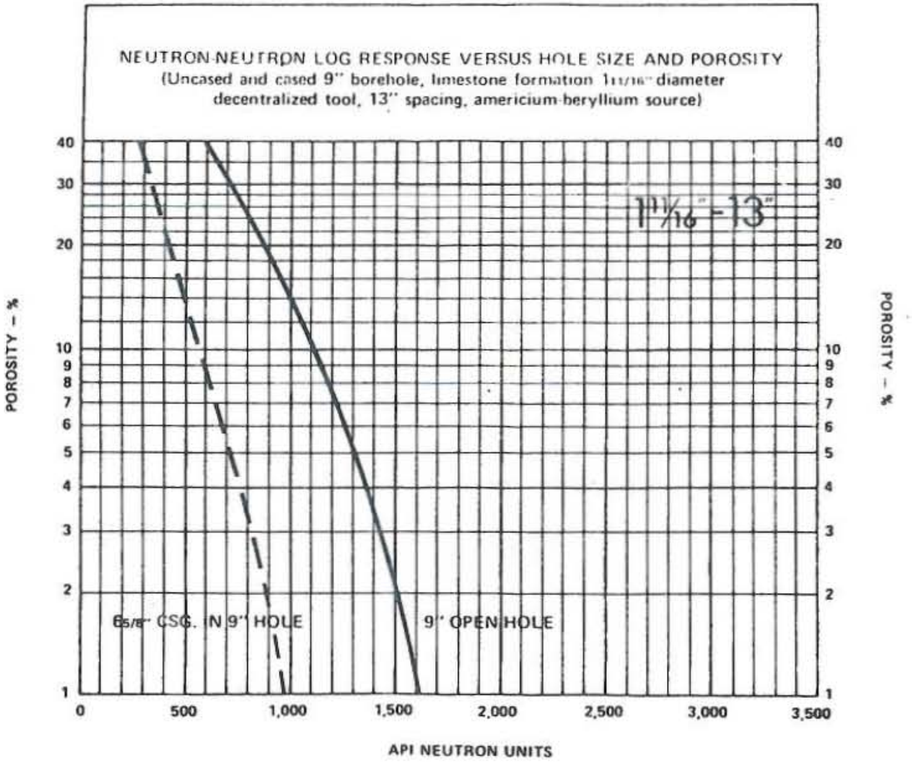

Fig. 7.2 Neutron-neutron log response versus limestone porosity for a 9" borhole. From Gearhart Owen Industries, Inc. (1976).

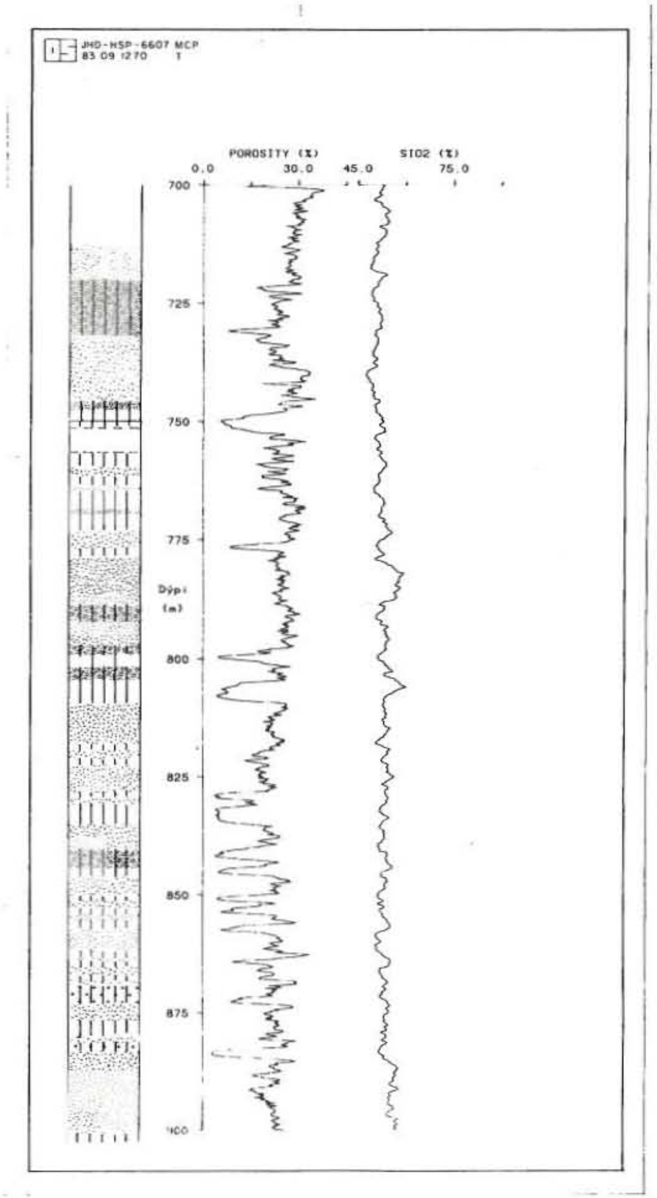

Fig. 7.3 KJ 17 porosity and silica content of the rocks versus depth.

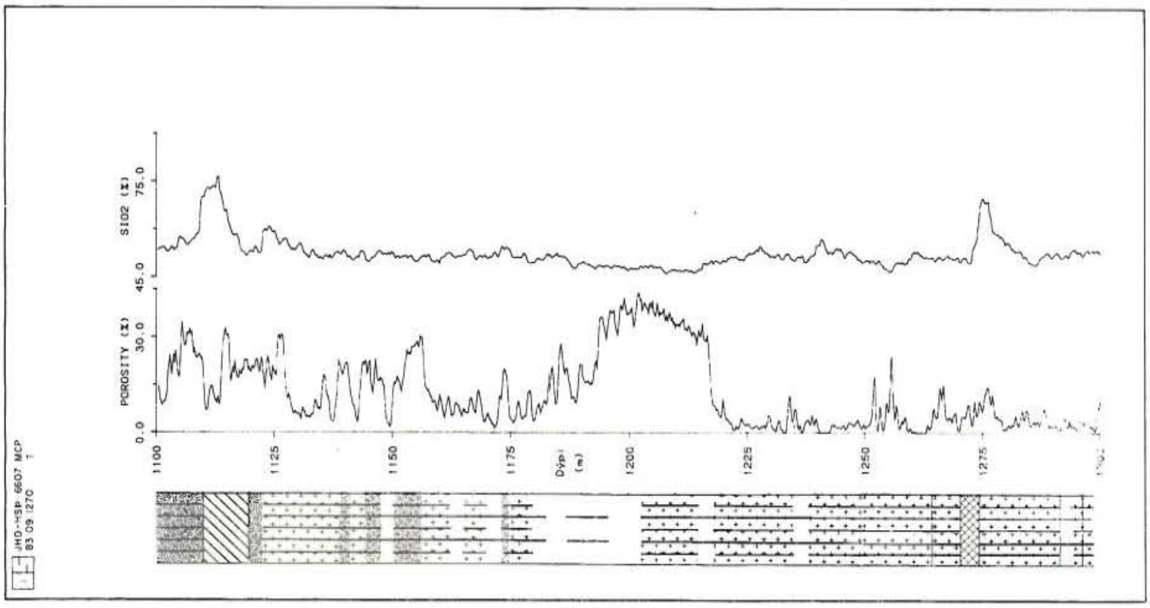

Fig. 7.3 Continued.

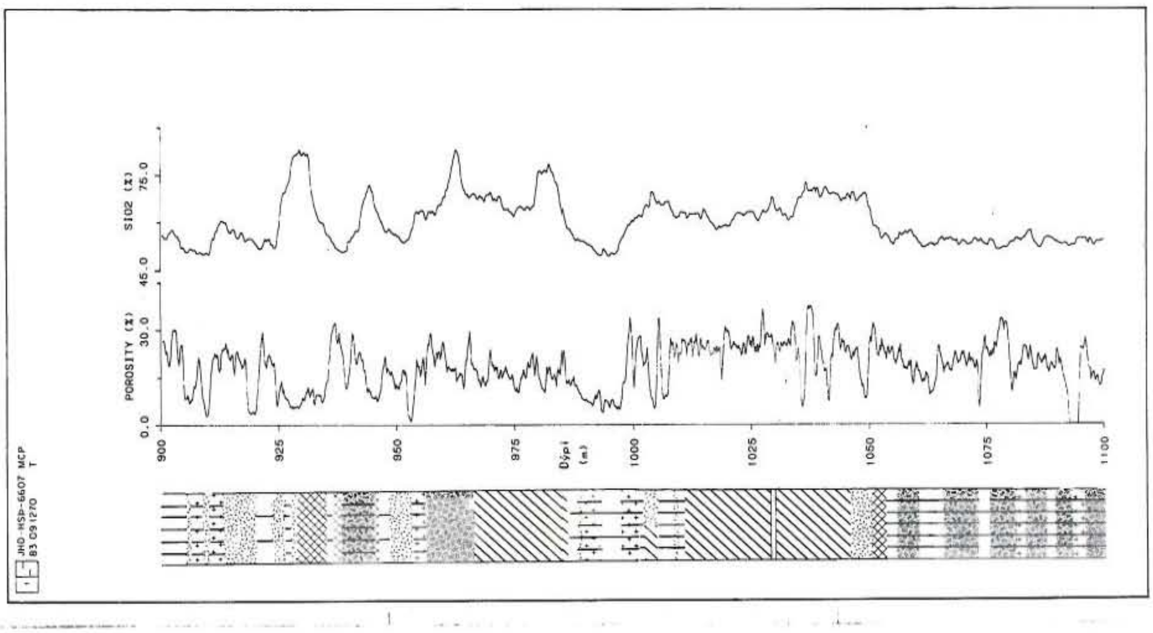

Fig. 7.3 Continued.

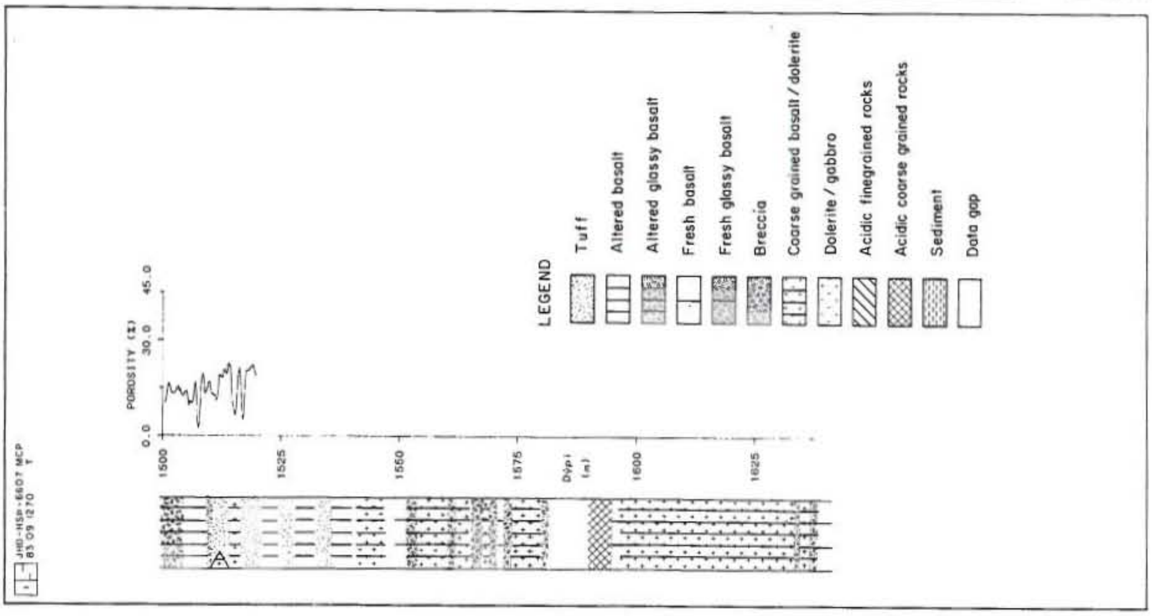

Fig. 7.3 Continued.

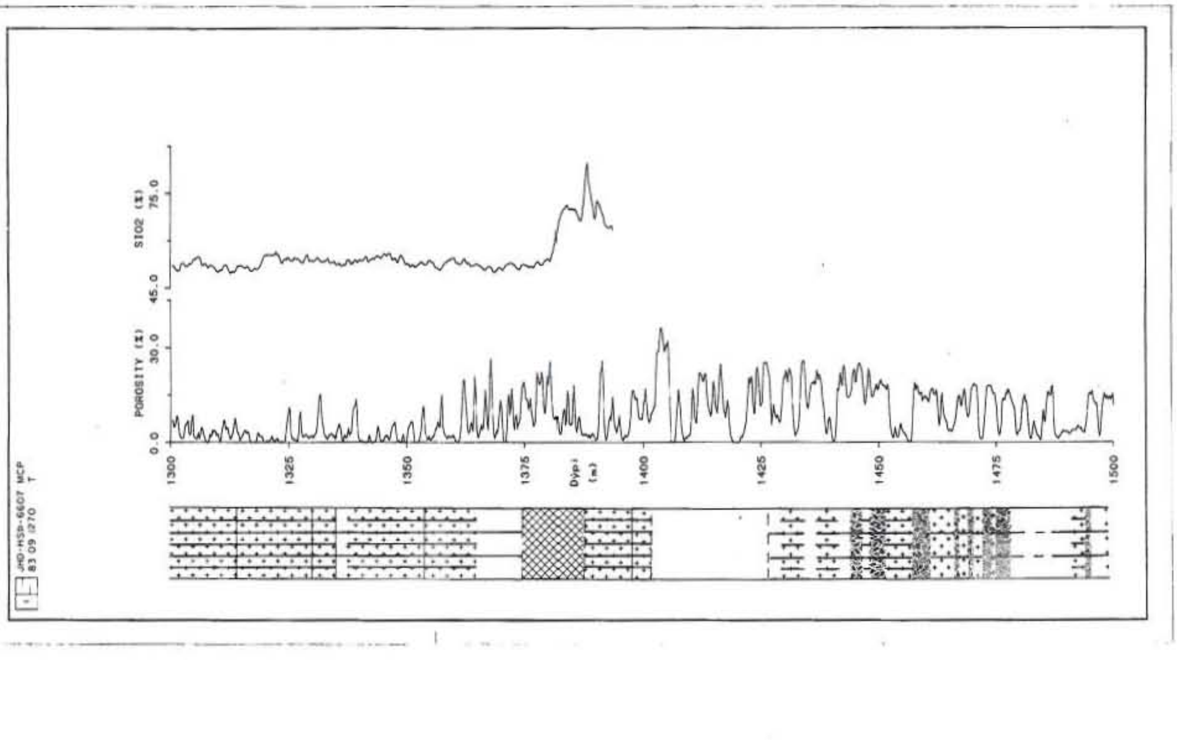

Fig. 7.3 Continued.

enriched in the Icelandic rocks by a factor of two. As a result of this relation between the radiogenic elements (U,Th,K) and SiO_2 in the IRDP hole, investigations have been initiated between the gamma intensity and the concentration of silica in the rocks in several wells in Iceland to establish a relation between those quantities. So far the relation:

$$GR(API) = 3.65\ SiO_2\ (\%) - 144$$

obtained from the IRDP hole has been found to be in good agreement with some other wells in Iceland. Furthermore, Stefansson et al. (1982 a) noted the following relations of the above mentioned radiogenic elements to silica contents in the IRDP hole:

$$(K_2O) = 0.169\ (SiO_2) - 7.79 \qquad R = 0.78$$
$$(Th) = 0.323\ (SiO_2) - 14.6 \qquad R = 0.93$$
$$(U) = 0.114\ (SiO_2) - 5.05 \qquad R = 0.91$$

where (SiO_2) and (K_2O) are concentrations in % of the total rock mass; (Th) and (U) are concentrations in ppm; and R is the correlation coefficient.

The above relationships were determined from the examinations of the core samples obtained from the IRDP hole and may not hold true for well KJ-17. Furthermore the involved parameters are interrelated and the equation:

$$GR(API) = C1\ K_2O + C2\ Th + C3\ U$$

and the relation:

$$GR(API) = f1\ (SiO_2); \qquad SiO_2 = f2\ (K_2O);$$
$$SiO_2 = f3\ (Th); \qquad SiO_2 = f4\ (U)$$

have no unique solution. However by assuming the above relation between the concentrations of U, Th, K_2O and SiO_2 for KJ-17 one possible arrangement of relative concentrations of the elements should be as shown in Table 7.1.

Fig. 7.3 shows the silica content of the rocks versusdepth in well KJ-17.

Table 7.1 Silica, Potassium, Thorium and Uranium concentrations for the different rock types in KJ-17.

Depth Interval, m	Rock type	SiO_2 (%)	K_2O (%)	Th (ppm)	U (ppm)
700-720	Tuff/hyaloclastite	52	1.0	2.2	0.8
955-965	Breccia	73	4.5	9.0	3.3
1037-1050	Fine grained acidic rock	69	3.9	7.7	2.8
1100-1110	Altered glassy basalt	55	1.5	3.2	1.2
1300-1330	Basalt/dolerite	50	0.7	1.6	0.7
1365-1375	Fresh basalt	51	0.8	1.9	0.8
1375-1388	Coarse grained acidic rock	72	4.4	8.7	3.2

8 CROSS PLOTS

The interpretation of the lithology from the geophysical well logs in igneous rocks is largely a matter of experience and the amount of corroborating data available. In each new area it is absolutely essential that some core data is available to develop interpretive criteria. Cross plots are various log parameters statistically plotted against other parameters. Adjustments can be made to these responses in order to fit better the local geologic conditions. Cross plotting of logs by using a computer is one of the most useful techniques for developing an understanding of log response in new rock types (Keys, 1979). In some cases cross plots of the log values are able to separate in clear groups the different rock types intersected by the well. This often leads to a better understanding for forming criteria for distinguishing rock types, especially in complex lithologies. Since cross plots can be adjusted to the local geologic conditions, these responses can be used for calibrating logs.

8.1 Resistivity - porosity cross plots

The pioneering effort in establishing the dependence of the resistivity factor of sedimentary rock formations upon porosity dates back to 1942 (Archie, 1942). Archie suggested the well-known empirical formula:

$$F = (Rf)/(Rw) = a \cdot \phi^{-m}$$

where F = formation factor, Rf = formation resistivity, Rw = resistivity of well bore fluid, a = constant (usually equal to 1 for sedimentary rocks), ϕ = porosity, and m = cementation factor.

Towle (1962) and Aquilera (1974 and 1976) pointed out that the resistivity log offers more versatility than other geophysical logs in distinguishing between fractured and intergranular reservoirs. This is supported by Brace et al (1965) who established a value of 1 for the exponent m in Archie's law in fractured crystalline rocks, whereas a value of 2 seems to be valid for non-fractured rocks. Stefansson et al.(1982 b) in their studies of the resistivity and porosity logs conducted in Iceland found that the Archie's exponent is close to 1 for Icelandic basalts. However, in their studies of the resistivity/ porosity relationship for Icelandic basalts, well KJ-17 was not included. The resistivity/porosity relation in KJ-17 will therefore be studied here and the value of m for KJ-17 compared to the trend for most Icelandic basalts.

The initial approach to determine the value of the exponent m in Archie's law for KJ-17 was to use the data from 700 -1519m. However, it resulted in a large scattering of log values and a positive m value. Hence, it was decided to take every 100m intervals in order to check the interval consistency of the data.

Figures 8.1 to 8.8 show the resistivity-porosity relations for 100m intervals in the KJ-17 with the exception of Fig.8.8, where the depth interval involved is 119.0m. For each depth interval the constants m and a x Rw were determined with the least squares method. Table 8.1 gives the summary of these calculations.

With the exceptions of 700 - 800m, 1100 - 1200m, 1200 - 1300m and 1300 - 1400m depth intervals the average value for the exponent (m) is calculated to be:

$$(m) = -0.70 \pm 0.17$$

and the average value for a x Rw is:

$$(a \times R_w) = 430 \pm 134 \text{ Ohmm}$$

In KJ-17 the fluid resistivity is assumed to be 10 Ohm-m. With this value the constant a in Archie's law is found to be:

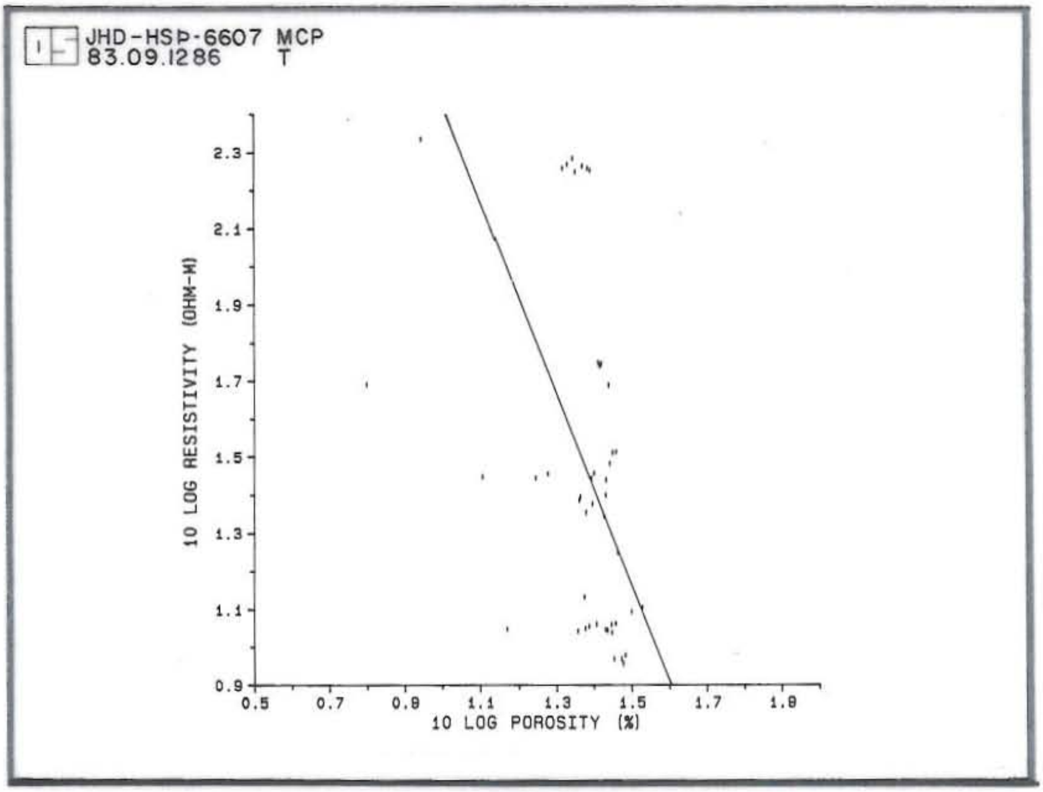

Fig. 8.1 Resistivity-porosity relation in the 700 - 800 m interval (2 meters running average).

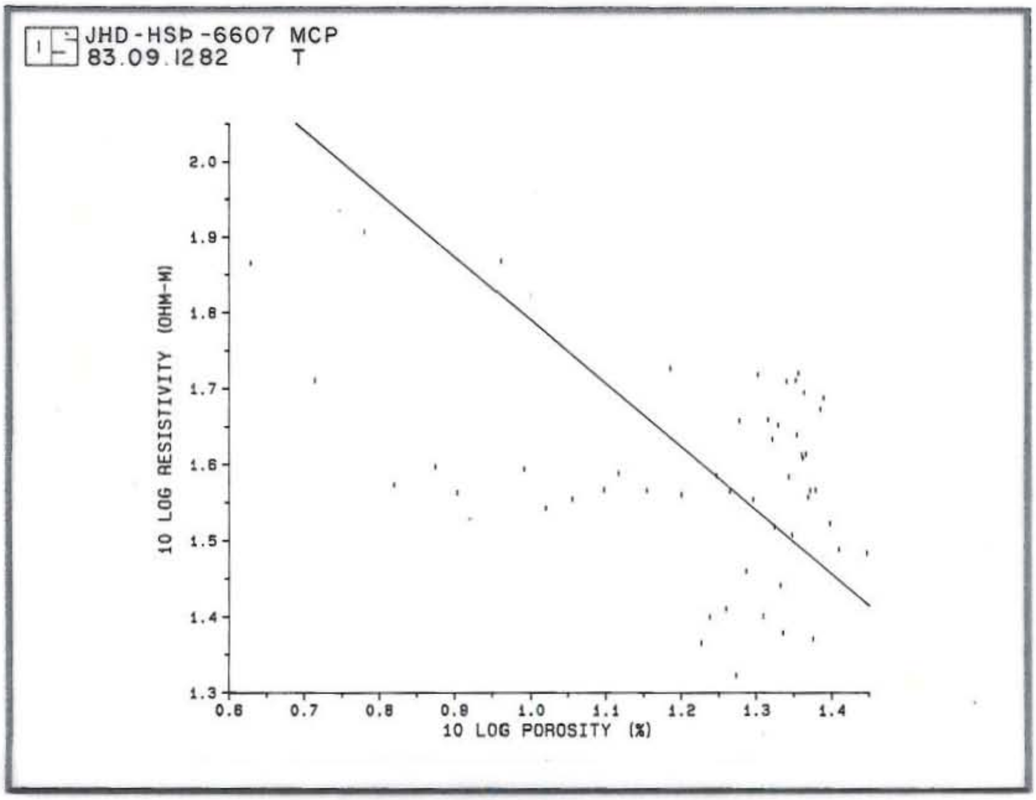

Fig. 8.2 Resistivity-porosity relation in the 800 - 900 m interval (2 meters running average).

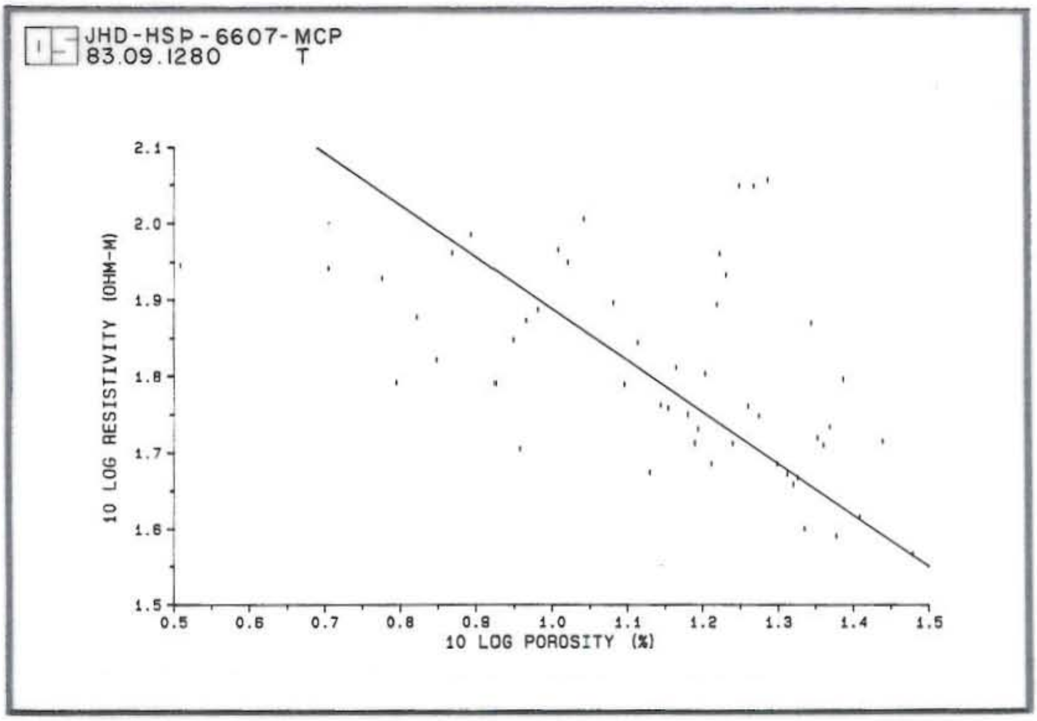

Fig. 8.3 Resistivity-porosity relation in the 900 - 1000 m interval (2 meters running average).

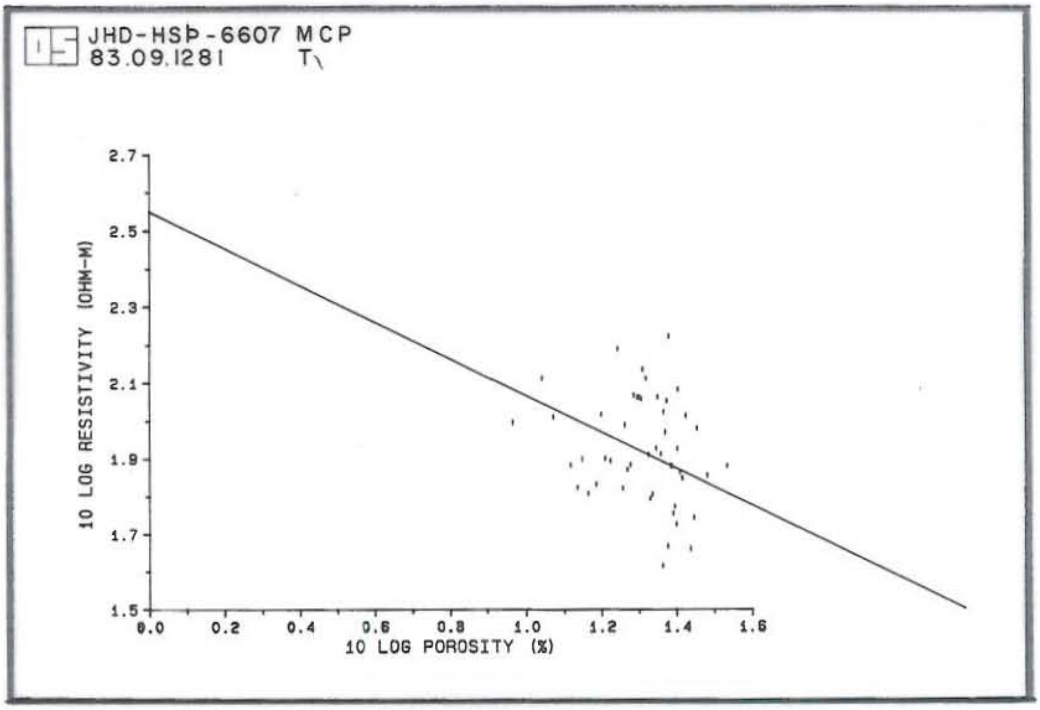

Fig. 8.4 Resistivity-porosoty relation in the 1000 - 1100 m interval (2 meters running average).

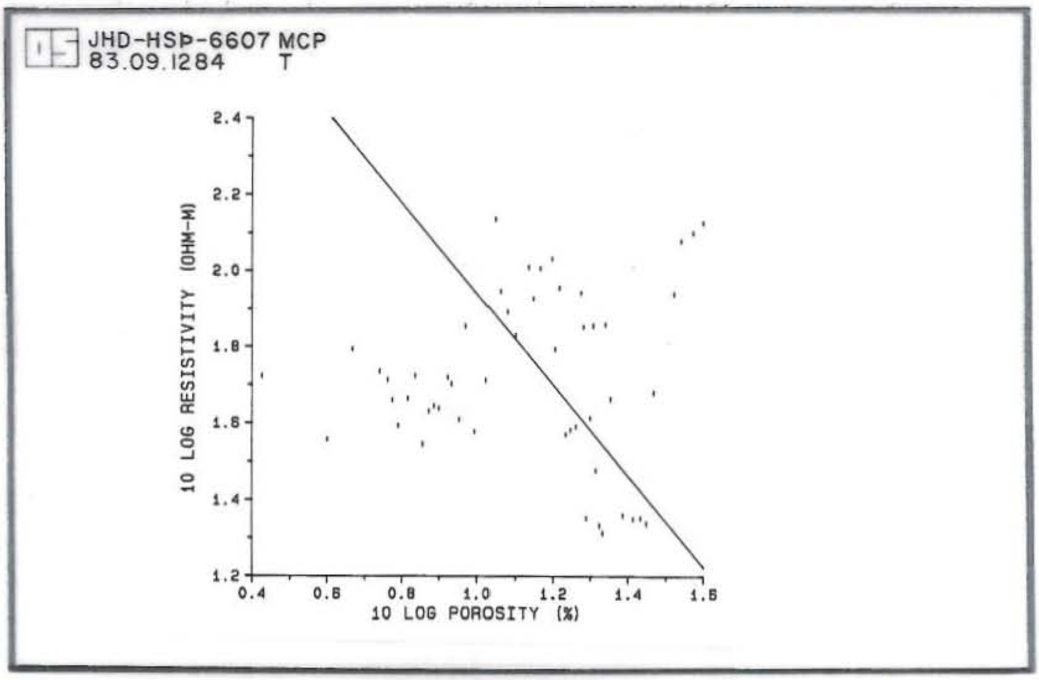

Fig. 8.5 Resistivity-porosity relation in the 1100 - 1200 m interval (2 meters running average).

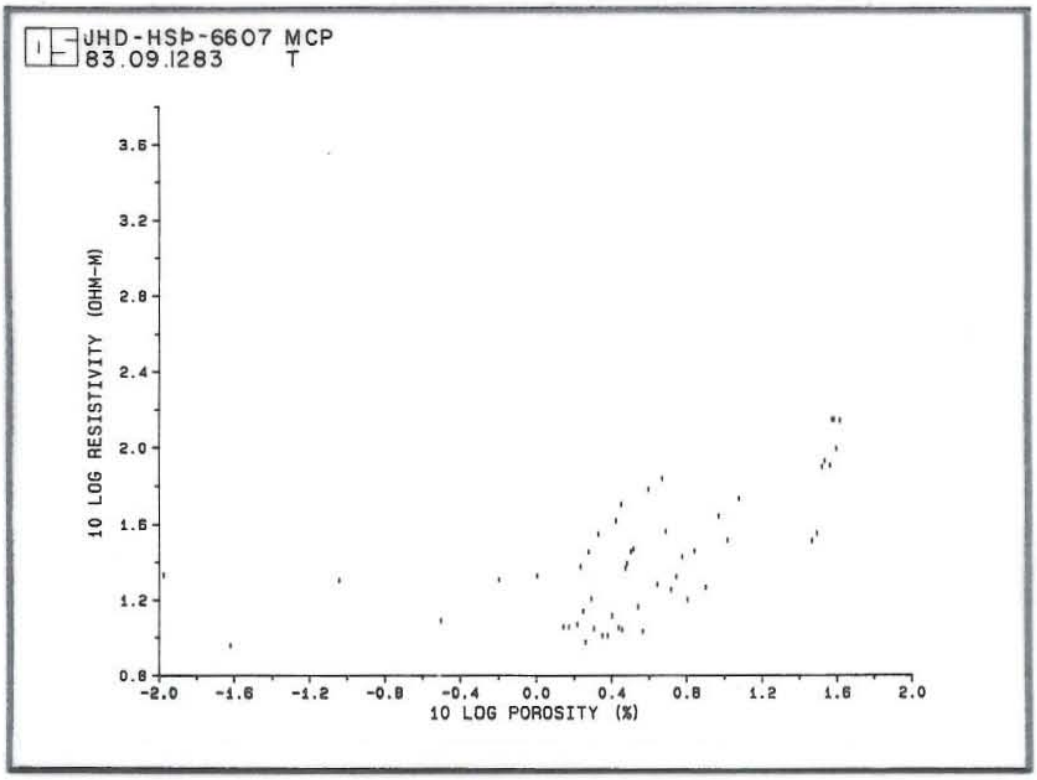

Fig. 8.6 Resistivity-porosity relation in the 1200 - 1300 m interval (2 meters running average).

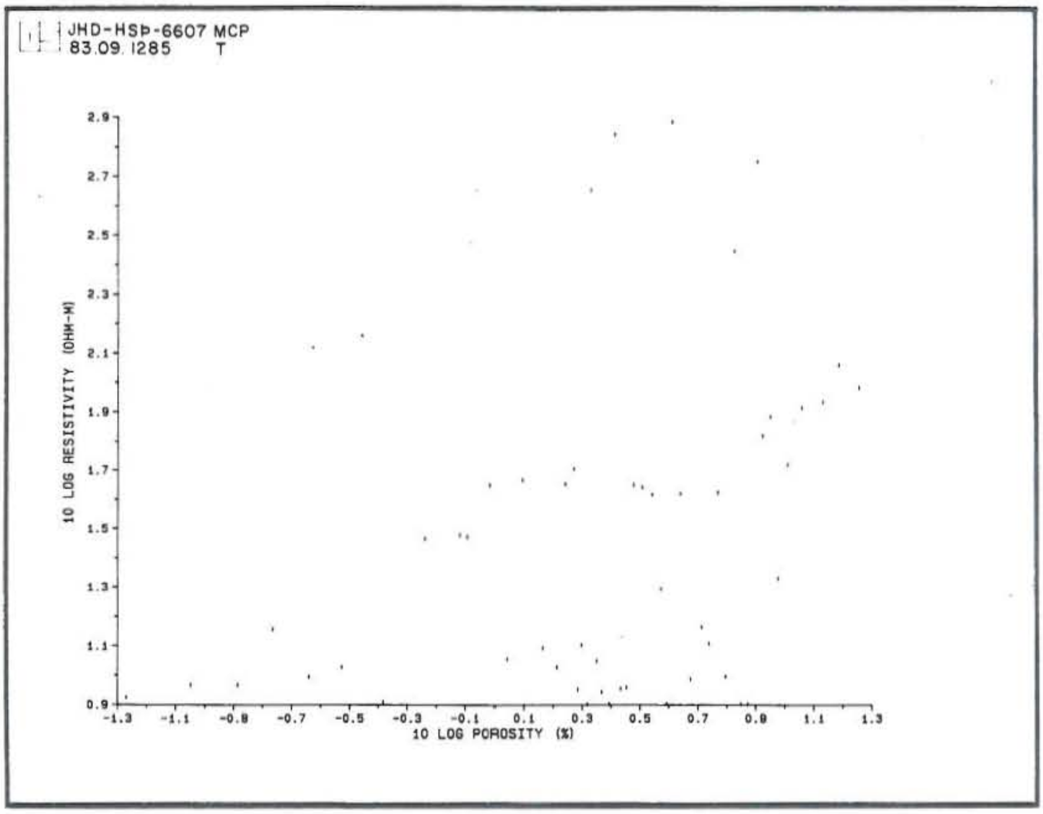

Fig. 8.7 Resistivity-porosity relation in the 1300 - 1400 m interval (2 meters running average).

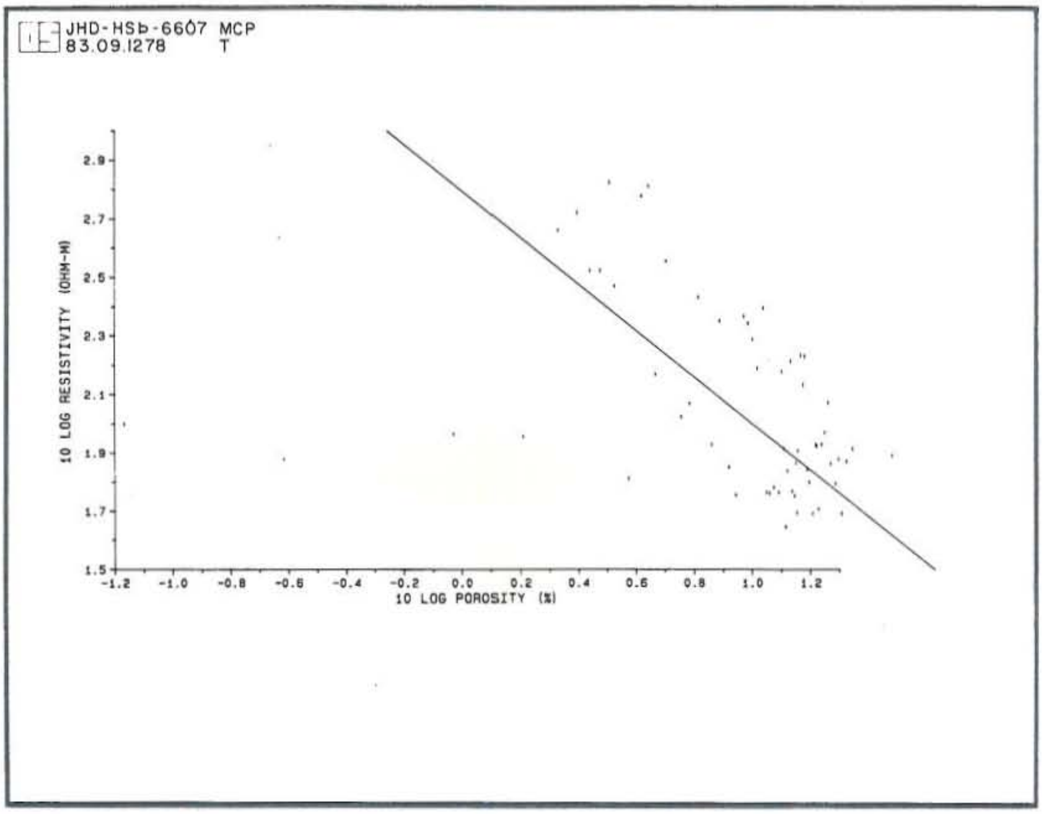

Fig. 8.8 Resistivity-porosity relation in the 1400 - 1519 m interval (2 meters running average).

a = 43 +/- 13

The resistivity - porosity relation for the 700-800m depth interval resulted in large values of constants m and a x Rw. This develops as the resistivity -porosity relation for this depth interval was approximated from the three groups of data as can be seen in Fig.8.1. These groups represent the three separate ranges of measured resistivity in the 700-800m depth interval (Fig.7.1) and should have been cross plotted separately.

The result of the resistivity - porosity cross plot for the 1100-1200m depth interval has a large uncertainty as far as the correlation coefficient is concerned. Hence, it is considered anomalous together with the results obtained from the 1200-1300m and 1300-1400m intervals, but both intervals gave positive m exponent in Archie's law. The positive m exponent in these depth intervals suggests that the resistivity is increasing with porosity, which is contradictory to the inverse relation of resistivity and porosity established by Archie (1942). These proportionality relations of resistivity and porosity in the 1200-1300m and 1300-1400m, and possibly in the 1100-1200m are hard to explain. The possibility of having some metallic elements in the formation having resistivities much lower than the resistivity of the formation fluid in these depth intervals is not in agreemen with the investigation of the rock cuttings.

8.2 The silica (natural gamma) - porosity cross plot

Figure 8.9 shows the silica - porosity cross plot for the 700-1390m depth interval. The running average for this plot is 20m. As shown in the figure, the log values are fairly distributed and do not show a dependence of silica content on porosity for KJ-17. The calculated silica-porosity relation for KJ-17 is:

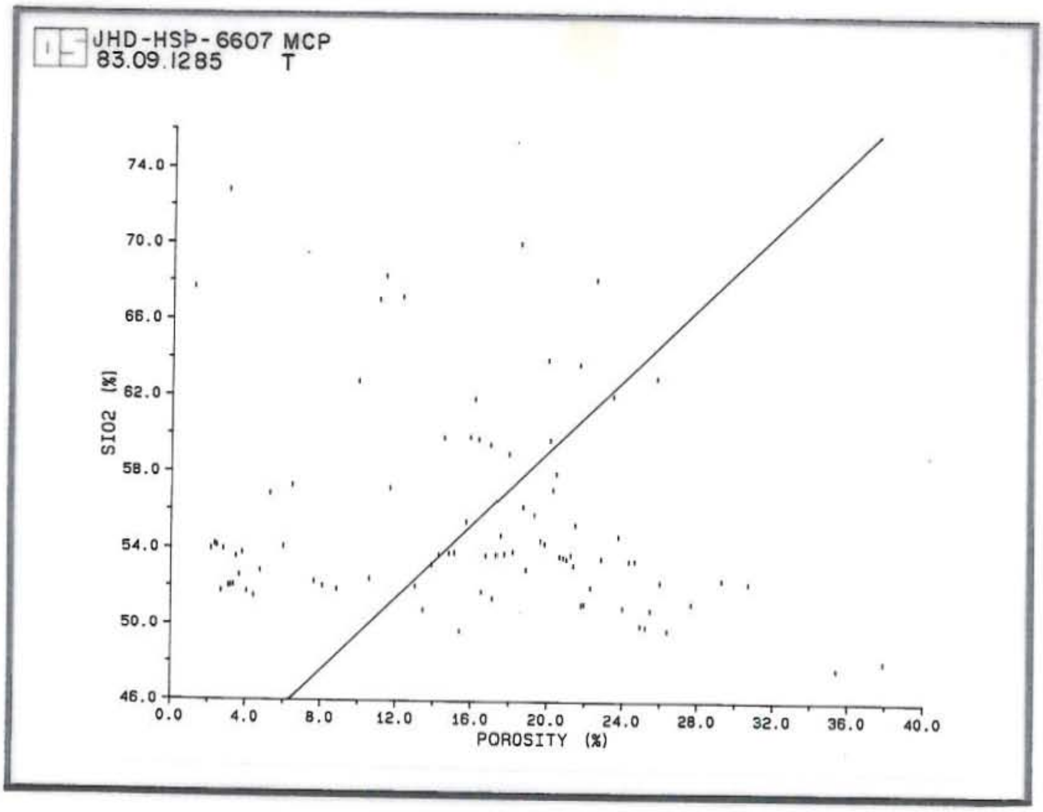

Fig. 8.9 Silica-porosity cross plot (700 - 1300 m, 20 m running average). $SiO_2 = 0.96\ \phi + 40$; R = 0.04.

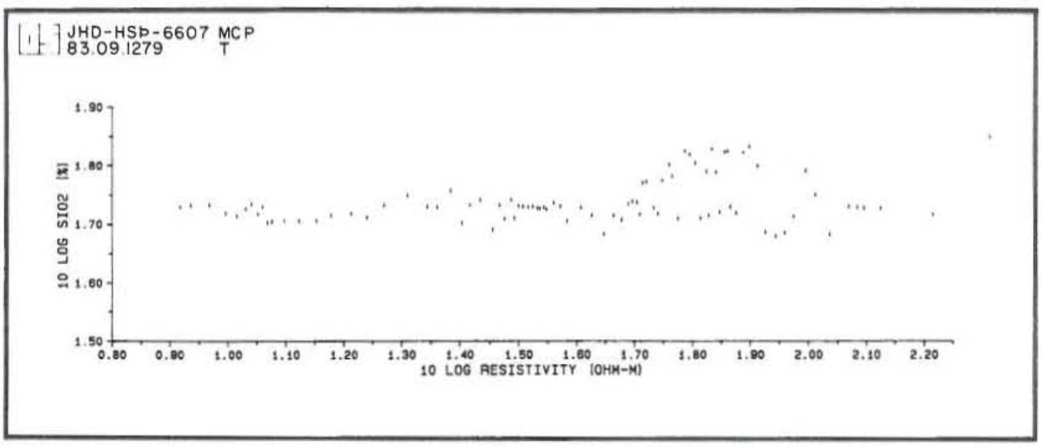

Fig. 8.10 Silica-resistivity cross plot (700 - 1390 m, 20 m running average.

$$SiO_2 = 0.96\phi + 39.8 \qquad R = 0.04;$$

which means that there is not a correlation between silica and porosity in well KJ-17.

8.3 The silica (natural gamma) - resistivity cross plot

The silica - resistivity cross plot for the 700-1390m depth interval in KJ-17 is shown in Fig.8.10. The running average for the plot is 20m. From the figure one can observe that the formation resistivity is not dependent on the silica content of rocks. One can notice that the silica content of the rocks for KJ-17 is fairly distributed along one line in the graph.

Table 8.1 Archie's coefficients for the resistivity-porosity cross plots in the KJ-17.

Depth interval (m)	Exponent (m)	a · Rw (ohm-m)	Correlation coefficient
700-800	- 2.53	91201	- 0.33
800-900	- 0.83	376	- 0.31
900-1000	- 0.68	364	- 0.49
1000-1100	- 0.49	355	- 0.41
1100-1200	- 0.99	641	- 0.06 (Anomalous)
1200-1300	+ (Anomalous)		
1300-1400	+ (Anomalous)		
1400-1519	- 0.80	623	- 0.40
Average	- 0.70 +/- 0.17	430 +/- 134	- 0.40

9 LARGE SCALE VARIATIONS

9.1 Resistivity histogram

The logarithmic distribution of the resistivity values in the 700-1800m interval was considered in an effort to classify the dominant units according to their resistivities. As shown in Fig.9.1, the logarithmic distribution of the resistivity in KJ-17 appears to be trimodal, suggesting that at least three rock types are forming these modes. The average resistivity value has been calculated to be 74 +/- 32 ohm-m.

The first mode with a resistivity range of 8-16 ohm-m (log 0.9-log 1.2) probably represents the tuff layers in the 700-900m depth interval. This group is about 12% of the formation penetrated by KJ-17 from 700-1800m.

The second group of resistivity values with a range 25-126 ohm-m (log 1.4 to log 2.1) probably derives from the altered basaltic pile interbedded in the 830-885m and 1055-1125m depth intervals. The lower values in the above range could be attributed to the fine grained basaltic pile. Calculations showed the second group to be about 51% of the pile penetrated by KJ-17 from 700-1800m.

The third group (from 158-850 ohm-m) probably represents the fine grained acidic rocks and the dolerite intrusions dominant in the intervals 1380-1390 and 1450-1800m. This group accounts for about 30% of the formation in the 700-1800m depth interval.

9.2 Porosity histogram

The porosity histogram is based on the calculated porosity values in the 700-1519m depth interval (Fig.9.2). The average porosity value for this interval is 15.3 +/- 10%. As shown in Fig.9.2, the distribution appears to be bimodal with the peaks at 2% and 23% porosities respectively.

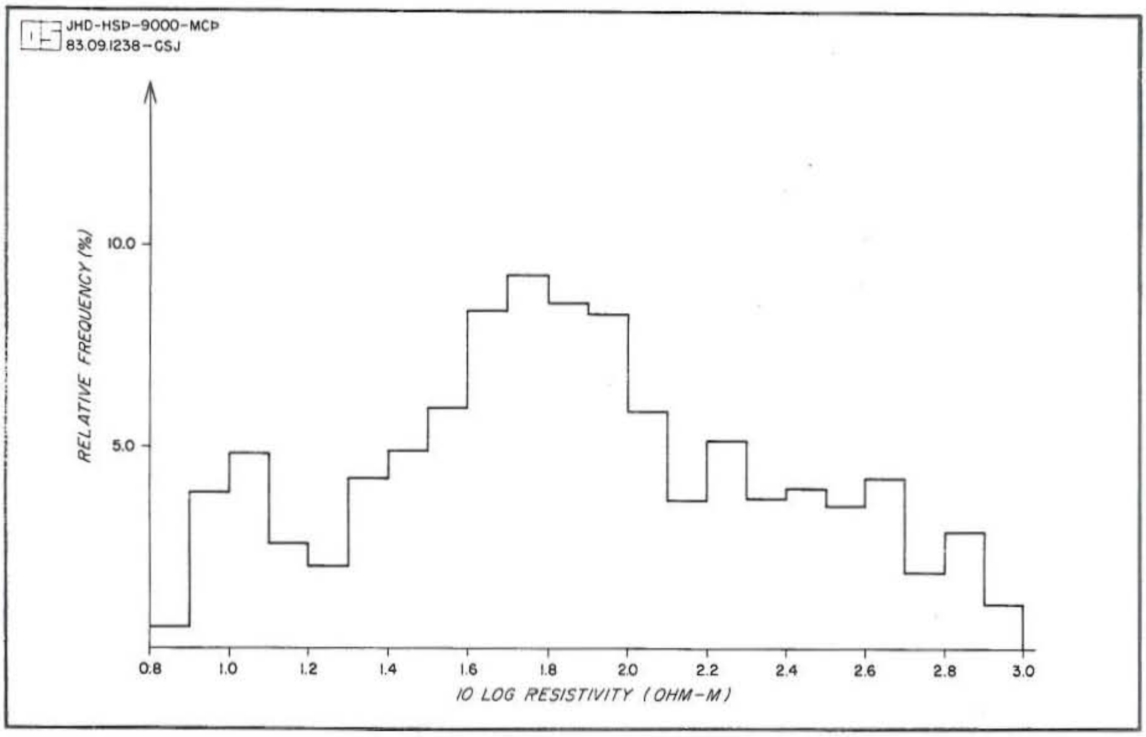

Fig. 9.1 Log distribution of the 64" normal resistivity in the interval 700 - 1800 m.
Average resistivity value = 74 +/- 3.2 ohm-m.

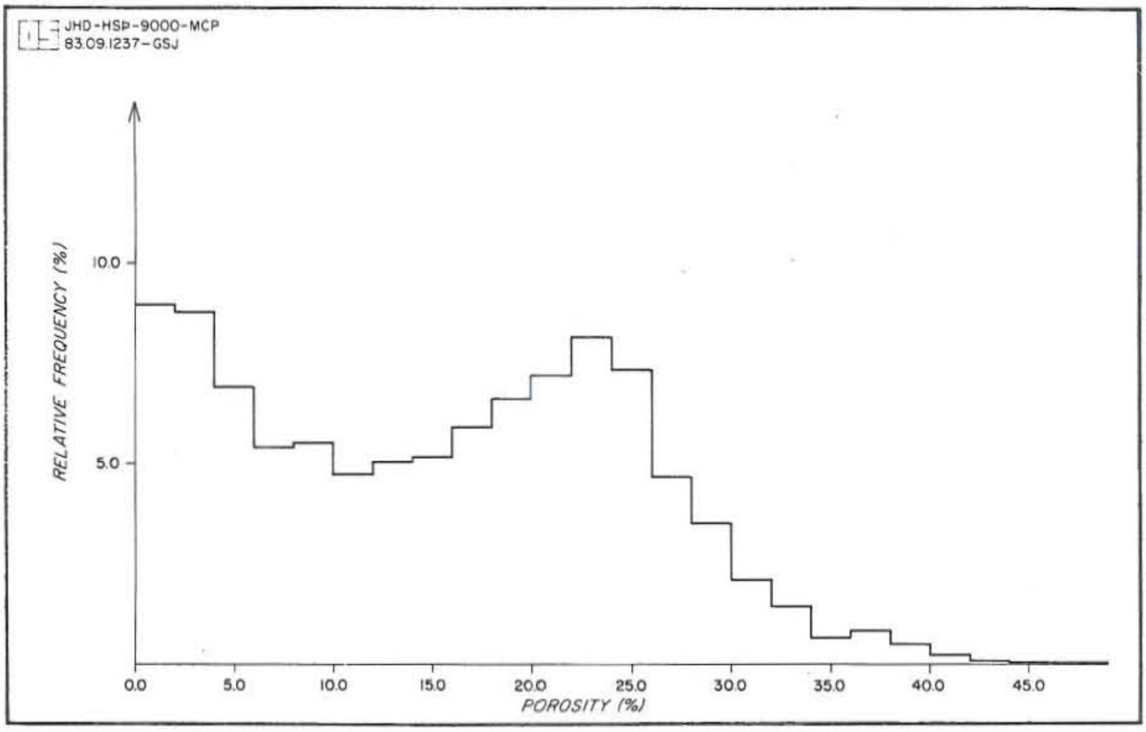

Fig. 9.2 Porosity histogram (700 - 1519 m).
Average porosity value = 15 +/- 10%

The first group with porosities ranging from 0-10% is about 36% of the pile penetrated by the well in the 700-1519m interval. These are interpreted to be the altered basalts in the 805-809 and 926-934m, the dolerite in the 989-998m, 1158-1182m and 1220-1405m depth intervals, the fresh basalts in the 1365-1375m, some contact zones like the contact zone between the coarsed grained acidic rocks and the dolerite intrusion in the 1387-1393m; and the intermittent occurences of the dolerite intrusions from 1405 to 1519m.

The second mode with porosities ranging from 10-40% comprises the rest of the pile in the 700-1519m depth interval. These are interpreted to be tuffs/hyaloclastite, altered glassy basalts, basalts and fine grained acidic rocks in the 700-1220m depth interval, the fine grained acidic rocks in the 1037-1040m interval, the occurences of dolerite and fresh basalt in the 1194-1215m interval, in some contact zones between the dolerite and an unknown formation in the 1402-1406m and 1422-1432m intervals, the breccia in the 1434-1452m interval, and some alternating occurences of breccia, altered glassy basalts and tuffs in the 1452-1519m depth interval.

9.3 Silica histogram

Fig. 9.3shows the silica distribution in the rocks of KJ-17. The silica average is 55 +/- 6%. Like the resistivity, the silica in KJ-17 exhibits trimodal characteristic with the peaks at 52.5, 63 and 69% silica respectively.

The first mode with silica ranging from 46-59% and which is about 83% of the pile in the 700-1390m depth interval of KJ-17 is interpreted to be the tuffs/ hyaloclastite, altered glassy basalt, altered basalt, fresh basalt and dolerite.

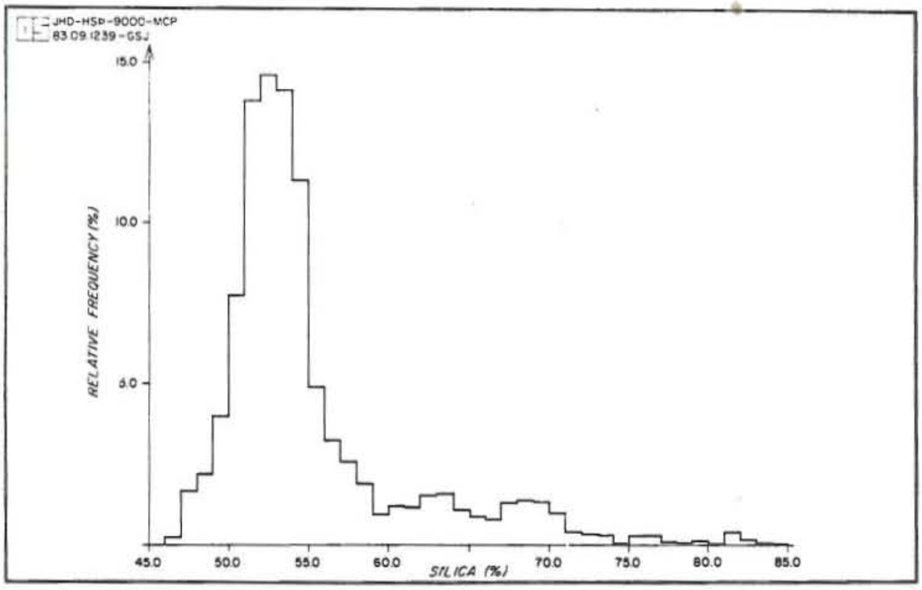

Fig. 9.3 Silica histogram (700 - 1390 m).
Average silica value = 55 +/- 6%.

The second mode with silica contents ranging from 59-66% is calculated to be about 8% of the pile in the 700-1390m depth interval. This is interpreted as breccia in the 955-965m and the layers of altered basalt and fine grained acidic rocks in the 1000-1025m depth interval.

The third mode with silica ranging from 66 to about 85% is interpreted as, the coarse grained acidic rocks in the 926-934m, the contact zone between breccia and fine grained acidic rocks in the 965-970m, the contact zone between the fine grained acidic rocks and the dolerite in 983-993m, and the contact zone between the fresh glassy basalt and the dolerite in the 1120-1125m depth interval.

9.4 Neutron, natural gamma and resistivity - large scale variations

The use of geophysical logs in mapping the large scale structure of the formation penetrated by the borehole has recently become an invaluable tool in lithological investigations. This has been noted by Stefansson and Tulinius (1983), and Jonsson and Stefansson (1982) in their investigation of a number of wells. Usually the logsarelowpass filtered and by this method pronounced zones penetrated by the well are clearly identified. In the case of KJ-17, a running average of 100m was applied to the neutron-neutron, natural gamma and resistivity logs. The results are shown in Fig. 9.4.

There are at least two distinct zones in the well. The first zone (I) is characterized by high natural gamma, moderate neutron-neutron and low resistivity values. The second zone (II) is characterized by low natural gamma and high neutron-neutron counting rates and a moderately low resistivity. If we look at the lithology logs, the first zone is characterized by frequent occurences of acidic intrusions interbedded with basalt and hyaloclastites.

By going into the details of the natural gamma ray log, it is quite clear that the high gamma count rate in the first zone (I) is caused by the acidic intrusions composed of fine and coarsed grained rocks and some occurrences of breccia. The response of the neutron-neutron log indicates that the intrusions are characterized by moderate porosities.

The lithology logs of the second zone show dolerite intrusions. The high neutron-neutron count rate suggests that the intrusion are of low porosity as shown in Fig.7.5. The low natural gamma response suggests that the intrusions are of basaltic composition. The response of the resistivity log for this zone is quite puzzling. While the neutron-neutron log indicates low porosity in contrast the resistivity log measures low resistivity. This is not easy to explain. The explanation that some metallic elements exist in these intrusive unit having resistivities much lower than the resistivity of the formation fluid is not from the geological point of view. This unusual porosity-resistivity relation was seen in the cross plots in these depth interval (1200-1300m and 1300-1400m, see Table 8.1). In the calculations, both depth intervals gave a positive exponent (m) of Archie's law which tend to suggests that the resistivity increases with increasing porosity.

It is also worth commenting on the smoothed resistivity log. From Fig. 9.4 it appears that the resistivity from 700-1350m is fairly constant whereas the resistivity from 1350-1800m increases with depth. This closely follows the trend observed in KJ-13 (Sarmiento, 1980).

In general, the pile penetrated by KJ-17 can be classified into two series with a zone of intrusions in between. The first series can be characterized as having moderate natural gamma intensity, moderate porosity and low resistivity. This series is intruded by acidic rocks. The second series cannot clearly be assessed as the neutron-neutron and the natural gamma logs do not reach below about 1400m. However, the resistivity log indicates increasing formation resistivity with depth.

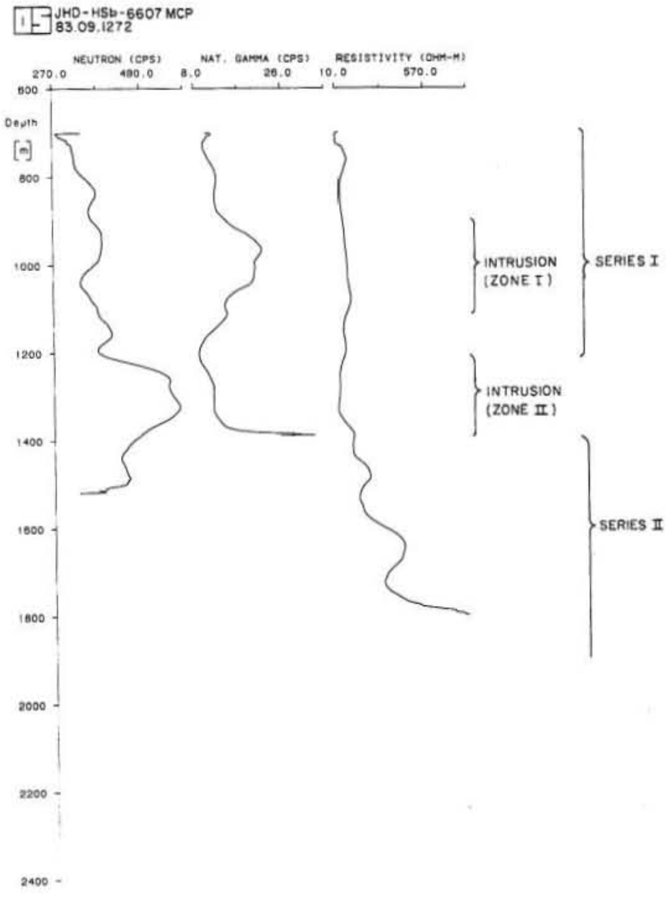

Fig. 9.4 Large scale variations (100 m running average) of neutron-neutron, natural gamma and resistivity.

10 CONCLUSION

1. In general, the geophysical and the lithology logs in KJ-17 are in good agreement.

2. The log responses of the three logs, the neutron-neutron and the natural gamma versus the resistivity logs in the interval 1191-1220m gave interesting results. The low neutron-neutron and the moderate natural gamma intensities coupled with high resistivity and some indications of cavities in this interval tends to suggest the existing of horizontal fractures in this formation. This observation is based on the relation of the horizontal fractures and the resistivity as determined by Stefansson et al., (1982b), Towle (1962). Aquilera (1974) and (1976), Hirakawa and Yamaguchi (1981). The relation as determined from their models pointed out that when the total porosity is dependent only in the horizontal fractures, the resitivity tends to be high. The moderate natural gamma values, are due to low concentration of K, U, and Th content in this formation (basalt/dolerite intrusions).

3. The maximum recorded porosity for KJ-17 is in the interval 1191-1220m. The minimum porosity is in the 1225-1400m depth interval which is also of basalt/dolerite intrusions.

4. The silica contents of the rocks in KJ-17 are in good agreement with the silica ranges for these types of rocks that have been established earlier by Stefansson et al., (1982a).

5. The mean average resistivity for KJ-17 in the 700/1800m depth interval is about 74 +/- 32 ohm-m.

6. The mean average porosity for the well in the 700-1519m depth interval is calculated to be 15 +/- 10%.

7. The silica distribution plot for KJ-17 shows the silica mean average in the 700-1390m depth interval to be 55 +/- 6%.

8. The results of the cross plots applied to the 1200-1300m and 1300-1400 depth intervals are in good agreement with the results of the large scale variations. The observation of increasing resistivity with neutron porosity for these depth intervals is hard to explain, and the hypothesis that some metallic elements having resitivities much lower than the resistivity of the formation fluid in these intervals is not in agreement with geological investigations. The caliper log for these depth intervals measured numerous cavities.

9. The pile penetrated by KJ-17 in the 700-1519m can be generally classified into two series with an intrusion in between them. The first series are characterized by moderate natural gamma intensity, moderate porosity and low resitivity. This series is also being intruded by an acid layer. The acidic intrusion is characterized by high secondary minerals, moderate porosity and low resitivity. The second series can not be assessed clearly due to depth limitation of the neutron-neutron and the natural gamma ray logs. However, the resitivity log showed the formation resitivity to be increasing with depth. The basalt/dolerite intrusions which separate the two series are characterized by low porosity, low resitivity and less to nil secondary minerals.

10. Some contact zones have also been detected notably, the contact zone between the breccia and the fine grained rocks of andesite composition in the 965-970m, the contact zone between the fine grained rock of andesitic composition and the basalt/dolerite in the 983-993m, the contact zone between the fresh glassy basalt and the basalt/dolerite in the 1120-1125m interval, and the contact zone between the basalt/dolerite and unknown formation in the 1402-1406 and 1422-1432m depth intervals.

11. The increasing resitivity with depth in KJ-17 follows closely with similar observation in other wells in the Krafla geothermal field.

12. The simultaneous recording of the amplitude intensity and the VDL in the acoustic cement bond log enhance greatly the interpretation of the CBL.

ACKNOWLEDGEMENTS

The author wishes to extend his thanks and appreciation to the organizers of the Geothermal Training Programme of the United Nations University and the National Energy Authority of Iceland for giving him the opportunity to participate in the 1983 geothermal course.

My sincere thanks are due to Dr. Ingvar B. Fridleifsson for his academic guidance and supervision of the entire course which has greatly enriched the knowledge of the author in geothermal technology, and to Dr. Valgadur Stefansson for his unselfish efforts in imparting theoretical and practical knowledge in borehole geophysics.

My special thanks are due to Steinar Thor Gudlaugsson for his ennumerable assistance and guidance in organizing and reviewing this report. The author feels that if not for his support the submission of this report would not have been timely.

Thanks are also due to Helga Tulinius for allowing the author to use some of her computer programs, and to Benedikt Steingrimsson, Hilmar Sigvaldason, Hordur Halldorsson and the rest of the NEA well loggers for imparting their practical experience in borehole geophysics. I wish also to thank Sigurjon Asbjornsson for his assistance during our stay in Iceland.

Finally, I wish to express my thanks and gratitude to the PNOC-EDC management for giving me a leave of absence and for making this training possible.

REFERENCES

Aquilera, R., 1974: Analysis of naturally fractured reservoir from sonic and resistivity logs, J. Pet. Tech., 26, p. 1233-1238.

Aquilera, R., 1976: Analysis of naturally fractured reservoirs from conventional well logs, J. Pet. Tech., 28, p. 764-772.

Archie, G.E., 1942: The electrical resistivity log as an aid in determining some reservoir characteristics, Trans. AIME, 146, p. 54-67.

Armannsson, H., Gislason, G., and Hauksson, T., 1978: Krafla, Temperature Conditions and Gases in the Geothermal Reservoir, OS-JHD-7846, National Energy Authority, Reykjavik, Iceland (in Icelandic).

Bjornsson, A., Johnsen, G., Sigurdsson, S., Thorbergsson, G. and Tryggvason, E., 1979: Rifting of the plate boundary in north Iceland 1975-1978, Journal of Geophysical Research, June 10, 1979, vol. 84, no. B6.

Benoit, W.R., Sethi, D.K., Fertl, W.H and Mathews, M., 1982: Geothermal well log analysis at Desert Park, Nevada , Geothermal log Interpretation Handbook, SPWLA Reprint volume August 1982.

Bodvarsson, G.S., Pruess, K., Stefansson, V., and Eliasson, E.T., 1983: Reservoir evaluation of the Krafla geothermal field, Iceland, LBL., Lawrence Berkeley Laboratory, Berkeley, California.

Brace, W.F., Orange, A.S and Madden, T.R., 1965: The effect of pressure on the electrical resistivity of water saturated crystalline rocks, J. Geophys. Res., 70, p. 5669-5678.

Brown, H.D., Grijalva, V.E., Raymer, L.L., 1970: New developments in sonic wave train display and analysis in cased holes, SPWLA eleventh Annual logging symposium, May 3-6, 1970.

Chang, H.T., 1981: Acoustic cement bond logging diagnostics for geothermal application, Geothermal resources council, Transactions vol. 5, p. 279-282.

Cochrane, J.E., 1966: Principles of log calibration and their application to log accuracy, Journal of Petroleum Technology, p. 817-826.

Czubek, J.A., 1981: Some aspects on nuclear well logging in igneous rock, notes on lectures presented at Orkustofnon, Iceland as a part of the International Atomic Energy Agency, Project ICE/8/02, Report OS81009/JHD05, p. 18-19 and 67-68.

Dresser Atlas, 1979: Well log review Hanndbook.

Fridleifsson, G. and Sigvaldason, H., 1981: Krafla-Hola KJ-17, Report # GOF-HS-81/02.

Gearhart Owen Industries, Inc., 1976: Formation Evaluation Data Handbook.

Gearhart Owen Industries, Inc., 1980: Cased hole engineer manual, vol.1.

Gearhart Owen Industries, Inc., 1981: Product catalog.

Gollwitzer, L.H., Masson, J.P., 1982: The cement bond tool, SPWLA Twenty Third Annual Logging Symposium, July 6-9, 1982.

Grosmangin, M., Kokesh, F.P., and Majani, P., 1961: A sonic method for analyzing the quality of cementation of borehole casings, Journal of Petroleum Technology, V. XII, no. 2, p. 165-171.

Sarmiento, Z.F., 1980: On Geophysical Logging of Geothermal wells with examples from KJ-13 in the Krafla Geothermal field, N-Iceland, A report for UNU geothermal training programme in Iceland.

Schlumberger, 1972: Log interpretation - Principles, Vol.1 p. 38.

Schlumberger, 1974: Calibration and Quality Standards Handbook.

Stefansson, V., 1981: The Krafla Geothermal Field, Northeast Iceland, Geothermal Systems: Principles and case histories, a 1981 Wiley and Sons publication, p. 273-294.

Stefnasson, V., Kristmannsdottir, H., and Gislason, G., Holubref 7, Orkustofnun 1977.

Stefansson, V., Gudmundsson, A. and Emmerman, R., 1982 a: Gamma ray logging in Iceland rocks, The log analyst, Nov.-Dec. 1982, p.11-16.

Stefansson, V., Axelsson, G. and Sigurdsson, O., 1982 b: Resistivity logging of fractured basalt, Eight Workshop on Geothermal Reservoir Engineering, Stanford University, Dec. 14-16, 1982.

Stefansson, V. and Tulinius, H., 1983: Geophysical logs from Lopra-1 and Vestmanna-1, Report OS-83088/JHD-18, 128 pp.

Stuckless, J.S., Bunker, C.M., Bush, C.A., Doering, W.P. and Scott, J.H., 1977: Geochemical and Petrological Studies of an Uraniferous Granite from the Granite Mountains, Wyoming, Journal of Research, Vol. 5, no. 1, p. 61-81.

Towle, G., 1962: An analysis of the formation resistivity factor porosity relationships of some assumed pore geometries, Paper presented at the third annual meeting of SPWLA, Houston, Texas.

Waller, W.C., Cram, M.E. and Hall, J.E., 1975: Mechanics of log calibration, Paper GG Transaction, SPWLA, Sixteenth Annual logging Symposium, June 4-7, New Orleans, LA.

Welex: Perforating for Production, a publication handbook.